BLF1-Mode of Action in Barley Leaf Size Control

Dissertation

AG Genetik-Institut für Biologie und Biochemie

zur Erlangung des akademischen Grades
"doctor rerum naturalium"
(Dr. rer. nat.)
in der Wissenschaftsdisziplin "Biologie"

eingereicht an der
Mathematisch-Naturwissenschaftlichen Fakultät
Institut für Biologie und Biochemie
der Universität Potsdam

Von

OUAD SOLTANI

Potsdam, 17. April 2023

Hauptbetreuer: Prof. Dr. Michael Lenhard

Betreuer: Dr. Jörn Lämke

Gutachter*innen: Prof. Dr. Michael Lenhard
Prof. Dr. Laura Rossini
Dr. Sarah McKim

Published online on the
Publication Server of the University of Potsdam:
https://doi.org/10.25932/publishup-60705
https://nbn-resolving.org/urn:nbn:de:kobv:517-opus4-607054

Table of contents

List of figures 5
Summary 9
Zusammenfassung 10
1. INTRODUCTION 11
1.1 Barley as a model for monocotyledonous species 11
1.2 The control of leaf growth and differentiation in Plants 12
1.3 *BLF1* gene controls leaf width in barley by limiting cell proliferation 16
1.4 IDD domain family proteins control plant growth in *Arabidopsis* by regulating auxin homeostasis and by fine-tuning GA signalling 17
1.5 RING E3 ligases play a key role in organ development and in abiotic stress responses in plants 18
1.6 Using natural variation in grasses to identify organ growth regulators 21
1.7 Aim of this study 22
2. MATERIAL AND METHODS 22
2.1 Plant materials 22
2.2 Seed sterilization 22
2.3 Seed germination 23
2.4 Growth conditions 23
2.5 Genomic DNA extraction 23
2.6 Phenotypic analysis 24
2.7 CRISPR/Cas9 related work 24
2.7.1 PCR and Sequencing of T0 Target Loci 24
2.7.2 Identification of Transgene-Free Mutant Lines 25
2.8 Gateway cloning 25
2.9 Yeast work 26
2.9.1 Yeast strains and vectors 26
2.9.2 Quick and easy yeast transformation 26
2.9.3 Library scale transformation 27
2.9.4 Cell number determination 27
2.9.5 Small scale mating on plates 28
2.9.6 Medium efficiency mating 28
2.9.7 Library scale mating 28
2.9.8 Identification of interactors via colony-PCR and test digest 29
2.9.9 Filter-Lift assay 29
2.9.10 Plasmid isolation from yeast 30
2.10 Transient Protein expression in tobacco leaves 30
2.10.1 *Agrobacteria* Preparation 30
2.10.2 Tobacco leaf infiltration 31

2.10.3 Confocal Imaging 31
2.10.4 Image Analysis 32
2.11 Co-immunoprecipitation 32
2.11.1 Generation of binary vectors 32
2.11.2 Nuclear protein extraction from tobacco cells 33
2.12 DAP-seq related work 34
2.12.1 Illumina library preparation and DAP-seq 34
2.12.2 In vitro protein expression and DNA/protein cross linking 34
2.12.3 Read mapping, filtering, and peak calling 35
2.13 *In vivo* ubiquitylation assay 35
2.13.1 Generation of plasmids 35
2.13.2 Rosetta cells co-transformation 36
2.13.3 Protein expression and purification 36
2.13.4 Western blotting 37
2.14 Confocal microscopy 37
2.15 Additional materials 37
3. RESULTS 41
PART1. TESTING THE HYPOTHESIS THAT BLF1 MODULATES GA SIGNALLING VIA AN INTERACTION WITH SLN1 41
1.1. Physical interaction of BLF1 / SLN1 proteins 41
1.2. Genetic interaction of *Blf1 / SLN1* genes 44
PART2. DISSECTING THE MOLECULAR MECHANISM OF *BLF1* GENE IN LEAF SHAPE CONTROL 48
2.1 Finding potential downstream targets of BLF1 using DAP-seq 48
2.2 Identifying BLF1 interacting protein using yeast-two-hybrid library screen 51
2.3 Confirmation of BLF1/candidate proteins interactions in planta 56
2.3.1 Ratiometric Bimolecular Fluorescence Complementation assay (rBiFC) 56
2.3.2 Co-Immunoprecipitation (Co-IP) 58
2.4 Functional characterization of the BLF1 interacting proteins 61
2.4.1 How closely does BLF1 interact with the E3 ligase related proteins? 61
2.4.2 Reconstitution of BLF1 ubiquitination cascade in Bacteria 65
2.4.3 Verification of BLF1 proteasomal degradation in barley 68
2.4.4 Analysis of genetic interaction of BLF1 and RING/U-Box E3 encoding genes 70
PART3. IDENTIFYING ADDITIONAL FACTORS ACTING TOGETHER WITH *BLF1* IN LEAF-SHAPE CONTROL BY EXPLOITING INDUCED MUTATIONS AND NATURAL GENETIC VARIATION 75
4. DISCUSSION 78
4.1 Test for physical and genetic interactions between *Blf1* and *SLN1* 78
4.2 Dissecting the molecular mechanism of the *BLF1* gene in leaf shape control 80
4.3 Identifying additional factors acting together with *BLF1* in leaf-shape control by exploiting natural genetic variation 88

5. CONCLUSION AND OUTLOOK 88
ACKNOWLEDGEMENTS 91
REFERENCES 92
HOMEPAGES CITED 105
APPENDIX A: OLIGONUCLEOTIDES 105
APPENDIX B: PLASMID CONSTRUCTS 108

List of figures

Figure 1. Yeast two-hybrid (yeast-two-hybrid) assays. 43
Figure 2. Schematic diagram of the experimental setup used to study the genetic interactio between BLF1 and SLN1 genes. 45
Figure 3. Leaf size parameters of wt, blf1, sln1d and blf1 Sln1d plants. 46
Figure 4. Flow-chart of the DAP-seq protocol & main results obtained in this study. 49
Figure 5. controls for fusion protein expression and bead binding. 50
Figure 6. Characterisation of positive clones obtained by yeast-two-hybrid library screening. 53
Figure 7. Confirmation of BLF1 and the candidate protein interactions by targeted yeast-two-hybrid assay. 55
Figure 8. Self-activation detection of the prey vector pDEST22-library by mating with pDEST32-EV. 55
Figure 9. Ratiometric Bimolecular Fluorescence Complementation (rBiFC) assay. 57
Figure 10. Flow-Chart of the Co-IP system established in this study. 59
Figure 11. validation of interaction between BLF1 and the candidate proteins using Co-IP. 60
Figure 12. Confirmation of the BLF1–RING/U-Box and BLF1–BTB/POZ interactions by FRET Measurements. 63
Figure 13. Quantification of the donor and acceptor signals before photobleaching from MG132 treated (+ MG132, mauve boxes) and untreated cells (-MG132, yellow boxes). 64
Figure 14. Bacterial system for expression and purification of ubiquitylated proteins. 66
Figure 15. Reconstitution of the BLF1 ubiquitylation in E. coli. 67
Figure 16. Effects of bortezomib treatments on the expression of pBLF1:BLF1-vYFP in barley. 69
Figure 17. Identification of mutations in the BLF1 and RING-E3 genes. 71
Figure 18. Phenotype of the ring-e3_2, blf1_a double mutant. 72
Figure 19. Small scale phenotyping of the ring-e3_1 mutant. 73
Figure 20. Large scale phenotyping of the ring-e3_1 mutant. 74
Figure 21. Schematic diagram of the experimental setup used to identify additional factors acting together with BLF1 in leaf shape control 76
Figure 22. Frequency distribution analysis of leaf 3 width phenotype in Landrace x blf1 crosses. 77

List of Tables

Table 1: Reaction components for the transformation mix used 26
Table 2: Calculation of the library screening mating efficiency 29
Table 3: Reaction components for the filter-lift assay 30
Table 4: SLiCE reaction mix 32
Table 5: PCR reaction mix 35
Table 6: Cycling conditions for the Phusion-PCR. 35
Table 7: List of used vectors 37
Table 8: Bacteria and yeast strains 38
Table 9: Chemicals 38
Table 10: Kits 39
Table 11: Buffers and media 39
Table 12: Quantification of the blf1 mutant phenotype 47
Table 13: Blast results of BLF1 interacting proteins 54

Declaration of authorship

I hereby declare, that this PhD thesis with the title "*BLF1*-Mode of Action in Leaf-size Control" is my own work; contribution or substantial help from other people is stated in the Material and Methods section, or cited in the text.

In brief: Some initial plasmid constructs and marker design of *blf1*, *Sln1d*, and landraces has been performed by Moritz Jöst. Leaf measurements were done with the help of Christian Kappel. DAPseq data analysis as well as Confocal imaging were done with the help of Moritz Jöst and Otto Baumann. The generation of CRISPR/Cas9 barley mutants was done by members of the group of Jochen Kumlehn, in particular Götz Hensel, at the IPK Gatersleben.

This PhD thesis was specifically prepared for submission to the faculty of science of the University of Potsdam and no part of this work has been submitted to any other University.

Potsdam, 26.09.2022	Ouad Soltani,
Ort, Datum	Name, Unterschrift

Eigenständigkeitserklärung

Hiermit erkläre ich, dass es sich bei dieser Doktorarbeit mit dem Titel "*BLF1*-Mode of Action in Leaf-size Control" um meine eigene Arbeit handelt; Beiträge oder wesentliche Hilfe von anderen Personen sind im Abschnitt Material und Methoden angegeben oder im Text zitiert.

Kurz gefasst: Einige erste Plasmidkonstrukte und das Design von Markern für blf1, Sln1d und Landrassen wurden von Moritz Jöst durchgeführt. Blattmessungen wurden mit Hilfe von Christian Kappel durchgeführt. Die Analyse der DAPseq-Daten sowie die konfokale Bildgebung wurden mit Hilfe von Moritz Jöst durchgeführt. Die Generierung von CRISPR/Cas9 Gerstenmutanten wurde von Mitgliedern der Gruppe von Jochen Kumlehn, insbesondere von Götz Hensel, am IPK Gatersleben durchgeführt.

Diese Dissertation wurde speziell für die wissenschaftliche Fakultät der Universität Potsdam erstellt und kein Teil dieser Arbeit wurde an einer anderen Universität eingereicht.

Potsdam, 26.09.2022	Ouad Soltani,
Ort, Datum	Name, Unterschrift

Summary

Establishment of final leaf size in plants represents a complex mechanism that relies on the precise regulation of two interconnected cellular processes, cell division and cell expansion. In previous work, the barley protein BROAD LEAF1 (BLF1) was identified as a novel negative regulator of cell proliferation, that mainly limits leaf growth in the width direction. Here I identified a novel RING/U-box protein that interacts with BLF1 through a yeast two hybrid screen. Using BiFC, Co-IP and FRET I confirmed the interaction of the two proteins in planta. Enrichment of the BLF1-mEGFP fusion protein and the increase of the FRET signal upon MG132 treatment of tobacco plants, together with an *in vivo* ubiquitylation assay in bacteria, confirmed that the RING/U-box E3 interacts with BLF1 to mediate its ubiquitylation and degradation by the 26S proteasome system. Consistent with regulation of endogenous BLF1 in barley by proteasomal degradation, inhibition of the proteasome by bortezomib treatment on BLF1-vYFP transgenic barley plants also resulted in an enrichment of the BLF1 protein. I thus demonstrated that RING/U-box E3 is colocalized with BLF1 in nuclei and negatively regulates BLF1 protein levels. Analysis of *ring-e3_1* knock-out mutants suggested the involvement of the *RING/U-box E3* gene in leaf growth control, although the effect was mainly on leaf length. Together, my results suggest that proteasomal degradation, possibly mediated by RING/U-box E3, contributes to fine-tuning BLF1 protein-level in barley.

Zusammenfassung

Die Festlegung der endgültigen Blattgröße bei Pflanzen ist ein komplexer Mechanismus, der auf der präzisen Regulierung zweier miteinander verbundener zellulärer Prozesse beruht, der Zellteilung und der Zellexpansion. In einer früheren Arbeit wurde das Gerstenprotein BROAD LEAF1 (BLF1), als ein neuartiger negativer Regulator der Zellproliferation identifiziert, der das Blattwachstum hauptsächlich in Richtung der Breite begrenzt. Hier habe ich durch einen Hefe-Zwei-Hybrid-Screen ein neuartiges RING/U-Box-Protein identifiziert, das mit BLF1 interagiert. Mittels BiFC, Co-IP und FRET konnte ich die Interaktion der beiden Proteine in der Pflanze bestätigen. Die Anreicherung des BLF1-mEGFP-Fusionsproteins und der Anstieg des FRET-Signals bei der Behandlung von Tabakpflanzen mit MG132 sowie ein *in vivo* Ubiquitylierungsassay in Bakterien bestätigten, dass das RING/U-Box-E3 mit BLF1 interagiert und dessen Ubiquitylierung und Abbau durch das 26S-Proteasom-System vermittelt. Darüber hinaus habe ich festgestellt, dass die Behandlung mit Bortezomib, einem Inhibitor des Proteasoms, bei BLF1-vYFP-transgenen Pflanzen ebenfalls zu einer Anreicherung des BLF1-Proteins führt. Ich zeige dass RING/U-Box E3 mit BLF1 in den Zellkernen kolokalisiert ist und den BLF1-Proteinspiegel negativ reguliert. Die Analyse der Knock-out-Mutante *ring-e3_1* legte eine Beteiligung das RING/U-Box-E3 Gen an der Kontrolle des Blattlänge nahe, was es zu einem guten Kandidaten macht, der die Funktion des *BLF1*-Gens regulieren könnte.

1. INTRODUCTION

1.1 Barley as a model for monocotyledonous species

Barley (*Hordeum vulgare ssp. vulgare*), is a self-pollinating monocotyledonous plant species that belongs to the *Poaceae* grass family which includes several major crops used in modern agriculture. Its initial domestication began with the wild species *Hordeum vulgare ssp. spontaneum* and took place in the Fertile Crescent (Zohary *et al.*, 2013)

Nowadays barley is ranked as the world's fourth most cultivated cereal after rice, wheat, and maize with a global production level (2018/2019) of 141 million tons (FAOSTAT website, available: http://faostat.fao.org). Worldwide, barley is mainly grown for animal feed (more than 70% of global production), for malting to produce alcoholic and non-alcoholic beverages (about 21%), and as human food (less than 6%) (Tricase *et al*., 2018). With an autogamous reproduction and a diploid genome (2n = 14, 5.1 Gb), barley has proven to be an excellent model plant for the Triticeae tribe, which includes the much more complex hexaploid wheat (Dawson *et al.*, 2015, Rotasperti *et al.*, 2020). As a result, extensive and well-characterized collections of morphological and developmental mutants, generated by several mutagenesis programs, have been assembled in repositories such as NordGen (https://www.nordgen.org/en/).

As one of the most widely spread crops, barley has the ability to adapt to different environmental conditions. Hence, its germplasm pool has a great genetic diversity allowing to breed for adaptation to different environmental conditions. Moreover, large collections of wild accessions, landraces and cultivars likely contain beneficial allelic variation that new genomic and breeding technologies can exploit (Munoz Amatriain *et al*., 2014).

A wide range of genomic and analytical tools have contributed to explore this variation and to understand the link between genetic diversity and inherited phenotypes, such as barley mutant analysis and genome-wide association studies (GWAS) in plants (Waugh *et al*., 2009). For example, the use of elite US and UK breeding germplasm (BarleyCAP and AGOUEB) coupled with the development of high-throughput barley SNP assays (Bayer *et al*., 2017) and an exome capture platform (Mascher *et al*., 2013) has allowed the detection of quantitative trait loci (QTLs) for biotic and abiotic stress resistance (Munoz Amatriain *et al*., 2014).

As a member of the *Triticeae* family, and given its close relationship to wheat (*Triticum aestivum L.*), barley can serve as a model species for the Gramineae family. Thus, discoveries in barley that have potential agronomic benefits can directly influence the yield of important cereal crops. Thanks to its diploid nature, studies of genetic mechanisms are greatly facilitated in barley compared to hexaploid wheat and, given their close genetic relationship, these are likely to be conserved between the two. Besides, its not possible to study the molecular mechanisms and traits specific to *Triticeae* in more distant model species such as maize, rice, or *Arabidopsis* (Hedges, 2002). Among the recent mechanisms identified in barley and proved to be conserved in wheat the *branched headt* (*bht*) locus which regulates spike branching in 'Miracle-Wheat' found by the identification of orthologs of the barley *compositum2* (*com2*)

mutant underlying spike-branching in 'Compositum-Barley. Sequence analysis of the *bht* locus in wheat revealed that a single mutation led to the domestication of 'Miracle-Wheat' (Dobrovolskaya *et al.,* 2015). Further examples are the non-fragile rachis genes *Btr1* and *Btr2* responsible for the change of brittle/weak rachis to nonbrittle rachis in barley (Pourkheirandish *et al.,* 2015). Both genes possess orthologs with similar functions in maize *BRANCHED SILKLESS 1* (*BD1*) (Chuck *et al.,* 2002), rice *FRIZZY PANICLE/BRANCHED FLORETLESS 1* (*FZP/BFL1*) (Zhu *et al.,* 2003), and *Brachypodium distachyon MORE SPIKELETS 1* (*MOS1*) (Derbyshire and Byrne 2013). Despite their crucial role for food safety and supply, yield gains of wheat and barley have remained moderate to stagnant within the last two decades which emphasize the urgent need of an ideotype crop plant, serving as a model plant rationally designed to combine morpho-physiological traits predicted to enhance the quality and/or quantity of the end product (reviewed by Schnurbusch (2019)).

Several studies suggest that the optimal plant architecture combines two main characteristics; smaller leaf angles from the upper canopy and narrower leaves as excessively wide leaf area could lead to surface overlapping of leaves, which reduces the light exposure of the shaded areas (Ort *et al.,* 2015). Ort *et al.,* (2015) have further demonstrated this hypothesis in their concept of smart canopy for crop biomass and yield. The concept refers to maximizing the potential of light penetration at the canopy level in a non-competitive manner between plants. Hence, a better understanding of the genetic and molecular mechanisms controlling tiller and leaf development is required for designing an optimal plant architecture, and efficient genomic and phenotyping tools are required to identify genes and alleles underlying these agriculturally important traits (Shaaf *et al.,* 2019).

1.2 The control of leaf growth and differentiation in Plants

Leaf growth up to a specific shape is tightly regulated within plant species, suggesting that a species-specific regulatory network terminates leaf growth in a coordinated and timely manner (Conlon and Raff, 1999; Mizukami *et al*., 2001). In grasses, the first leaf primordia are produced by the shoot apical meristem (SAM), during embryogenesis. For example, in barley, 3–4 leaf primordia are present in the seed and they carry on with growth post-embryonically (Kirby and Appleyard, 1987). The SAM can thus be viewed as a cell-generating machine that produces a naive tissue which will undergo in the next stages the different mechanism(s) of morphogenesis and differentiation (Fleming, 2004). Based on histological analysis of median longitudinal sections of shoot apices, the first sign of leaf initiation is described as localized periclinal cell divisions at some distance from the SAM centre (Raghavan, 2000).

The SAM is composed of two major compartments: the "central zone" (CZ) and the peripheral zone (PZ). The CZ is formed by a population of undifferentiated cells that maintain a slower division rate called the stem cell population. Surrounding the CZ is the PZ, in which cells divide faster and leaf and flower primordia are initiated, respectively, under the control of auxin (de Jager *et al.,* 2005). As soon as they migrate from the stem cell niche to the periphery zone, cells lose their identity and start dividing faster to give rise to lateral organs. Hense, the positioning of a cell in the SAM is the major determinant of its fate (Shaaf *et al.,* 2019).

The identity of stem cells in the CZ is determined by the opposing functions of two gene pathways: a positively acting pathway that promotes stem-cell identity (based on the homeodomain transcription factor *WUSCHEL* (*WUS*)) and a negatively acting pathway that suppresses it (based on a series of *CLAVATA* gene products) (Clark *et al.,* 1997; Brand *et al.,* 2000; Schaaf *et al.,* 2019). The *CLAVATA* genes encode a putative secreted peptide ligand (*CLV3*) and two Leu-rich repeat (LRR) receptor-like proteins (*CLV1* and *CLV2*) (Clark *et al*., 1997; Fletcher *et al*., 1999). The two pathways interact so that the *WUS*-based pathway promotes the activity of the negatively acting pathway, and the negatively acting *CLV* pathway suppresses activity of the positively acting *WUS* pathway (Lenhard *et al.,* 2002). This mutually dependent feedback loop is required to maintain both the stem cell niche and the underlying WUS-expressing population. Thus, any increase in the number of stem cells resulting from an increase in *WUS* activity leads automatically to suppression of this latter via the *CLV* pathway. Although the *WUS/CLV* pathways dispose of an overlapping gene expression pattern, they are still spatially separated (Fleming, 2004).

A further key meristem regulator is a homeobox gene of the KNOTTED class, known as *SHOOT MERISTEMLESS* (*STM*), and the loss of function mutation in *STM* results in a non-functional shoot meristem. In addition, *stm* mutants have fused cotyledon petioles, suggesting that *STM* has two functions: it maintains the undifferentiated cellular state characteristic of meristematic cells and prevents outgrowth of the cells separating the cotyledon primordia in the periphery (Long *et al.,* 1996; Lenhard *et al.,* 2002).

During leaf development, growth and differentiation proceed in a coordinated way to reach the final mature leaf shape, and this occurs by establishing polarity along the proximal-distal, medio-lateral and abaxial-adaxial axes. The initial primordia P0 is formed when groups of founder cells, recruited from the CZ to the PZ of the SAM, lose their meristematic identity and become specified as leaf primordia. P0, in its turn, grows along the proximal–distal axis mainly through cell proliferation. Then, adaxial–abaxial structures are differentiated in the P2 stage. Subsequently, cells proliferate along the medial–lateral axis leading to flat and symmetric leaves (Scanlon *et al.,* 1996; Lewis and Hake 2016, reviewed by Iwakawa *et al.,* 2020). According to research realized on maize, until the P2 stage, the developing leaf is entirely formed by blade tissue and the first emergence of the sheath takes place between P3 and P4. But this differentiation along the proximal-distal axis may differ in timing between species. In maize for example, the pre-ligular band (i.e., the group of cells that will give rise to the ligule) forms before P6 (Lewis and Hake 2016), whereas this step occurs at P3 in rice (Itoh *et al.,* 2005).

Leaves continue to grow from meristematic zones located at the bases of leaf blade and sheath (Briggs 1978; Itoh *et al.,* 2005; Jöst *et al.,* 2016). Starting from the tip of the leaf, cells stop dividing and switch to the expansion and later the maturation phases. This proliferation arrest spreads then toward the base, in a way that when cells at the leaf tip are fully differentiated, cells at the base are still dividing (Kazama *et al*. 2010; reviewed in Nelissen *et al.,* 2016). Once proliferation has ceased, cells transition to elongation-based growth and grow to their mature size by expansion. Leaves reach maturity once cells have differentiated and both cell

proliferation and expansion have ceased (Sharman 1942; Sylvester *et al*. 1990; Donnelly *et al*. 1999; Nath *et al*. 2003; Kazama *et al*. 2010; Tsukaya, 2013). In the transition phase from proliferation-based growth to cell expansion, both modes of growth co-occur, dividing the leaf into the following separate zones: the division zone, the elongation zone and the maturation zone (Green 1976; Fiorani and Beemster 2006; Andriankaja *et al*. 2012).

It was shown in maize that the transition from cell division to cell elongation depends on gibberellin (GA) levels. GA levels peak at the transition from the division to the elongation zone; decreasing or increasing GA levels shift this transition zone more proximally or distally, resulting in shorter or longer leaves, respectively (Nelissen *et al*. 2012). Thus, the size of the division zone, as well as the residence time of cells within this region, can influence mature leaf size (Fiorani and Beemster 2006). Consequently, depending on their positioning along the proximal-distal axis, cells undergo maturation at the distal end, expansion in the central region or division in the proximal zone (Fournier *et al.*, 2005). Spatial and temporal coordination of these processes leads to the final leaf structure. Leaf length for example, is controlled by two main factors: leaf elongation duration (LED) and leaf elongation rate (LER), which are determined by the division zone (reviewed in Nelissen *et al*., 2016). LER and LED, as it has been shown in maize and barley, are controlled by distinct mechanisms (Baute *et al.*, 2016; Digel *et al.*, 2016).

As boundaries between cell types are often the origin of new tissue development, the role of boundary formation in axillary meristem development has been an intense area of study (Bar and Ori, 2014; Lewis and Hake, 2016). The barley *Uniculm2* (*Cul2*) gene has been shown to control the axillary meristem development, as *cul2* mutant plants lack lateral branches (tillers). A genetic screen for *cul2* suppressors unravelled two recessive alleles of *ELIGULUM-A* (*ELI-A*), encoding an unannotated protein containing a highly conserved RNaseH-like domain. Functional characterisation suggested that *ELI-A* is involved in boundary formation between the blade and sheath but not in boundary development for axillary meristem development (Muehlbauer *et al*., 2018).

To identify genes with dual roles in boundary demarcation and leaf and axillary meristem development, Johnston *et al*. (2014) proposed a conserved genetic system that establishes axillary meristems and determines leaf shape in maize. Transcriptome analysis from the maize preligule region identified homologous genes that are expressed at the blade-sheath boundary as well as at the lateral organ initiation (Johnston *et al*., 2014). Among the differentially expressed genes were the maize *CUC2* and *BOP* homologs. RNA in situ hybridization experiments showed maize *CUC2*-like transcripts accumulating in the preligule band and at the lateral branch initiation. The maize BOP-like transcripts accumulated in developing ligules, leaf axils, and axillary meristems (Johnston *et al*., 2014). The BOP homolog in barley *UNICULME4* (*CUL4*) is expressed in developing ligules, leaf axils, and axillary meristems and is shown to have a similar function to the maize *BOP* homolog in the formation of the ligule boundaries and axillary bud development (Tavakol *et al*., 2015).

In grasses, the concentric domains forming the PZ are the origin of the upper and lower regions of the leaf which meet at a midplane boundary. Three main parts characterise the PZ: The

central, lateral, and marginal domains. The *NARROWSHEATH* genes (*NS1* and *NS2*), members of the *WUSCHEL-RELATED HOMEOBOX* (*WOX*) gene family, are responsible for the control of the marginal identity (Scanlon *et al*., 1996; Nardmann *et al*., 2004). A resent study by Richardson *et al.* (2021) aimed to understand the origin of the evolutionary mechanism underlying the sheathing leaf aspect that characterize grasses and other monocots. Based on the "petiole-sheath" hypothesis proposed in the 19th century, suggesting that the grass sheath is the homolog of the petiole and the blade the homolog of the lamina, they tried to create a growth model that aims to verify this hypothesis by understanding how does the PZ control primordia outgrowth and leaf morphogenesis.

The model was based on two growth polarity fields: an orthoplanar field perpendicular to the outer surface and a planar polarity field parallel to the surface. To study the orientation of growth polarity in barley, they performed a cell tracking and expression analysis of the auxin transporter *SISTER-OF-PINFORMED1* (*SoPIN1*), known as an early indicator of epidermal polarity, and the CUC2 boundary gene in the wild type and ns1/2 mutant (Conklin *et al*., 2019, Richardson *et al.*, 2021). The results suggested two functions for NS1/2: (i) extension of the PZ and midplane to encircle the meristem and (ii) growth promotion perpendicular to orthoplanar polarity to drive primordium emergence. To study the link between grass and dicot leaves, the same model was created for the *Arabidopsis*. Taken together, the results were in favour of the petiole-sheath hypothesis.

In rice, characterisation of the *narrow leaf1* (*nal*1) mutant revealed that *NAL1* regulates leaf morphology by affecting vein patterning and cell division (Qi *et al*., 2008; Li *et al*., 2015). Histological analysis showed the *nal1* mutant phenotype results from an enhanced cell proliferation in the periclinal direction and suppressed cell division in the anticlinal direction during primordia outgrowth (Li *et al*., 2015). A combination of RNA-Seq and RT-qPCR analysis was used to identify through which mechanism *NAL1* regulates cell proliferation. Analysis of the differentially expressed genes between wt and the *nal1* mutant suggested that *NAL1* positively regulates the expression of the auxin transporters (PINs). A recent study by Qi *et al* (2019) shows that *NAL1* is also involved in the regulation of cell expansion through up-regulation of genes encoding Expansins (OsEXP).

In addition to an increase in the number of tillers, the high-tillering mutant of barley (*Hvhnt1*) also presented narrower leaves and shorter plants compared to the wild-type. Molecular mapping showed that *HvHNT1* encodes a trypsin family protein. Additionally, expression pattern analysis of *HvHNT1* confirmed its involvement in tiller formation and leaf development. A putative cyclophilin-type peptidyl-prolyl cis/ trans-isomerase (HvPPIase) was identified as a substrate of the HvHNT1 protein. Taken together, these results suggested that HvHNT1 interacts with HvPPIase to control tiller development and leaf width in barley (Ye *et al*., 2019). Tillering is also one of the important agronomic traits that have a great impact on crop yield. There are three stages in tiller development in grasses: (i) axillary meristem initiation, (ii) bud formation, and (iii) tiller outgrowth (Digel *et al.*, 2016 ; Grbic and Bleecker, 2000). Bud formation is known as a genetically controlled aspect. Mutation in genes such as *barren stalk1* (*ba1*; Gallavotti *et al*., 2004) and *barren inflorescence2* (*bif2*; McSteen *et al*.,

2007) in maize (Zea mays) and *monoculm1* (*moc1*; Li *et al*., 2003) in rice resulted in the inhibition of bud formation due to defects in axillary meristem initiation. By contrast, axillary bud outgrowth is regulated by genes, phytohormones, environmental factors, and their interactions. Mutants such as *Teosinte branched1* (*Tb1*; Doebley *et al*., 2006) and *Grassy tillers1* (*gt1*; Whipple *et al*., 2011) in maize; and *Teosinte Branched1* (*OsTB1*; Takeda *et al*., 2003), *Ideal Plant Architecture1* (*Ipa1*; Jiao *et al*., 2010), *Dwarf27* (D27; Lin *et al*., 2009), *D14/HTD2* (Arite *et al*., 2009), and *D53* (Jiang *et al*., 2013) in rice are proved to inhibit the tiller bud's outgrowth.

Thanks to extensive research in dicot species, mainly in *Arabidopsis*, a very complex network of molecular factors that either affect cell division and/or elongation is already known. In contrast, although research has grown strongly in the last few years on monocot species, we still lack such a complex picture. Although monocot and dicot species are known to be genetically distant, several molecular aspects have been shown to be conserved between them. Nelissen *et al.*, 2016 in their review summarized conserved genetic and molecular mechanisms controlling leaf growth in dicots and monocots, based on research in rice, maize and *Arabidopsis.* By contrast, only few barley leaf mutants were well characterized. Regardless of the pleiotropic phenotypes in leaf and shoot architecture traits that often characterize individual mutants, which complicates the classification of barley mutants according to their leaf size, mutants still can be categorized as having narrow (e.g., *angustifolium*, *fol*), wide (e.g., *broad leaf1*, *blf1*), long (e.g., *curly3*, *cur3*) or short leaves (e.g., *curly dwarf1*, *cud1*) (Shaaf *et al.*, 2019).

1.3 *BLF1* gene controls leaf width in barley by limiting cell proliferation

Among all available barley leaf-size mutants, only three have been functionally characterized and the molecular mechanisms underlying the altered leaf shapes have been identified: the high-tillering mutant (*Hvhnt1*) with narrower leaves and shorter plants compared to the wild-type, the recessive *narrow leafed dwarf1* (*nld1*) mutants characterized by reduced plant height, narrower leaf blade, but similar blade length compared to wild type (Yoshikawa *et al.*, 2016), and the *broad leaf1* (*blf1*) mutants, with an opposite phenotype to *nld1*, with wider but slightly shorter leaf blades compared to the wild type. The following paragraphs focus on the molecular aspects underlying the *blf1* mutant phenotype.

Histological and morphological analysis of *blf1* performed by Jöst *et al.*, (2016) showed that this increase in leaf width is exclusively due to an increased number of cell files, without affecting the overall cell patterning, as the number of other cell types such as bundle sheaths and stomata increased to a similar extent as epidermal cell files. Interestingly, this increase in width was observed in all leaf blades, including the flag leaf, and in palea and lemma; but not in the leaf sheath, suggesting the existence of shared genetic mechanisms controlling medial-lateral growth between these organs and leaves. The effect on blade width starts from P6 onward and young leaf analysis showed no difference in leaf size between Bonus and *blf1*. Additionally, imaging of cleared embryo apices from mature grains confirmed that the sizes of the SAM, P1, and P2 primordia were comparable between the two genotypes. Taken together, these results indicate that *BLF1* functions to limit cell proliferation in the medial-lateral axis,

during primordia outgrowth, without affecting the initial recruitment of founder cells as *NS1/2* do (Jöst *et al.*, 2016, Shaaf *et al.*, 2019).

Positional cloning, analysis of independent alleles, and transgenic complementation confirm that *BLF1* encodes a presumed transcriptional regulator of the INDETERMINATE DOMAIN family. In contrast to loss-of-function mutants, moderate overexpression of *BLF1* decreases leaf width below wild-type levels. A functional BLF1-vYFP fusion protein expressed from the endogenous promoter shows a dynamic expression pattern in the shoot apical meristem and young leaf primordia. Hence, this suggested that the *BLF1* gene regulates barley leaf size by restricting cell proliferation in the leaf-width direction (Jöst *et al.*, 2016).

1.4 IDD domain family proteins control plant growth in *Arabidopsis* by regulating auxin homeostasis and by fine-tuning GA signalling

The predicted BLF1 protein is a member of the *INDETERMINATE DOMAIN (IDD)* family encoding a putative nuclear protein with four zinc finger domains and a coiled-coil domain. Many IDD genes have been functionally characterized and were shown to be involved in various biological functions, including leaf polarity, seed maturation and germination, flowering, root development, shoot gravitropism, sugar metabolism, cold-stress signalling, GA signalling, auxin biosynthesis and transport, and ammonium uptake (reviewed in Kumar *et al.*,2019). IDDs are known to form extensive interaction networks to ensure precise transcriptional control and thereby cell-fate specification and hormonal signalling. Phylogenetic analysis indicated that BLF1 has three orthologs in *A. thaliana*, two in maize and one in sorghum, *Brachypodium*, rice, and wheat (Jöst *et al.*, 2016). Functional characterization of the *Arabidopsis* proteins IDD14, IDD15, and IDD16 proved their involvement in lateral organ morphogenesis and gravitropic responses by directly targeting the promoter region of *YUCCA5 (YUC5), TRYPTOPHAN AMINOTRANSFERASE of ARABIDOPSIS1* (*TAA1*), and *PIN-FORMED1* (*PIN1*) genes to induce their expression and thus to promote auxin biosynthesis and transport. Consequently, several *idd* mutants exhibit different auxin-related traits, including variations in free IAA levels and reduced auxin transport (Cui *et al.*, 2013).

A gain-of-function mutant of *Arabidopsis IDD14* presents transversally down-curled leaves and a reduced width-to-length ratio (Cui *et al.*, 2013), which is similar to the phenotype resulting from over-expressing *BLF1* in barley (Jöst *et al.*, 2016). However, in *Arabidopsis*, loss of function mutants in *IDD14*, *IDD15*, and *IDD16* do not have obvious leaf phenotype (Cui *et al.*, 2013), in contrast to the *blf1* loss of function mutant (Jöst *et al.*, 2016). This might have two different explanations: it could either be due to the different cellular mechanisms controlling leaf growth between the two species, with a well-defined basal proliferation zone for grasses in contrast to more-diffuse proliferation activity without clear cell files in *A. thaliana* leaves, or simply to the different leaf morphology between monocots and dicots. Expression pattern analysis showed that *BLF1* and the three *IDD* genes are expressed in the prospective veins, which further support the hypothesis that *BLF1* may similarly influence auxin transport.

Gibberellin (GA) is another essential plant hormone that has a crucial role in plant development, from embryogenesis to senescence. DELLA proteins, members of the GRAS domain transcription factor family, act as key negative regulator of GA signalling. Although disposing of a strong transcriptional activity, DELLA proteins lack a DNA binding domain, and act as transcriptional coregulators with other DNA-binding factors (Yoshida *et al.,* 2014).

Notably, five IDD members, AtIDD3, AtIDD4, AtIDD5, AtIDD9, and AtIDD10/JACKDAW (JKD), interact with DELLA and the GA-positive regulator *SCARECROW-LIKE3* (*SCL3*) to fine-tune GA signalling (Yoshida *et al.,* 2014; reviewed in Kumar *et al.,*2019). JKD, known also as a member of IDD family protein, binds to two GRAS family transcriptional regulators SHORT-ROOT (SHR) and SCARECROW (SCR), to inhibit ectopic periclinal divisions in the outer cortex layer of the root. Hence, the ground tissue with three layers observed in the *jkd* mutants is due to ectopic divisions resulting from a reorientation of the cell-division plane oppositely to the root-length direction (Welch *et al.,* 2007; Ogasawara *et al.,* 2011). Taken together, these results lead to the hypothesis that BLF1 as an IDD family protein may also interacts with the unique barley DELLA protein SLENDER1 (SLN1) in barley (Chandler *et al.,* 2002) to regulate GA response.

1.5 RING E3 ligases play a key role in organ development and in abiotic stress responses in plants

As sessile organisms, plants have to adapt to variable environmental changes by perceiving and transmitting internal and external signals, and during these processes, post-translational protein modifications are frequently employed (Callis, 2014). In fact, modifications, such as protein methylation, acetylation, phosphorylation and ubiquitination, have been shown to play a crucial role in plant development and plant–environment interactions (Wilson *et al*., 2016).

The ubiquitin proteasome system (UPS) in particular plays a central role in regulating cell homeostasis and function and coordinates plant growth (e.g. hormonal responses, seed dormancy and germination, root growth, floral development and cell cycle progression) and biotic and abiotic stress responses (e.g. drought and high salinity), by regulating the abundance, activities or subcellular localizations of proteins in eukaryotic cells (Ingvardsen and Veierskov, 2001; Kurepa and Smalle, 2008).

The UPS is a serial cascade process of protein ubiquitination and degradation. Substrate proteins destined for degradation are tagged with poly-ubiquitin chains made up of 76 amino acid ubiquitin protein and then hydrolyzed by the 26S proteasome. Substrate ubiquitination involves three steps catalyzed by three different enzymes or enzyme complexes: ubiquitin-activating enzyme (E1), ubiquitin-conjugating enzyme (E2), and ubiquitin protein ligase (E3) (Liu *et al*., 2021). The first step of the ubiquitylation process consists in the activation of ubiquitin by E1, in an ATP-dependent manner, by creating a thioester bond between the C-terminus of ubiquitin and a cysteine residue of E1. In a second step, the thioester-linked ubiquitin is transferred onto a cysteine residue of E2 (Haas *et al*., 1982). In the third step, the ubiquitin from E2 is transferred to a lysine, cysteine, serine or threonine residue of a substrate protein via E3 (Ishikura *et al*., 2010, Shimizu *et al*., 2010, Chen *et al*., 2016). Hence, in the past

several decades research has focused on studying the molecular function of different types of E3 ligases as they play key roles in determining substrate specificity in a temporally and spatially regulated manner by recruiting specific targets to ubiquitylated E2 (Vierstra, 2009).

E3 ligases are divided into two main groups. The first group includes E3s that act as a single subunit such as the RING (Really Interesting New Gene) (RING)/U-box and HECT (Homology to E6-AP Carboxyl Terminus) E3s (Dreher and Callis, 2007; Vierstra, 2009). E3s among the second group act as multi-subunit Ub ligases, such as Cullin-RING box1- Ligases (CRLs), which are further divided in four subfamilies: SCF (S-phase kinase-associated protein 1–Cullin 1–F-box), BTB (Bric-a-brac–Tramtrack–Broad complex), DDB (DNA Damage-Binding domain-containing) and APC (anaphase-promoting complex) (Vierstra, 2009; Park *et al*., 2011; Sadanandom *et al*., 2012)

RING-type E3s are considered as the largest family of E3s, which bind both a ubiquitin-like proteins (UBLs)-loaded E2 and a protein substrate targeted for UBL transfer (Metzger *et al*., 2014). More than 477 genes encoding putative RING E3 Ub ligases have been identified in *Arabidopsis*; which makes them the third largest gene family in *Arabidopsis* and the most abundant single subunit-type Ub ligases (Kraft *et al*., 2005; Stone *et al*., 2005; Vierstra, 2009). This diversity of RING E3s is clear evidence for their important role in the sessile life cycle of plants (Vierstra, 2009). Several RING-type E3 ligases are also involved in determining seed size through regulating gametogenesis and cell cycle processes. In *Arabidopsis*, DA2 act synergistically with the ubiquitin receptor DA1 to negatively regulate seed size by decreasing cell proliferation in developing seeds and by interacting synergistically with DA1, a ubiquitin receptor known also as a key regulator in seed size control (Xia *et al*., 2013, Li and Li 2016). OsGW2, the ortholog of DA2 in rice, negatively affects grain size and final yield through mediating cell division (Song *et al*., 2007). Similarly, the orthologs of OsGW2 in maize (Zea mays), ZmGW2-CHR4 and ZmGW2-CHR5, also act in the control of kernel size and weight (Li *et al*., 2010). These studies further confirm that RING E3 Ub ligases can positively or negatively regulate organ growth mechanisms in both monocot and dicot model plants.

Given the enormous variability in the RING-E3 targets, regulation of substrate recognition and ubiquitylation undergoes also diverse mechanisms. One RING-type E3 can target multiple substrates and several E3s can have the same substrate (Metzger *et al*., 2014). Binding of substrates by RING E3s may occur directly or indirectly. In fact, RING-type E3 do exist in different structural contexts, as single chain enzymes, or as homodimers such as RNF4, BIRC7 and the U-box proteins CHIP and Prp19, or as heterodimers such as BRCA1-BARD1 and RING1B-Bmi1 (Joukov *et al*., 2001; Brzovic *et al*., 2001; Cao *et al*., 2005).

Additionally, RING-type E3s can also exist in multi-subunit assemblies. One of the well characterized examples for this is the Cullin RING Ligase (CRL) superfamily (Petroski *et al*., 2005). A CRL subfamily complex consists of a cullin protein (Cul-1, 2, 3, 4a, 4b, 5, or 7), a small RING protein (in most cases Rbx1/Roc1/Hrt1), and either an adaptor protein that binds the substrate recognition elements or, in some cases such as CRL3, it binds both to the cullin protein (Cul-3) as well as the substrate (Sarikas *et al*., 2011), which explains the large plasticity in substrate specificity for the CRL subfamily.

All these aspects make it a significantly hard task to identify E3 ligase substrates. Characterization of some E3 ligases led to the identification of conserved targeting sequences in substrates which allow the prediction of putative substrates. Examples for this, are the Nedd4 E3 ligase containing three or four WW domains which bind proline-rich domains in target proteins (Chen *et al*., 1995; Kanelis *et al*., 2001; Sarikas *et al*., 2011).

Post-translational modifications play also a significant role in ligase–substrate recognition. For example, binding of UBR5 E3 ligase to phosphoenolpyruvate carboxykinase to ensure its ubiquitylation and degradation is mediated via acetylation-dependent recognition under high glucose conditions (Jiang *et al.*, 2011).

Additionally, many factors represent significant technical challenges in ligase–substrate recognition. (1) The dynamic nature of protein ubiquitylation: Ubiquitylation is tightly controlled by E3 ligases and DUBs acting in a co-ordinated manner to add or remove ubiquitin chains in response to changing cellular environments (Komander *et al*., 2009). (2) The weak physical interaction and rapid dissociation rate between some E3–substrate complexes: Once the substrate binds to E3 ligase, ubiquitylation occurs at a very short time and the complex dissociates. So, the substrate can only be enriched by E3 ligase in the presence of a proteasome inhibitor (Pierce *et al*., 2009). (3) The low cellular abundance of substrates may also be a delimiting factor (Yoshida *et al*., 2009). (4) The relatively slow, low-throughput biochemical methods: The dynamic equilibrium between E3 ligase and substrate requires more sensitive techniques and is partly addressed by 'trapping' approaches. Ubiquitin ligase trapping and proximity labelling can detect transient, low-affinity E3–substrate interactions and low-abundance substrates (Mark *et al*., 2014). (5) Functional redundancy and multiplicity: A single substrate may be targeted by multiple E3 ligases at different sites, and similarly a single E3 ligase may target multiple substrates under different conditions or in different cellular compartments. This partly explains the huge diversity in spatial and temporal control of ubiquitylation (reviewed by Jain and Barton, 2009). In this context, cellular localisation is an important consideration, as substrate–ligase complexes identified by biochemical methods may not be expressed or interact in the same sub-cellular compartment. (6) Rapid degradation of ubiquitylated proteins: Without the use of proteasome inhibitors, it can be difficult to identify ubiquitylated proteins destined for degradation by the proteasome, and the use of such inhibitors may cause additional confounding biological effects (Harper *et al*., 2012).

The relative insensitivity of many methods to post-translational modifications of substrates, E3 ligases or ubiquitin may be considered as a complicating factor in E3 ligase substrate identification, as they have the potential to alter activity and substrate binding (Kim *et al*., 2011; Swatek and Komander, 2016). The recently developped systematic approaches to identify E3 ligase substrates, such as yeast-two-hybrid assay, global proteome analysis, protein array, global protein stability profiling, luminescent *in vitro* ubiquitylation assay and high-throughput quantitative microscopy, are providing a potent mechanistic insight into ubiquitin signalling. Additionally, combination of genetic models (i.e. modulating E3 ligase expression or activity) with powerful functional genomics or proteomics have rapidly expanded our understanding of diversity of the ubiquitin-modified proteome (ubiquitome) in various contexts (Komander, 2009; Sylvestersen *et al*., 2013 and Ordureau *et al*., 2015)

Differences in the catalytic domains of HECT, RING and RBR classes of E3 ligases also present additional challenges in the variable methods used for the identification of substrates, as they include different mechanisms of Ub binding and transfer, variations in regulatory mechanisms and the requirement of accessory/adaptor proteins (Iconomou and Saunders, 2016). Unfortunately, comparison of the relative performance of each method against different E3 classes is not available yet, which makes it difficult to draw definitive conclusions. While interacting proteins of E3 ligases represent potential substrates, further validation by orthogonal methods is necessary to attribute status as *bona fide* substrates.

In Barley, *BLF1* gene is proved to have an overall very low expression level in the shoot meristem and growing leaves. *BLF1* overexpression decreases leaf width below wt level, but it also inhibits seed formation leading to plant sterility (Jöst *et al.*, 2016). Consequently, the observed low expression level indicates that the BLF1 protein is regulated in a dosage-dependent manner to maintain cell homeostasis and normal plant development. These results suggest that the BLF1 protein may be regulated through ubiquitylation and proteasomal degradation to maintain an overall low protein content.

1.6 Using natural variation in grasses to identify organ growth regulators

Despite the well-established studies in understanding the genetics of organ growth in cereals, advanced genetic studies to explore its natural variation are still missing. For that, Schnurbusch *et al.* (2018) aimed to offer a better understanding of the natural genetic variation of leaf blade area (LA) in barley, by using 215 worldwide spring barleys. The accessions included 92 accessions with the high photoperiod-sensitivity *PHOTOPERIOD RESPONSE LOCUS 1* (*Ppd-H1*) allele and 123 accessions with reduced photoperiod sensitivity (*ppd-H1*). Measurements of LA showed that *Ppd-H1*-carrying accessions are smaller than *ppd-H1*-carrying ones. GWAS analysis revealed that the accessions carrying the *ppd-H1* allele had more genetic variation in LA than the Ppd-H1 carrying ones. Additionally, several major QTLs affecting LA variation were found close to plant heading time, phytohormone- and sugar-related genes. These results proved that natural variation of LA could be of great interest for improving plant environment interactions, canopy architecture and crop yield of cereals.

Another study performed by Buescher *et al*. (2014) aimed to identify the genetic network controlling the expressivity of the semi dominant *Liguleless narrow* (*Lgn-R*) mutant allele identified in maize and known to affect to affect ligule and auricle development and to result in a narrow leaf phenotype. To map the *Lgn-R* modifiers, *Lgn-R* positive mutants introgressed in a B73 background were crossed to B73 x Mo17 (IBM; Lee *et al.* 2002) recombinant inbred lines (RILS) and the *Lgn-R* mutants from the F1 generation were used to measure their leaf length and width. The data processing and quantitative trait locus (QTL) mapping allowed identifying a major QTL on chromosome 1 (sympathy for the ligule; sol) from the Mo17-background that suppresses the *Lgn-R* mutant phenotypes. Additionally, this QTL has been shown to genetically interact with a locus on chromosome 7 corresponding to the *lucifer* (*lcf*) allele from the B73-background to increase the ability of the *solMo17* allele to suppress *Lgn-R*.

Using natural modifiers to identify genes controlling leaf traits has been well studied in rice but not in temperate cereals. Hence, investigating the natural variation in leaf size and shape existing in diverse barley collections could be of great interest to identify candidate genes associated with leaf shape and positioning and to understand the genetic architecture of these agronomic traits.

1.7 Aim of this study

Leaves of cereal crops convert solar energy into the bulk of calories consumed by humans. However, the genetic and molecular mechanisms governing growth of cereal leaves to their final sizes and shapes remain poorly understood. A previous characterisation of the *BLF1* gene proved its involvement in leaf width control by limiting cell proliferation in width direction during primordia outgrowth (Jöst *et al.,* 2016). BLF1 protein has been described as a member of the IDD family of putative transcriptional regulators. An emerging model for the function of IDD proteins is that they provide a DNA-binding platform for transcriptional regulators of the GRAS family, including the DELLA repressors of gibberellic-acid (GA) signalling. Based on this previous work, this project particularly focuses on studying the molecular function of the *BLF1* gene. To this end, I have pursued the following objectives: (1) test the hypothesis that BLF1 modulates gibberellin signalling in the growth zone of barley leaves by investigating genetic and physical interactions with the barley DELLA protein SLENDER1 (SLN1) and characterizing the growth phenotype in more detail; (2) identify BLF1 interacting proteins and downstream targets in an unbiased way by exploiting the availability of a functional BLF1-YFP line; 3) isolate genetic modifiers of the *blf1* mutant phenotype from natural and induced variation in barley as a means to find interacting regulators of cereal leaf growth.

2. MATERIAL AND METHODS

2.1 Plant materials

The original *blf1-l* (herein called *blf1*) mutant line is available as stock GSHOI 393 from the National Genetic Resources Program Germplasm Resources Information Network (NGRP/GRIN) at http://www.ars-grin.gov/. The *BW58* mutant line was obtained by introgression of *blf1-l* into Bowman. The *Sln1d* mutant lines were kindly provided by Peter Michael Chandler (CSIRO Plant Industry, Australia). The *ring-e3_1* and *ring-e3_2*, *blf1_a* CRISP/Cas9 mutant lines were generated by the group of Prof. Goetz Hensel and Dr. Jochen Kumlehn at the IPK Gatersleben. They used a construct with three sgRNAs, two against *BLF1* (TTCGGGTCGTCGTTGCAGAT-exon1, ACTTCCGGCGC-AAGCACAG-exon2), one against the *RING/U-BOX* gene (GTCCAGATCCGAGCACGAGG-exon1). F2 populations from crosses of the *blf1-1* mutant to 20 genetically diverse barley landraces from the IPK Gatersleben germplasm collection, were obtained from previous work.

2.2 Seed sterilization

- **Barley**

Sodium hypochlorite solution (12% NaCl, Roth, Karlsruhe) was diluted to 6% with H2O and added to uncoated seeds in a 50 mL Falcon tube. The seeds were incubated for 2 min under

agitation. Sodium hypochlorite solution was then completely removed and seeds were washed 2-3 times with H2O. 70% EtOH was added to the seeds and incubated for 5 min under agitation. EtOH solution was then completely removed and seeds were washed 2-3 times with H2O.

- ***Arabidopsis***

30 mL of 70% EtOHtech was added to sieved seeds in a 50 mL Falcon tube. EtOH was then completely removed with Pasteur pipet. Seeds were then incubated in 30 mL of the sodium hypochlorite solution (the same as for barley) for 5 min. The solution was then completely removed and seeds were washed 2-3 times with 100% EtOH. EtOH was completely removed, and seeds were dried in vacuum (may be heated to 50°C). For small amounts of seeds: Eppendorf tubes were used, and the volumes were adjusted appropriately.

2.3 Seed germination

- **Barley**

After sowing on wet filter paper, seeds were stratified in the dark at 4°C for 2-3 d depending on the age of the seeds. Seeds are then incubated at room temperature in the dark for 2-3 days. Germinated seeds are then planted in soil. In the analyses, the day of potting is referred to as day zero.

- ***Arabidopsis***

Sterilized *Arabidopsis* seeds were plated on MS solid media and stratified in the dark at 4°C for 2-3 d. Plates were then placed in growth chambers.

2.4 Growth conditions

Barley plants for detailed phenotypic analysis were grown in the glasshouse or a growth chamber under long day conditions (16 hours light and 8 hours dark), 80% relative humidity and at a constant temperature of 22°C. Barley plants for simple DNA or RNA extractions and *Arabidopsis* plants were grown in growth chambers under the same growth conditions.

2.5 Genomic DNA extraction

All the buffers and solutions required for this experiment were prepared as described by Bartlett *et al.* (2017).

<u>Sample preparation</u>

- For genotyping purpose

DNA was extracted from a piece of 1.5-inch leaf segment at a seedling stage. The harvested plant tissues were placed in a 2.2 mL 96 deep-well plate and frozen overnight at -70°C. Plates were then transferred to a freeze-dryer to dry samples overnight. One ball bearing was added into each well and samples were grinded using Spex GenoGrinder for 5 min at 25 r/s to a fine powder.

- For DAP-seq library preparation

DNA was extracted from stem and leaves of 3–4-day old barley seedlings. The harvested plant tissues were placed in 1.5 mL collection tubes with ~200 µL glass beads (2mm) and frozen in liquid nitrogen. Tubes were shaken on a paint shaker for 10-15 min to grind the tissues to a fine powder.

Extraction

The extraction buffer (0.1M Tris-HCl pH 7.5, 0.05 EDTA pH 8.0, 1.25% SDS) was preheated to 65°C and 500 µL was added to each sample. The plate/tube was sealed with caps, shaked thoroughly and incubated at 65°C for 30 min. Next, the plate/tube was cooled down to room temperature by placing them in the fridge for about 15 min. 250 µL of 6M ammonium acetate, which was stored at 4°C, was added to each sample. The mixture was shaken vigorously and incubated for 15 min in the fridge. The plate/tube was centrifuged for 20 min at 4,000 rpm and 4°C in a Beckman centrifuge (in an Eppendorf centrifuge for 1,5 mL tubes) to collect the precipitated proteins and plant tissue. 600 µL of the aqueous phase was transferred into a new 96 deep-well plate/1,5 mL tube containing 360 µL of isopropanol in each well. The solution was mixed thoroughly and incubated for 5 min at room temperature to allow the DNA to precipitate. Samples were centrifuged for 20 min at 4,000 rpm and 4°C in order to pellet the DNA. 500 µL of 70% ethanol was added to each sample (wash step) and the plate/tube was centrifuged for 20 min at 4,000 rpm and the supernatant was discarded again. The pellet was dried at room temperature then resuspended in 200 µL of ddH2O. The DNA was dissolved overnight at 4°C in the fridge. The un-dissolved cellular debris were collected by centrifugation of the plate/tube for 20 min at 4,000 rpm. 150-200 µL of the DNA supernatant was transferred into a 96-well PCR plate/1,5 mL tube. The DNA concentration of random samples was estimated using Nanodrop (50-150 ng/µL).

2.6 Phenotypic analysis

For leaf widh, length, and overall blade area measurements, with the help of Christian Kappel, leaves were segmented from digital images using Matlab. Size parameters were extracted from the binary images.

2.7 CRISPR/Cas9 related work

2.7.1 PCR and Sequencing of T0 Target Loci

Primers producing amplicons covering genomic target loci were designed (Appendix A) and tested/optimized using wildtype DNA extracted to achieve specific clean amplification. Following PCR cycling, 5 µL of each reaction was run in an agarose gel made with an appropriate percentage of agarose relative to the expected band sizes. Large deletions resulting from targeted mutagenesis may be visible by a band shift to a lower position relative to a wild-type control. The remaining 15 µL of PCR was purified using the Sera-Mag™ Select beads (Merck, GE29343052). Purification was made according to the manufacturer´s instructions. Purified PCR products are used for Sanger sequencing over target loci on both strands by setting up reactions containing the following: 20 ng PCR product +10 µM Primer, adjusted to

a final volume of 14 µl. Completed reactions were sent to LGC sequencing company. Indels at target loci may be visible as double peaks starting from or near to the expected Cas9 cut cite. T0 lines where mutagenesis has been detected were grown to seed and examined again in T1 for mutation inheritance.

2.7.2 Identification of Transgene-Free Mutant Lines

Seeds from the 5 selected T0 active lines were germinated and 20 T1 plants per T0 active line were generated. After around 1 week the plants were well established and leaf material was sampled and used for DNA extraction. The DNA is used for PCR/sequencing, as described above, with the aim of identifying indels or larger deletions. This time due to chromosome segregation there is a much higher likelihood of identifying homozygous mutants. To test for the presence or absence of the T-DNA, we conducted a PCR with a Forward primer targeting the promoter (Ubi), and a Reverse primer targeting the Cas9 sequence: F_ TTTAGCCCTGCCTTCATACG, R_ TTAATCATGTGGGCCAGAGC. Following cycling, 5 µL of each reaction was run in 2% agarose gel. Where the T-DNA is present, a single band of 700 bp was amplified, and where it is not, it indicates T1 lines that are transgene free. A no template negative control was included as well as a positive control of a genomic DNA sample known to contain the T-DNA. In parallel, the 100 T1 plants were amplified with primers covering the target loci, and the purified PCR products from all the 100 T1 plants were sequenced. Samples that contain no T-DNA but have been observed to contain targeted mutations are classified as transgene-free mutants as the mutations must have been inherited and are not merely somatic mutations, because Cas9 is no longer present. As only heterozygous or biallelic mutant lines have been identified, it was necessary to go into T2 via another round of selfing to produce homozygous mutants that are transgene free. To genotype T2 plants, Indel and dCAPs primers specific to each mutant allele were designed (Appendix A). T2 plants were grown under controlled green-house conditions (see above) and leaf 3 and leaf 4 were collected from each plant and used to measure their maximum-width, length and average blade area.

2.8 Gateway cloning

The Gateway BP clonase II and LR clonase II Enzyme Mix by Invitrogen were used for Gateway cloning. pDONR221 from Invitrogen was used as an entry clone. The full-length cDNA from each cloned gene was amplified with the appropriate Gateway adapted primers (Appendix A). The reaction mixture for each enzyme was prepared according to the manufacturer´s instructions. For the yeast two-hybrid (Y2H) assay, entry clones were recombined into pDEST22 and pDEST32 destination vectors (N-terminal fusions to Activation domain [AD] and DNA-Binding domain [BD] of the *S. cerevisiae* transcriptional activator Gal4, respectively) (Dreze *et al.*, 2010). For ratiometric bimolecular fluorescent complementation (rBiFC) assay in *N. benthamiana* plants, entry clones were recombined into pBiFCt-2-in-1-NN destination vector (N-terminal fusions of the N- and C- terminated parts of yellow fluorescence protein [YFP], respectively) (Hecker *et al.*, 2015). For Förster resonance energy transfer (FRET) assay in *N. benthamiana* plants, entry clones were recombined into pFRETgc-2-in-1-NN destination vector (N-terminal fusions of the mCherry- and mEGFP-fluorescent tags, respectively) (Mehlhorn et al., 2018). For DNA Affinity Purification

sequencing (DAP-seq) assay, entry clones were recombined into pIX-Halo destination vector (Bartlett *et al*., 2017). Sanger sequencing was used to validate in-frame cloning and the sequence integrity of all constructs using appropriate primers (Appendix A).

2.9 Yeast work

2.9.1 Yeast strains and vectors

MaV103 (Mat a) and MaV203 (Mat α) strains were kindly provided by Mathieu Waroquier (Université de Namur, Belgium). These strains originate from crosses of PCY2 and MaV99 which are described in more detail in Chevray and Nathans (1992). They contain the three *GAL4*-inducible reporter genes *LacZ, HIS3* and *URA1*. Their activity can be assayed colorimetrically and via growth on plates lacking histidine and uracil, respectively. Haploid strains of *S. cerevisiae* were transformed with CDS-containing pAD and pBD (pDEST22 and pDEST32, respectively) plasmids. The plasmids pDEST22 and pDEST32 are used for the assembly of bait and prey fusion proteins. They contain the genes *TRP1* and *LEU2*, respectively, as selectable markers. These confer the ability to grow on media lacking Tryptophan and Leucine. cDNA library generated from young barley inflorescences and cloned in pDEST22 with an average size of 1kb/insert was kindly provided by Prof. Sarah McKim (University of Dundee, Scotland). The library was transformed in MaV103 strain and mated with MaV203 strain pre-transformed with pDEST32-BLF1.

2.9.2 Quick and easy yeast transformation

This protocol was adapted from Gietz and Woods (2002). Generally, this protocol can be used with a liquid culture or cells grown on a plate as starting material (liquid method proved to be more efficient). First, 5 mL of liquid medium were inoculated and grown shaking overnight at 30°C. 2 mL of culture was harvested on the next day and harvested for 5 min at 5.000 x g. The following components were added to the pellet.

Table 1: Reaction components for the transformation mix used

COMPONENT	VOLUME/µL
PEG 3350 50% (w/v)	240
1M Lithium Acetate	36
ssDNA (10 mg/mL)	10
Plasmid DNA (min. 1 µg) plus water	74
ddH2O	Until 360

After thorough resuspension, the cells were incubated in a water bath at 42°C for 40 min. Afterwards, the cells were harvested and the supernatant removed. The pellet was resuspended in 1 mL ddH2O and 100 µL were spread on selective plates. Cells were grown for 2- 4 days at 30°C.

2.9.3 Library scale transformation

Preparation of ss carrier DNA: high molecular weight salmon testis DNA (Sigma, Taufkirchen, #D1626) was dissolved in sterile TE to a final concentration of 2 mg/mL (takes several h). The DNA was aliquoted and stored at -20°C. Prior to use, an aliquot is boiled for 5 min and quickly cooled in ice.

5 mL YPDA was inoculated and incubated with shaking overnight at 30°C. The overnight culture was counted (see below) and 50 mL was inoculated in warm YPDA to OD600 = 0.217 (5× 10^6 cells/ ml). The culture was grown to an OD600 = 0.87 (1,1 x 10^8) (30°C, 180 rpm). Cells were harvested for 5 min at 1.500 x g, then washed with 25 mL sterile H2O dd. The pellet was resuspended in 1 mL 1× LiAc (0.1 M Lithium acetate), then harvested again at 1.500 x g for 15 s. The pellet was resuspended in 0.5 mL in 1× LiAc. 50 µL cell suspension was aliquoted for each transformation in an Eppendorf tube. The cell suspension was harvested at 1.500 x g for 15 s.

The transformation mix (see library scale protocol) and DNA (1 µg) was added to the cell pellet. The cells were resuspended and mixed well by vortexing. The mixture was incubated for 30 min at 30°C (without shaking), then heat shocked for 17.5 min at 42°C. The cells were harvested and resuspended in appropriate amount of H2O dd. (1 µg of library plasmid was resuspended in 3 mL and plated on 9 large plates (12 cm × 12 cm)). Cells were plated on selective plates and incubate at 30°C for 2-5 days or until colonies are visible.

For the library transformation, the transformation efficiency was determined (1.62×10^4 cfu/µg of plasmid DNA), and the transformed cells were transferred into frozen stocks as follows: 2 mL TE were added to a large plate (12 cm × 12 cm) and cells were resuspended with a spreader. Cells were then transferred to a centrifuge tube. The wash step was repeated once. Cells were then harvested for 5 min at 1.500 x g. The cell pellet was washed twice with at least one pellet volume of H2O dd and resuspended in one pellet volume of glycerol solution (65% (w/v) glycerol, 0.1 M MgSO4, 25 mM Tris/ HCl, pH 8.0). The suspension was aliquoted in a 50 µl single use aliquots and stored at -70°C.

2.9.4 Cell number determination

0.1% (w/v) Trypan Blue solution was mixed in a 1:1 ratio with a 1:10 dilution of the cell culture. After 1 min of incubation time, the cells were counted under a microscope. Dead cells appeared blue.10 µL of this dilution was delivered onto a counting chamber and the number of cells was counted in four successive squares from the 16 large grid squares of the chamber using a 10x objective lens. The counted number was then multiplied by 4 (total number of grid squares), by 10,000 (the inverse of the volume of the whole central square) and by 0,1 (the dilution factor) to obtain the titer in the diluted suspension.

Number of cells / mL= Σ counted cells x 4 x 0,1 x 10,000

2.9.5 Small scale mating on plates

This protocol is used to mate two different yeast strains easily but with rather low efficiency. A small amount of cells was scraped off a selecting plate and streaked in a small circle on a YPDA plate. This was done for the other strain, too and the cells were mixed carefully. Plates were incubated overnight at 30°C, all cells scraped off the circle and resuspended in 500 µL of sterile water. 100 µL was streaked on plates selecting for diploids (SD/-LT).

2.9.6 Medium efficiency mating

5 mL of single drop-out liquid culture were inoculated with each of the yeast strains and grown shaking overnight at 30°C. 2 mL of each culture was harvested and resuspended in 200 µL of sterile water. The different mating type cells were mixed via pipetting and filled up to 1 mL with sterile water. 100 µL of cells were plated on YPDA over night at 30°C and mated cells were transferred on SD/-LT plates selecting for diploids.

2.9.7 Library scale mating

This protocol is used to mate cells containing the bait construct with cells carrying the prey library. 5 mL of selective medium were inoculated with about 3 colonies of the MaV203 strain pretransformed with pDEST32-BLF1, and grown shaking over night at 30°C. Cells were counted on the next day and 2.5 x 10^8 cells added to 50 mL of selective medium. Cultures were grown shaking at 30°C for 3 to 5 hours till the cell titer reached at least 2 x 10^7 cells/mL. Cells were then harvested and centrifuged for 5 min at 1.500 x g. The pellet was resuspended to 1 x 10^9 cells/mL and 200 µL (~ 2 x 10^8 cfu) of the bait strain was mixed with 160 µL (~ 1 x 10^8 cfu) of the MaV103 strain pretransformed with the library. Cells were harvested, resuspended in 120 µL YPDA medium and plated on YPDA plates which were incubated overnight at 30°C. The cell lawn was washed off the plate with SD/-LT medium and the cell suspension was filled up to 100 mL. The cultures were incubated shaking for 6 hours at 30°C, pelleted and washed with 30 mL sterile water. Cells were resuspended in 40 mL water and 450 µL each were plated on ~60 large plates selecting for diploids and interaction (SD/-LTH + 3-AT). To test the mating efficiency, 100 µL of 10^{-4} to 10^{-6} dilutions were plated on SD/-L, SD/-T and SD/-LT plates and all were incubated for 3-5 days at 30°C. The following table presents the calculation of the library screening mating efficiency.

Table 2: Calculation of the library screening mating efficiency

Mating strain (plasmid)	Selective media	Selects for	Dilution	No. of cfu/ml	Viability in cfu/ml	Mating efficiency (% Diploids)
MaV103 (pDEST22-library) + MaV203 (pDEST32-BLF1)	-Trp	pDEST22-library (Bait)	1:10,000	100	1×10^7	= 5%
	-Leu	pDEST32-BLF1 (Prey)	1:10,000	5,000	5×10^8	
	-Leu/-Trp	Diploids (pDEST22-library) + (pDEST32-blf1)	1:1000	50	5×10^5	

$$\frac{\text{No. of cfu/ml of diploids} \times 100}{\text{No. of cfu/ml of limiting partner}} = \% \text{ Diploids}$$

(The strain (Bait or Prey) with the lower viability is the "limiting partner")

2.9.8 Identification of interactors via colony-PCR and test digest

To identify putative interactors after successful library scale mating and selection on SD/-LTH + 3-AT media, a colony PCR and subsequent test digest was done. A minimum amount of cells was picked from a SD/-LTH plate and resuspended in 40 µL of 1x MyTaq-buffer. The well plate was sealed and incubated at 96°C for 5 min. 20 µL were used for the colony PCR. Primer pairs used for PCR and expression analysis are listed in Appendix A. Next, a test digest with the enzymes AluI and HpaII (both NEB) was done and 8 µL of the PCR product was used with water adjusted accordingly. The gels were analyzed and similar restriction patterns between colonies were searched for (Fig. 6D).

2.9.9 Filter-Lift assay

A filter-lift assay was done to check for LacZ activity in putative interactors. Plates with freshly grown yeast cells were covered with sterile filter paper and the paper was pressed lightly against the agar. Afterwards, the paper was lifted off, immersed in liquid nitrogen and kept to thaw in a petri dish. Under a fume hood, the filter-lift mix was prepared and a fresh filter paper was soaked in another petri dish. The thawed filter paper was placed onto the prewet paper with the cell side up. Plates were sealed and incubated at 30°C for up to two days.

Table 3: Reaction components for the filter-lift assay

Component	Volume
20 mg/mL X-Gal in N, N- Dimethylformamide	90 µL
β-Mercaptoethanol	5 µL
Z-buffer	1.8 mL
For 1 L Z-buffer	
Na_2HPO_4 x 7 H2O NaH_2PO_4 x H2O	16.1 g
KCl	5.5 g
$MgSO_4$ x 7 H2O	0.75 g
$MgSO_4$ x 7 H2O	0.25 g

2.9.10 Plasmid isolation from yeast

Plasmid extraction was used to transform putative interactors into cells containing the bait as a control for found interactions. A colony of the mated cells which grew on -His, -Leu, -Trp and identified as a putative interactor was grown in 5 mL SD/-LT liquid medium for 24 hours with shaking at 200 rpm and 30°C. 4 mL were harvested at 1.500 x g for 15 min and resuspended in 2 mL TE-buffer. The suspension was centrifuged again at 1500 x g for 15 min and the supernatant discarded. The pellet was resuspended in 300 µL Resuspension buffer (see Table 11) and 40 µL of 0.4 U/µL Zymolase mix was added. The suspension was incubated at 37°C for 30 min and 300 µL lysis buffer (see Table 11) was added. After 5 min of incubation at room temperature, 300 µL of precooled neutralization buffer (see Table 11) was added and the lysate incubated on ice for 5 min. The suspension was centrifuged at 14000 x g for 10 min at 4°C and the supernatant carefully transferred to a new 2 mL tube. 800 µL of Chloroform: isoamyl-alcohol (24:1, v/v) was added, vortexed and centrifuged at full speed for 1 minute. The supernatant was pipetted into a new 1.5 mL tube and 500 µL isopropanol was added and incubated 10 min at room temperature. A centrifugation at 14000 x g for 30 min followed and the aqueous phase was carefully decanted. The DNA pellet was washed with 70% ethanol and again centrifuged for 10 min at full speed. Pellets were dried and dissolved in 30 µL of sterile water. The DNA concentration was estimated via gel electrophoresis.

2.10 Transient Protein expression in tobacco leaves

All the used media and reagents were prepared according to the Mehlhorn *et al.* (2018) protocol.

2.10.1 *Agrobacteria* Preparation

The different 2-in-1 vectors described above were introduced into *Agrobacterium tumefaciens* strain GV3101(pMP90) (Koncz and Schell, 1986) via electroporation and transformed cells

were selected on Luria-Bertani (LB) plates supplemented with the appropriate antibiotics (rifampicin 50 µg/mL, gentamicin 20 µg/mL, and Spect 50 mg/mL). 5 mL LB medium containing the same antibiotics was inoculated with a single positive colony and incubated overnight (28 °C, 200–230 rpm). 500 µL of the overnight culture was transferred into 4.5 mL of fresh LB medium supplied with rifampicin, gentamycin, and specific antibiotic and incubated for another 3–4 hours (28°C, 200 rpm) to an OD595 of approximately 0.2–0.8. the culture was centrifuged at 4.000 x g for 15 min at 4°C and the cell pellet was washed once or twice with 5 mL of 4°C cold water. The cell suspension was adjusted to a final OD595 of 0.8 with 4°C cold AS medium and incubated for at least 1h on ice.

2.10.2 Tobacco leaf infiltration

3–4-week-old (8th–10th leaf stage) *N. benthamiana* plants were watered 4–6 hours prior to infiltration. The *Agrobacterium* suspension was injected into the abaxial side of the third to fifth youngest leaves with a 1 mL syringe (without cannula). For this purpose, the syringe was placed between leaf-veins and the injection was supported by gentle counter pressure with a finger on the adaxial side. After infiltration, plants were covered and returned to the growth chamber. Confocal analysis was performed after approximately 36–48 hours post-infiltration.

2.10.3 Confocal Imaging

A leaf section of approximately 1 cm^2 was cutted and mounted upside down on a slide. A bit of water wad dropped on the slide and a coverslip was placed over the tissue. Our studies are done using the Zeiss LSM710 and LSM880 confocal microscopes with laser lines diode 405, pulsed 440, pulsed 470, Argon 488, 496, 514, DPSS 561, HeNe 594, and HeNe 633, respectively. The ZEN 3.6 (blue edition) software was used for Image acquisition and analysis.

- **rBiFC**

The confocal microscope was set up for YFP fluorescence with 514 nm excitation and 520–560 nm emission range and for RFP fluorescence with 561 nm excitation and 570–630 nm emission range. Sequential scanning was applied to avoid spectral overlap. A bright field channel was included for guidance from transmission of either laser line. The 40x/0.75 NA water-immersion objective was used to focus on epidermal cells. The negative control was first used to adjust the gain and-if necessary-offset to get rid of any autofluorescence and for an optimal dynamic range. The settings were adjusted to yield a mean fluorescence intensity ratio between YFP and RFP of one. Once the parameters are adjusted, 20–30 images of randomly selected areas were selected and saved for quantification.

- **FRET assay**

For mEGFP fluorescence, the confocal microscope was set up with 488 nm excitation and 490–530 nm emission range, and for mCherry fluorescence with 561 nm excitation and 565–610 nm emission range. Sequential scanning was applied to avoid spectral overlap and a bright field channel was included for guidance from transmission of either laser line. The 40x/0.75 NA water-immersion objective was used. The gain and offset settings for samples were adjusted to exploit the full dynamic range. The FRET-AB mode from the dropdown menu in the LAS X software was selected and the donor and acceptor settings were adjusted as mentioned before.

The acceptor-excitation-laser intensity in the “bleach” tab was set up to 100% and the frames between 300 and 500. An area where both proteins of interest are sufficiently expressed was selected for the bleaching procedure. Images before and after bleaching were captured automatically using the LAS X software and the FRET efficiency was calculated according to the following formula: FRETeff = (Dpost - Dpre) / (Dpost).

where Dpost is the fluorescence intensity of the Donor after acceptor photobleaching and Dpre the fluorescence intensity of the Donor before acceptor photobleaching. The FRET efficiency was considered as positive when Dpost > Dpre.

2.10.4 Image Analysis

For image analysis, the ImageJ software (freely available at http://imagej.net/ Downloads) was used. First, an RFP image was selected and the button M, or STRG-M (measure) was pressed to calculate the area, mean, and min/max fluorescence intensity. Next, the corresponding YFP image was selected and measured again. All images were analysed accordingly. The ratio between the mean fluorescence intensity values of YFP and RFP was calculated for each image and used for graphical display after including statistical analysis.

2.11 Co-immunoprecipitation

2.11.1 Generation of binary vectors

The same 2-in-1-BiFCt-NN constructs created for rBiFC assay were used for this experiment. Only the epitope tagged were modified as follows: HA-tag was replaced with Halo-tag, and Myc-tag was replaced with 3xFLAH-tag. For that, the original plasmids were linearized by PCR amplification using primers flaking the epitope-tags from both sides (see Appendix A). The Halo sequence was amplified from the pIX-Halo vector using primers that contain 25 bp-overlapping sides with the backbone sequence (see Appendix A). The 3xFLAG adapter sequence with 25 bp-overlapping sides was designed by the LGC sequencing company (see Appendix A). The vector and insert fragments were ligated using the SLiCE cloning strategy as follows:

Table 4: SLiCE reaction mix

Component	**Volume**
Linearized vector (50-200 ng)	-
Insert (1:1-1:10 molar ratio of vector:insert)	-
10X SLiCE buffer (see Table 11)	1 μL
SLiCE extract	1 μL
ddH20	to 10 μL

The SLiCE reaction mix was incubated at 37°C for 1 hour using a PCR machine or a water bath, and then place on ice. For electroporation, 1 μL of the assembly reaction was transformed into 20 μL of electrocompetent cells.

2.11.2 Nuclear protein extraction from tobacco cells

Proteins were transiently co-expressed in tobacco leaves by transfection of the binary vectors into tobacco epidermal cells via *Agrobacteria* media transformation and leaf infiltration (see above).

- **Tissue homogenisation**

The midvein was removed from leaves and 3–5 g of them were shopped into small pieces. the plant material was treated with ice-cold diethyl ether (2–3 ml/g) for 3–5 min in a glass container. Ether-drained leaves were rinsed with ice-cold Nuclei Isolation Buffer (NIB, see Table 11) (3–5 ml/g fresh weight). Plant tissues were grinded in 5–10 volumes of ice-cold NIB in 50 mL Falcon tube with a homogenizer set on its lowest speed (8,000 rpm) 3–5 times, each 5 seconds, until the tissue is completely disrupted.

- **Filtration**

The homogenates were slowly decanted through two Corning® cell strainers with 100 μm and 40 μm mesh pores, respectively.

- **Lysis of contaminating**

10% Triton X-100 was added dropwise to the solution until a final concentration of 0.5% is reached. The solution was gently agitated for 20 min at positive 4°C. The homogenate was centrifuged at 1.000 × g for 10 min. The pellet was slowly resuspended with Pasteur pipette in 10 mL of NIB. 5 mL of 2.5 M sucrose was added into a pre-cooled 50 mL Falcon tube. 5 mL of 60% Percoll solution were carefully overlayed with a Pasteur pipette to avoid mixing the sucrose and Percoll layers.

- **Isolation of nuclei using Percoll/sucrose density gradient**

The crude preparation of nuclei was carefully loaded on the top of the density gradient by drawing the extract into a Pasteur pipette and slowly releasing the solution onto the side of the tube above the 60% Percoll layer. The gradient was subjected to centrifugation in a swinging bucket rotor at 1.000 × g for 30 min at 4°C. The liquid above the gradient was removed. The 60% Percoll layer that contains most of the nuclei was carefully removed with a Pasteur pipette. The Percoll suspension containing tobacco nuclei was slowly diluted with 5 volumes of NIB and 0.5% Triton X-100 using a Pasteur pipette and incubated for 10 min under gentle shaking.

- **Purification of nuclei on 35% Percoll cushion**

The pellet of nuclei was diluted in 5 mL of NIB and the solution was overlayed on 5 mL of a 35% Percoll solution. The mixture was centrifuged at 1.000 × g for 10 min. The nuclei were washed by resuspending the pellet in 5 mL of NIB and centrifuged as previously (washing step). The nuclei were then resuspended in 500 μL of nuclei storage buffer (see Table 11), frozen in liquid N2 and stored at −70°C until use.

- **Nuclear protein extraction**

Total proteins were extracted using TRizol reagent according to the manufacturer's instructions (Invitrogen).

- **Purification of HaloTag® Fusion Proteins**

500 µl of nuclear protein extracts was added to 100 µl of pre-equilibrated Magne® HaloTag® Beads (as described by the manufacturer). The mixture was incubated for 1 hour at room temperature (22–25°C) with constant mixing to make sure that the beads remain in suspension. The mixture was then placed on a magnetic stand for 30 seconds and the supernatant was carefully removed. 150 µl of the cleavage buffer (see Table 11) was added to the beads, and incubated at room temperature for 90 min with constant mixing. The supernatant containing the cleaved proteins was carefully removed and reserved. The eluted proteins were then analyzed by Western blot.

2.12 DAP-seq related work

2.12.1 Illumina library preparation and DAP-seq

A genomic DNA library (gDNA) was prepared according to Bartlett *et al.* (2017). 5 µg of genomic DNA was diluted in EB (10 mM Tris-HCl, pH 8.5) and sonicated to 200 bp fragments in a Covaris S2 sonicator. DNA was purified using AmpureXP beads at a 2:1 bead:DNA ratio. Samples were then end repaired using the End-It kit (Lucigen) and cleaned using Qiaquick PCR purification (Qiagen) according to the manufacturer's recommendations. Purified samples were A-tailed using Klenow 3–5′exo- for 30 min at room temperature and then purified using Qiaquick PCR purification as described above. Purified samples were then ligated overnight with a truncated Illumina Y-adapter (Appendix A) as described in Bartlett *et al.* (2017). Libraries were purified by bead cleaning using a 1:1 bead:DNA ratio, eluted from the beads in 30 µl of EB and quantified with the Qubit HS fluorometric assay.

2.12.2 In vitro protein expression and DNA/protein cross linking

50 µL TNT SP6 Coupled Wheat Germ Extract System (Promega, cat. no. L4130) expression reaction was assembled in a 96-well PCR plate according to the manufacturer's specifications, using 1 µg of pIX-Halo-ORF plasmid DNA per reaction. 40 µL of expression reaction were added to 10 µL of washed Magne-Halo beads (Promega) and rotated for 1 hour end-over-end to keep the beads in solution.

Beads were then washed four times in 1X PBS (see table 11) + NP40 (0.005%) and resuspended in 100 µl of 1X PBS. One microgram of genomic DNA library was diluted to a final volume of 60 µL in 1X PBS and added to the protein bound beads. Protein bound beads and gDNA were rotated for 1 hour at room temperature. Beads were washed four times in 1X PBS + NP40, followed by two washes with 1X PBS. Beads were transferred to a new tube and DNA was recovered by resuspending in 25 µl EB and boiling for 10 min at 98 °C. Eluted samples were enriched and tagged with dual indexed multiplexing barcodes by performing 20 cycles of PCR in a 25 µL reaction as described in the following tables.

Table 5: PCR reaction mix

Component	Amount per reaction (µL)	Final concentration
Water	9.5	-
5x Phusion HF buffer	10	1x
10 mM dNTPs	2.5	500 µM
Primer A (25 µM)	1	0.5 µM
Primer B (25 µM)	1	0.5 µM
Phusion DNA Polymerase (2000 U/mL)	1	2 U

Table 6: Cycling conditions for the Phusion-PCR.

Cycle Number	Denature	Anneal	Extend
1	95°C for 2 min	---	---
2	98°C for 30 s	---	---
3-22	98°C for 15 s	60°C for 30 s	72°C for 2 min
23	---	---	72°C for 10 min

Samples were pooled and sequenced on a NExtSeq500 with 75 bp single end reads. A total of 10–30 million reads were obtained for each sample.

2.12.3 Read mapping, filtering, and peak calling

Data analysis was essentially performed as described in Bartlett *et al*. (2017). The quality of the sequence-reads was analyzed using FastQC (Andrews, 2010). Reads were mapped to the barley reference genome of the cultivar Barke (Jayakodi *et al.* 2020) with BWA-MEM (Li H. 2013). Mapped reads were filtered for unmapped and non-uniquely mapped reads using samtools. Filtered reads were used for subsequent analysis. Peak calling was peformed with GEM v3.4 (Guo *et al.*, 2012). Peaks were visualized and inspected with IGV genome browser (James *et al.*, 2011). Motif discovery was performed with MEME-CHiP (Machanick & Bailey, 2011).

2.13 *In vivo* ubiquitylation assay

2.13.1 Generation of plasmids

To created the pGEN4 plasmid, cDNAs from *HvUbc11(E2)* and *HvUba2(E1)* were PCR amplified using primers with 25 bp overlapping ends (Appendix A). The backbone sequence was amplified from the original pGEN4 plasmid. The vector and insert fragments were combined using the SliCe reaction (see above). To create the pCOG5 plasmid, cDNAs from *BLF1*, *RING/U-Box* (E3) and *PTB/POZ& MATH* (E3) were PCR amplified using primers with

25 bp overlapping ends (Appendix A). The backbone sequence was amplified from the original pCOG5 plasmid. The vector and insert fragments were Combined using the Slice ligation reaction (see above).

2.13.2 Rosetta cells co-transformation

Rosetta2™(DE3) competent cells were thawed on ice for 5 min. 1 µL from each plasmid (50 ng/ul) was added to the cells and mixed gently. the mixture was incubated in ice for 5 min, then heat shocked for 30 s at 40 °C using a water bath. The tubes were then placed on ice for 2 min. Cells were then resuspended in 250 µL of SOC media and mixed gently. The tubes were incubated at 37°C and 220 rpm. The cell suspension was then plated on LB plates containing the following antibiotics at specific concentrations: chloramphenicol (34 µg/ml.), Ampicillin (50 µg/ml) and KanR (50 µg/ml). Incubate the plates at 37°C O/N.

2.13.3 Protein expression and purification

- **Preculture**

5 mL of TB medium containing chloramphenicol (34 µg/ml.), Ampicillin (50 µg/ml) and KanR (50 µg/ml) was inoculated with a single colony of the Rosetta double transformed cells. The culture was grown overnight at 37◦C.

- **Main culture**

5 mL of the overnight culture was transfered to a new 100 mL of TB mediumpositive antibiotics and measure OD600 (=0.1). The culture was then grown to an OD600 of 0.5 to 0.7 (3 to 5 hours) at 37◦C and 220 rpm. 100 µL of 1 M IPTG was added to the culture and cells were grown again for 16-20 hours at 30°C and 200 rpm overnight. The culture was then chilled on ice. Cells were harvested by centrifugation for 10 min 5.000 x g at 4°C. The pellet was resuspended in 5 mL bacterial cell lysis buffer (see Table 11) in a ratio of 1 g cell weight / mL. The cells were sonicated in an ice bucket for 3 x 10 sec or more if the cells are not completely disrupted. 1 µL of DNase solution (1 mg/mL) was added per 1 mL of cell suspension and the solution was incubated at 4°C for 30 min. The solution was centrifuged at 20.000 x g (13,000 rpm) for 20 min at 4°C. 50 µl of the supernatant (containing the protein extract) was transferred into a fresh tube and used as an input control before purification for SDS-page analysis. 5 mL of the supernatant was added to preequilibrated beads (see below). The mixture was incubated for 1 hour at room temperature under an end-over-end agitation. The mixture was centrifuged at 500 x g for 5 min and the supernatant was collected for measuring the binding efficiency by Western blot analysis (Flow through). The Sepharose beads were resuspended in 100 µL PBS (washing step) and centrifuged at 500 x g for 5 min. The supernatant was collected in a fresh tube. The washing step was repeated twice for total of 3 washes. The beads were resuspended in 50 µL of GST elution buffer (see Table 11) and incubated for 5-10 min at room temperature with gentle agitation. The mixture was centrifuged at 500 x g for 5 min and the supernatant was collected in a fresh tube (there should be clean protein inside). The elution step is repeated twice for total of 3 washes and the eluates were analysed separately by Western blot.

- **Preparation of Glutathione-sepharose beads**

The beads were vigorously mixed and 100µl (bead slurry volume) was transferred in fresh tubes. The gel was sedimented by centrifugation at 500 x g for 5 min (this will give 50 µL of Bed volume) and the supernatant was carefully removed. Beas were washed with 100µl of 1xPBS (wash1), then centrifuged at 500 x g for 5 min. The supernatant was carefully removed. The wash step was repeated 3-4 times. The beads were resuspend in 50 µl PBS.

2.13.4 Western blotting

Samples were transferred onto a nitrocellulose membrane and incubated with mouse anti-Halo epitope tag antibody (1:1000 dilution in PBS), mouse anti-GST antibody (1:1,000 dilution in PBS), mouse anti-Ub epitope tag antibody (1:5000 dilution in PBS) or mouse anti-3xFLAG epitope-tag antibody (1:5000 dilution in PBS), and Anti-Digoxigenin from mouse IgG1κ (clone 1.71.256) secondary antibody (1:10 000). Scanning was performed with the NightOWL LB 983 Fluorescence preclinical imaging system imaging system (Berthold) in accordance with the manufacturer's instructions at 600 and 800 nm.

2.14 Confocal microscopy

- **Tissue fixation and ClearSee treatment**

ClearSee solutions were prepared by mixing xytol powder [final concentration 10% (w/v)], sodium deoxycholate [final concentration 15% (w/v)] and urea [final concentration 25% (w/v)] in water. Barley shoot apices were fixed with 4% (w/v) Paraformaldehyde in 1X PBS for 30-120 min under vacuum (~690 mmHg) at room temperature. Fixed tissues were washed twice for 1 min each in 1x PBS and cleared with CleaSee solution at room temperature for at least 4 days to 4 weeks or more, depending on the tissue type. For post-staining, cleared tissues were stained with Calcofluor White [final concentration 100 µg / mL] in ClearSee solution overnight. After staining, tissues were washed in ClearSee for 1 hour.

- **Imaging**

With the help of Moritz Jöst, confocal microscopy pictures from dissected shoot apices were taken with a Zeiss LSM880 using a 514 nm excitation laser line. Signal was detected at 519-537 nm for the vYFP and 600-750 nm for FM4-64.

2.15 Additional materials

Table 7: List of used vectors

Plasmid	Purpose of use	Origin	Cat.nbr
pDON221attB1B2	Entry clone for gateway cloning	Invitrogen	12536017
pDON221attB1B4	Entry clone for Gateway cloning	Lab stocks	ML1330

pDON221attB2B3	Entry clone for gateway cloning	Lab stocks	ML1331
pDEST22	Destination vector for Gateway cloning	Invitrogen	PQ1000101
pDEST32	Destination vector for Gateway cloning	Invitrogen	PQ1000101
2-in-1-BiFCt-NN	Destination vector for Gateway cloning	Lab stocks	ML1334
2-in-1-FRETgc-NN	Destination vector for Gateway cloning	Lab stocks	ML1344
pIX-HALO	Destination vector for Gateway cloning	Lab stocks	CN139
pCOG5	In vivo ubiquitylation apparatus	Gali Prag lab	-
pGEN4	In vivo ubiquitylation apparatus	Gali Prag lab	-

Table 8: Bacteria and yeast strains

	strain	**origin**
E. coli	Rosetta2(DE3)	Novagen
	BL21	Lab strain
Agrobacterium tumefaciens	GV3101 pMP90	Lab strain
Saccharomyces cerevisiae	MaV103(mating type a)	Mathieu Waroquier (Université de Namur, Belgium)
	MaV203 mating type α)	Mathieu Waroquier (Université de Namur, Belgium)

Table 9: Chemicals

Product	**Company**	**Catalog Nbr.**
Magne® HaloTag® Beads	Promega	G7281
TnT® Coupled Wheat Germ Extract System	Promega	L4130
Amino Acid Mixtures	Promega	L4461
HaloTEV Protease	Promega	G6601
Anti-HaloTag® Monoclonal Antibody	Promega	G9211
GST Tag Monoclonal Antibody	Thermofisher	MA4-004
Glutathione Sepharose® 4B	Sigma Aldrich	GE17-0756-01
Reduced Glutathione	Sigma Aldrich	G4251-10G
Monoclonal Anti-Ubiquitin antibody	Merk	SAB2702288

ANTI-FLAG® antibody	Merk	SAB4200071
GST Tag Monoclonal Antibody	Invitrogen	MA4-004

Table 10: Kits

Purpose	Kit name	Manufacturer
Yeast plasmid extraction	QIAprep Spin Miniprep Kit	Qiagen
Plasmid miniprep	NucleoSpin Gel and PCR Clean-Up	Macherey & Nagel
Plasmid midiprep	NucleoBond® Xtra Midi kit	Macherey-Nagel
Gel DNA extraction	NucleoSpin Gel and PCR Clean-Up	Macherey & Nagel
PCR purification	NucleoSpin Gel and PCR Clean-Up	Macherey & Nagel
Illumina sequencing	NextSeq 500/550 High Output Reagent Kit v2 (75 Cycles)	Illumina

Table 11: Buffers and media

Buffer/Medium	Composition
Nuclei isolation buffer (NIB)	10 mM MES-KOH (pH 5.4), 10 mM NaCl, 10 mM KCl, 2.5 mM EDTA, 250 mM sucrose, 0.1 mM spermine, 0.5 mM spermidine, 1 mM DTT.
Note: 4× stock solution of NIB was prepared without spermine, spermidine and DTT, and stored at 4°C. 1× NIB was prepared from the 4× stock and supplemented immediately before use with spermine, spermidine and DTT from the stocks of 100 mM spermine, 100 mM spermidine and 1 M DTT in deionized H2O.	
Nuclei storage buffer	20% glycerol, 20 mM HEPES-KOH (pH 7.2), 5 mM $MgCl_2$, 1 mM DTT. Store at −20°C.
Beads equilibration buffer	PBS (phosphate-buffered saline) with 0.005% IGEPAL® CA-630
1X PBS (pH 7.5)	137 mM NaCl 2.68 mM KCl 1.47mM KH_2PO_4 8.1 mM Na_2HPO_4

Cleavage buffer	4.5 µl of HaloTEV Protease and 145.5 µL of 1X PBS
Bacterial cell lysis buffer	PBS Ph=7.4 10% glycerol 0.1% Triton X-100 100 ug/ml lysozyme 1mM PMSF 5mM $MgCl_2$ 1 µL DNase solution (1 mg/mL)
GST-fusion elution buffer	1 x PBS, 10 mM reduced Glutathione, pH 8.0
1x PBS buffer (pH 7.4)	8 g Sodium chloride 0.2 g Potassium Chloride 1.44 g Sodium Phosphate Dibasic 0.245 g Potassium Phosphate Monobasic ddH2O = 1 L
TB media	20 g Bacto Tryptone 24 g yeast extract 4 mL glycerol ddH2O = 900 ml 100 mL 10X TB salt (added after autoclaving)
10X TB salt	23.135 g KH_2PO_4 125.41 g K_2HPO_4 ddH2O = 1 L
10X SLiCE buffer	500 µL 1 M Tris-HCl pH 7.5 50 µL 2 M $MgCl_2$ 100 µL 100 mM ATP 10 µL 1 M DTT ddH20 to 1 mL Store at -20 C in 40-60 µl aliquots.
YPDA medium	10 g Yeast extract 20 g Peptone 100 mg Adenine hemisulphate ddH2O = 1 L 40 mL 50% (w/v) sterile Glucose (added after autoclaving)
Yeast synthetic drop-out media:	6.7 g Yeast Nitrogen base Yeast Synthetic Drop-out medium (Sigma): 1.62 g -Leu (Y1376) 1.92 g -Trp (Y1876) 1.54 g -Leu, -Trp (Y0750) 1.46 g -Leu, -Trp, -His (Y2146) 1.46 g -Leu, -Trp, -Ura (Y1771) ddH2O = 1L 40 mL 50% (w/v) sterile Glucose (added after autoclaving)

3. RESULTS

Part1. Testing the hypothesis that BLF1 modulates GA signalling via an interaction with SLN1

The aim of this part of the study was to test the hypothesis that BLF1 may provide a DNA-binding platform for the GRAS-domain containing DELLA protein SLN1 and thus influence GA signalling. An analogous role has been shown for AtIDD3, AtIDD4, AtIDD5, AtIDD9, and AtIDD10/JACKDAW (JKD), that interact with DELLA and the GA-positive regulator SCARECROW-LIKE3 (SCL3) to fine-tune GA signalling (Yoshida *et al.*, 2014; reviewed in Kumar *et al*., 2019). In principle, two main strategies to study the functional network of a gene are exploited: genetic and protein-protein interactions. The major advantages of the two approaches is that genetic interactions capture functional relationships between genes using phenotypic readouts, while protein-protein interactions identify physical connections between gene products. These complementary networks provide a global view of the functional architecture of a gene. The following sections discuss the results of the BLF1/SLN1 interaction analysis.

1.1. Physical interaction of BLF1 / SLN1 proteins

To study a possible physical interaction between BLF1 and SLN1, we performed a pair-wise yeast-two-hybrid assay. The full length CDS (Coding Sequence) of BLF1 was cloned into pDEST32 (Fig. 1A), and the full-length CDS of SLN1 was cloned into pDEST22 (Fig. 1B). To create diploid yeast cells the yeast mating phenomenon was exploited: two yeast strains with opposite mating types, MaV103 (*Mat a*) and MaV203 (*Mat α*), pretransformed with pDEST22-SLN1 and pDEST32-BLF1, respectively, were mated together. Two positive controls provided by Prof. Sarah McKim expressing each two proteins with a medium and strong interaction intensities, and a negative control carrying pDEST32-BLF1 and pDEST22-EV, were used for this experiment. Mated cells were spotted onto double dropout medium lacking Leu and Trp to confirm their diploidy. Growth on SD/-LT of all the tested protein combinations proved that that they all carry both bait and prey constructs. To test for interaction between proteins, mated cells were spotted on triple dropout media lacking Trp, Leu and His (SD/-LTH) or Trp, Leu and Ura (SD/-LTU), to select for medium and strongly interacting proteins, respectively. Only the two positive controls were able to grow on SD/-LTH, whereas no growth was detected for BLF/SLN1 and for the negative control. For the SD/-LTU, only the positive control with strong interaction was able to grow (Fig. 1C). This leads to two possible explanations: either the BLF1 and SLN1 proteins do not interact physically, or this lack of interaction is due to defective expression of either fusion protein.

To further test the latter hypothesis, we performed positive controls: as BLF1 was shown to interact specifically with other proteins (see below, Part2), we focused on SLN1 and tested its interaction with the barley GA-receptor GA INSENSITIVE DWARF1 (GID1) in the same yeast two-hybrid system. We chose this positive control based on previous findings in rice and *Arabidopsis*, showing that GID1 perceives bioactive GA (GA4 is the major bioactive GA in this plant) and undergoes conformational changes that enable the interaction between GID1

and DELLAs, ultimately leading to DELLA degradation. Recent genetic, biochemical, and structural studies have elucidated GA-GID1-DELLA as a pivotal regulatory module for plant growth and development in *A. thaliana* and rice (Sun, 2010; Zhao *et al.*, 2017; Jathish, 2022). As GID1 has not yet been functionally characterised in barley, we speculated that its function might also be conserved in barley. For that, we cloned the full-length CDS of GID1 into pDEST22. The construct was then transformed into the MaV103 yeast strain, then mated with the MaV203 strain pretransformed with SLN1. The same procedures as for BLF1/SLN1 were followed for SLN1/GID1. SLN1 and GID1 had the same growth profile on SD/-LTH and SD/-LTU as the medium positive control, suggesting that the two do interact physically (Fig. 1D). Taken together, these results indicate that both proteins BLF1 and SLN1 are expressed in yeast cells and argue that these two proteins do not interact physically.

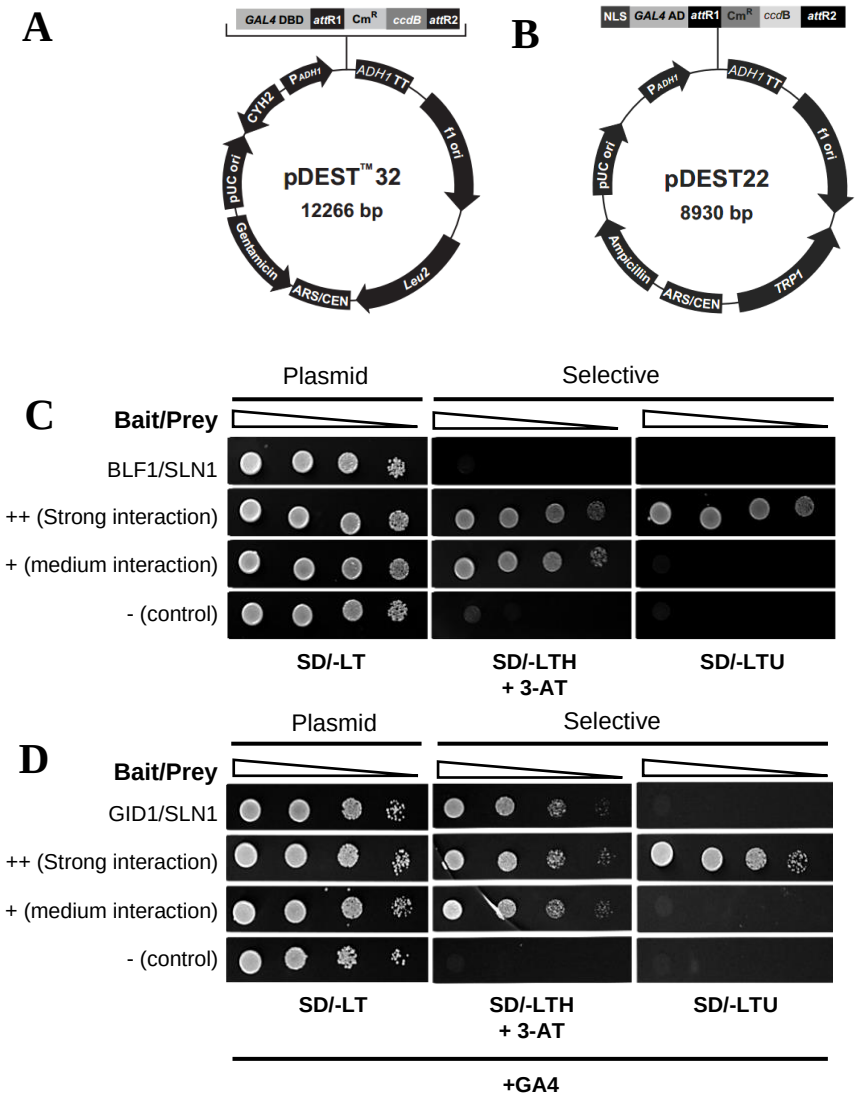

Figure 1. Yeast two-hybrid (yeast-two-hybrid) assays.
(**A), (B)** Plasmids used for the yeast two-hybrid assay. TRP1 and LEU2 *reporter genes* confer the ability to grow on media lacking Tryptophan and Leucin, respectively. **(C)** Assay of the interaction between BLF1 and SLN1. **(D)** Assay of the interaction between BLF1 and GID1. Full length cDNA of BLF1 or GID1 were fused to the to GAL4 binding domain (BD), and the full length SLN1 cDNA was fused to GAL4 activating domain (AD). Diploid cells carrying both bait or prey constructs were plated in serial 10-fold dilutions (open triangles above panels) and spotted onto a non-selective medium lacking Trp and Leu (SD/-LT; control) or a stringent selection medium lacking Trp, Leu and His (SD/-LTH) with 10 mM 3-AT or Trp, Leu and Ura (SD/-LTU), with or without 100 µM GA4. Positive controls for strong and medium protein-protein interactions in yeast were supplied by Prof. Sarah McKim. BLF1 x EV was used as a negative control.

1.2. Genetic interaction of *Blf1 / SLN1* genes

In a complementary approach, to study a possible genetic interaction of *Blf1 / SLN1*, we generated double mutants between the strong loss of function allele *blf1-1* (herein called *blf1*) from the BW58 mutant line obtained in cultivar Bowman (Jöst *et al*., 2016), and the dominant gain-of-function allele *Sln1d* obtained in cultivar Himalaya (Chandler *et al*., 2002) (Fig. 2). The *BW58* mutant was obtained from a previous work by introgression of the *broad leaf-l* locus, originally induced in the barley cultivar Bonus using X-ray mutagenesis (Lundqvist & Franckowiak, 1997), into the barley cultivar Bowman (Druka *et al.* 2011). As described in Figure 2, the single mutant lines were crossed and F1 seeds were generated. Then, an F2 population was created by selfing F1 plants, and the F3 population was created by selfing F2 plants. As these mutants are in different genetic backgrounds (Bowman for *blf1* versus Himalaya for the *Sln1d* mutations), their combination in the hybrids may modify the phenotypic expression of the mutations. Therefore, to account for this possibility we generated segregating F3 populations that are fixed for a mutant or the respective wild-type allele at one of the loci, but segregate for the other locus (i.e., fixed *Blf1* wild-type, segregating for *Sln1d*; fixed *blf1* mutant, segregating for *Sln1d*; and vice versa). This approach has the advantage that unrelated background genetic variation that segregates independently from the *SLN1* locus will affect the *SLN1* wild-type and *Sln1d* mutant plants similarly and will thus cancel out when comparing the average values of the two genotype classes. If for example the *Sln1d* mutation is epistatic to *blf1*, this would be detectable by *BLF1 Sln1d* and *blf1 Sln1d* plants from the above populations having the same leaf width and the *sln1c* mutation thus causing a stronger decrease in leaf width in a *blf1* than in a *BLF1* background. This in turn would support the notion that *BLF1* acts as a positive factor in GA signalling, which would become dispensable when the suppression of GA signalling by SLN1 is abolished.

For each segregating group, we determined leaf dimensions for the 3rd and 4th leaves and genotyped for the segregating locus (Fig. 2). As expected, leaf 3 of *blf1* mutants is 21% wider than wt leaves (Fig. 3A, Table 12) and its blade length was decreased by ~22% (Fig. 3B and Table 12). This differential length and width phenotype led to a compensation in the overall leaf size resulting in a non-significant change in the overall blade area of leaf 3 in *blf1* mutant plants (Fig. 3C, Table 12). *Sln1d* mutant plants however, show a slight decrease in leaf 3 width of ~8% (Fig. 3A, Table 12), and a more pronounced decrease in leaf 3 length of ~44% compared to the wt (Fig. 3B, Table 12). This, resulted in a similar decrease in the leaf blade area (46%) (Fig. 3C, Table 12). For the double mutant plants (*blf1 sln1d*), leaf 3 is 14% wider than wt (Fig. 3A and Table 12) but it shows no significant difference from the *blf1* mutant plants. The double mutant plants also presented a highly significant decrease in leaf 3 length (~63%), exactly equivalent to the additive effects of the two single mutants with 22% and 44% reduction in leaf 3 blade length for *blf1* and *sln1d* mutant plants, respectively (Fig. 3B, Table 12). A similar additive effect was also observed on leaf 3 blade area which was decreased by 56%, almost the equivalent of the additive effects of the two single mutant plants representing 3% and 46% reduction in leaf 3 blade area for *blf1* and *sln1d* mutant plants, respectively (Fig. 3C, Table 12). These results were further confirmed with leaf 4 measurements, representing comparable changes in all the analysed leaf parameters (Fig. 3A-C, Table 12).

In this combination of *blf1* with the *SLN1* allele we only observed additive phenotypes, indicating independent effects of the two loci on leaf growth.

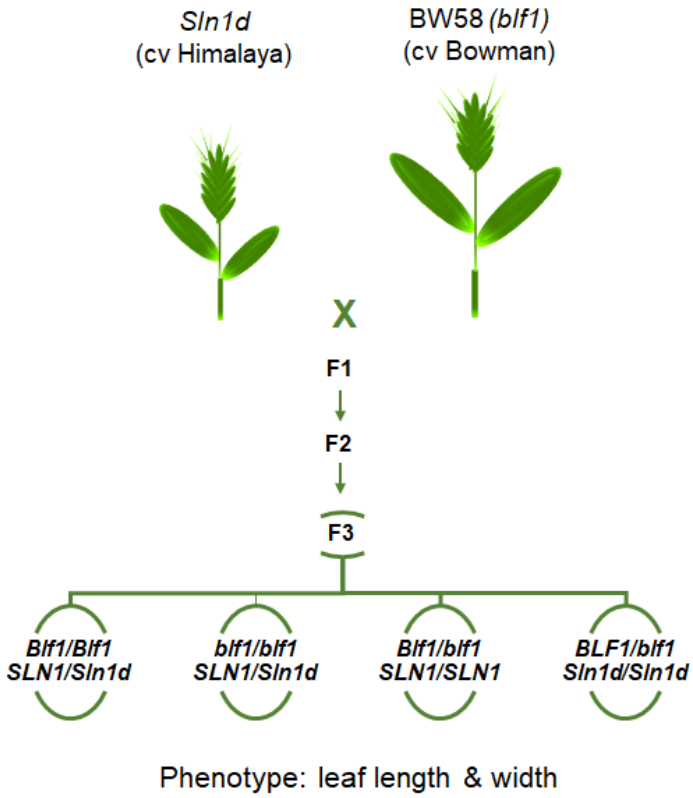

Figure 2. Schematic diagram of the experimental setup used to study the genetic interactio between *BLF1* and *SLN1* genes.
blf1 loss of function mutant line BW58 obtained in cultivar Bowman was crossed to the Sln1d dominant gain-of-function allele obtained in Himalaya cultivar. F3 populations were generated and 4 alternative homozygous groups segregating for both alleles were selected for phenotyping. Leaf 3 and 4 from 200 plants belonging to each group were analyzed for leaf width, length and area.

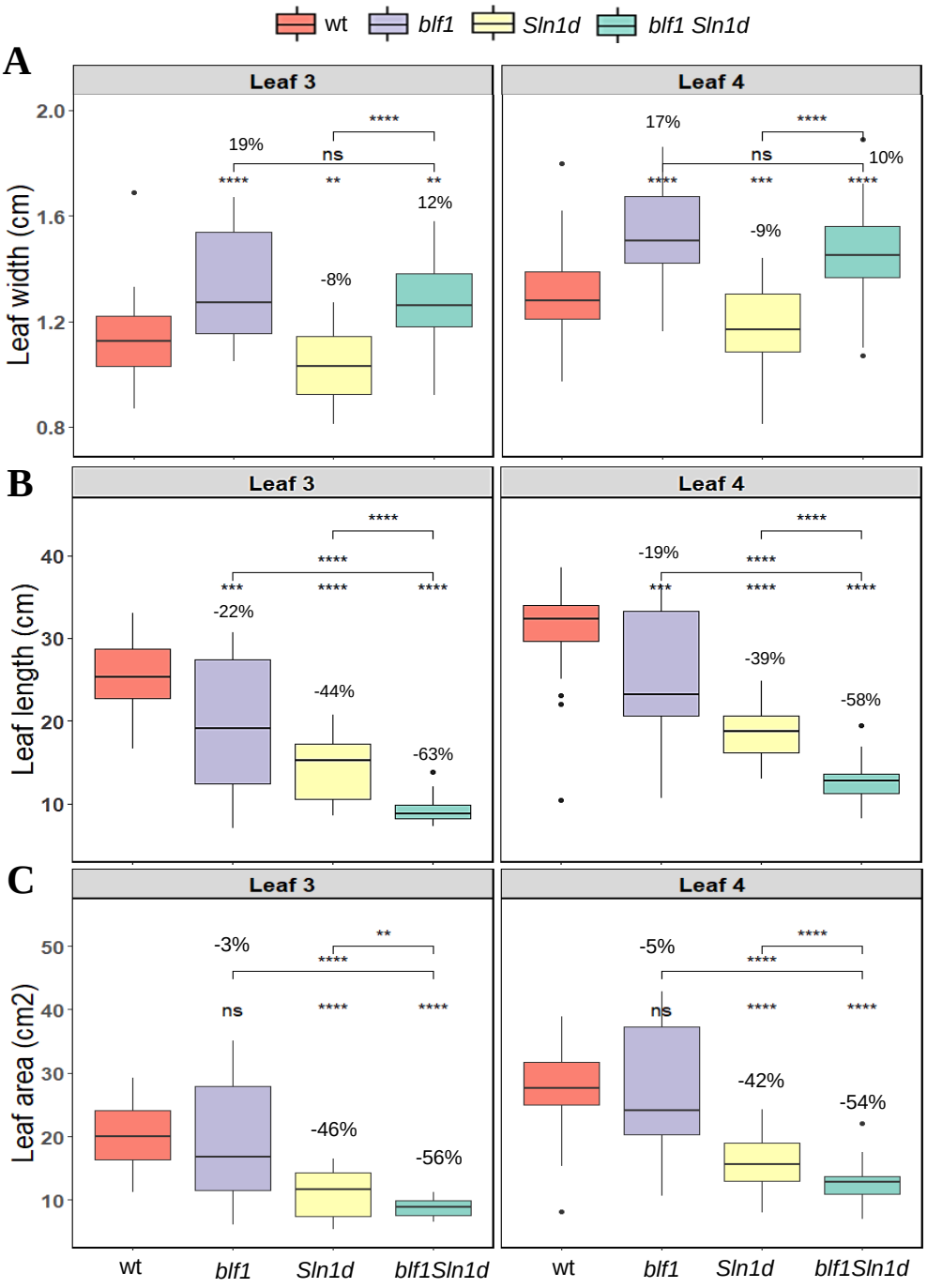

Figure 3. Leaf size parameters of wt, *blf1*, *sln1d* and *blf1 Sln1d* plants.
Maximum width **(A)**, length **(B)** and area **(C)** of mature leaf blades from wt, *blf1*, *Sln1d*, and *blf1 Sln1d* plants. Orange boxes refers to wt, mauve boxes to *blf1*, yellow boxes to *Sln1d* and green boxes to *blf1 Sln1d*. Legend for x-axes applies throughout **(A-C).** Box plots are mean ± SEM from 200 plants with the median as the horizontal line within each box. Asterisks indicate significant differences after Student's t-test at p<0.05 (*), p<0.01 (**), p<0.001 (***) and p<0.0001 (****) or not significant (ns). Increase in size of single and double mutant plants relative to the wt is given in percent.

Table 12: Quantification of the blf1 mutant phenotype

Maximum width, length and area of mature leaf blades (Leaf 3 & 4). Relative increase or decrease in *blf1*, *sln1d* or *blf1 sln1d* versus wt is given under Δ (%). All values are mean ± SEM of the indicated numbers (n) of plants per genotype. P-values are from Student's t-test against wt.

Leaf 3	**Maximum width (cm)**	**Δ (%)**	**n**	**P-value**
wt	1.12 (± o. 253)		48	
blf1	1.34 (± o. 422)	19	30	$8.6E^{-06}$
Sln1d	1.03 (± o. 210)	-8	51	0.004
blf1 Sln1d	1.26 (± o. 198)	12	23	0.001
Leaf 3	**length (cm)**	**Δ (%)**	**n**	**P-value**
wt	25.4 (± 6. 568)		48	
blf1	19.8 (± 16. 030)	-22	30	$7E^{-04}$
Sln1d	14.2 (± 6. 075)	-44	51	$1.71E^{-16}$
blf1 Sln1d	9.3 (± 1.020)	-63	23	$2.24E^{-16}$
Leaf 3	**Area (cm^2)**	**Δ (%)**	**n**	**P-value**
wt	20.4 (± 8. 49)		48	
blf1	19.7 (± 16. 187)	-3	30	0.69
Sln1d	10.9 (± 5. 055)	-46	51	$1.11E^{-16}$
blf1 Sln1d	5.9 (± o. 285)	-56	23	$1.26E^{-16}$
Leaf 4	Maximum width (cm)	Δ (%)	n	P-value
wt	1.30 (± o. 195)		49	
blf1	1.52 (± o. 225)	17	30	$5E^{-07}$
Sln1d	1.18 (± o. 213)	-9	71	0.00013
blf1 Sln1d	1.44 (± o. 198)	10	47	$1.5E^{-05}$
Leaf 4	**length (cm)**	**Δ (%)**	**n**	**P-value**
wt	31.04 (± 2. 068)		49	
blf1	25.2 (± 10. 230)	-19	30	0.00092
Sln1d	18.75 (± 3. 075)	-39	71	$1.16E^{-16}$
blf1 Sln1d	12.82 (± 2.020)	-58	47	$2.6E^{-16}$
Leaf 4	**Area (cm^2)**	**Δ (%)**	**n**	**P-value**
wt	27.84 (± 6. 63)		49	
blf1	27.7 (± 17.358)	-5	30	0.68
Sln1d	15.93 (± 6. 075)	-42	71	$2.16E^{-16}$
blf1 Sln1d	12.74 (± 4. 285)	-54	47	$7.57E^{-16}$

Part2. Dissecting the molecular mechanism of *BLF1* gene in leaf shape control

The second part of this study was dedicated to the identification of the BLF1 molecular mechanism in an unbiased manner. For that, we used two complementary approaches; yeast two-hybrid [Y2H] screening to search for BLF1-interacting proteins and an *in vitro* method, called DAP-seq (Barlett *et al*., 2017) to identify putative BLF1 targeted genes.

2.1 Finding potential downstream targets of BLF1 using DAP-seq

As described in Figure 4, the Dap-seq experiment was conducted in accordance to the paper from Barlett *et al.* (2017). First, we prepared a gDNA library formed of 200 bp native genomic DNA fragments (Fig. 4a, 4b). Next, we expressed BLF1 as our transcription factor of interest (Fig. 5A) and as a positive control the homeodomain transcription factor Variation at the six-rowed spike 1 (VRS1) (Fig. 5B), as Halo-tagged proteins in wheat-germ extract (Fig. 4c). VRS1 is known as the main gene determining spike row-type in barley (Komatsuda *et al*., 2007). For that, we assumed that VRS1 might be a relevant positive control to assess the efficiency of DAP-seq approach in identifying downstream targets of a transcription factor. In vitro expressed proteins (Fig. 4c) were couple to Halo-beads (Fig. 4d) and used to enrich for bound DNA fragments from the gDNA (Fig. 4e). Both protein expression and subsequent binding to the beads from the two independent protein mixtures were verified by Western blot analysis using anti-Halo antibody (Fig. 5). Input analysis, used to assay the *in vitro* protein expression, showed specific bands at ~100 kDa for the Halo-BLF1 fusion protein (Fig. 5A-a), and at ~60 kDa for the Halo-VRS1 fusion protein (Fig. 5B-a) fusion proteins, corresponding to the size of each of the proteins of interest BLF1 (55 kDa) and VRS1 (26,3 kDa), respectively, plus the Halo-Tag (~34 kDa). This confirmed the successful *in vitro* expression of both proteins. Analysis of the supernatants (Flow-through, FT) obtained after bead binding, revealed a moderate decrease in amount of proteins for BLF1 (Fig. 5A-b) and VRS1 (Fig. 5B-b) compared to the expression reaction (Input) (Fig. 5A-a and Fig. 5B-a, for BLF1 and VRS1, respectively). A degradation control was included in this experiment, which consists on treating the input similarly to the FT by incubation at room temperature for 2 hours, to verify if the lower protein level observed in Figure 5A-b and 5B-b is due to bead binding rather than protein degradation. As Halo-tag binds covalently to the magnetic beads, the only way to asses bead binding is through reduction of the Halo-tagged proteins in the FT. No change in the amount of proteins was observed between the input and the degradation control (Fig. 5A-c and Fig. 5B-c), indicating that the decrease of proteins observed in the FT is indeed due to their uptake by the beads. The bound gDNA fragments are then eluted and used for Illumina sequencing (Fig. 4f, 4g). The sequencing reads were mapped to the barley reference genome then filtered in order to restrict the number of reads mapping to multiple locations in the genome. Filtered reads were then used for peak calling and motif enrichment analysis.

Unexpectedly, the sequence motifs identified from the top 600 peaks of the three replicates of each TF, were very similar (Fig. 4h) and they simply correspond to some repetitive elements from the barley genome. Similarities between these motifs show that BLF1 and the VRS1 DAP-seq experiments did not find any clear peaks, nor any enriched sequence motifs.

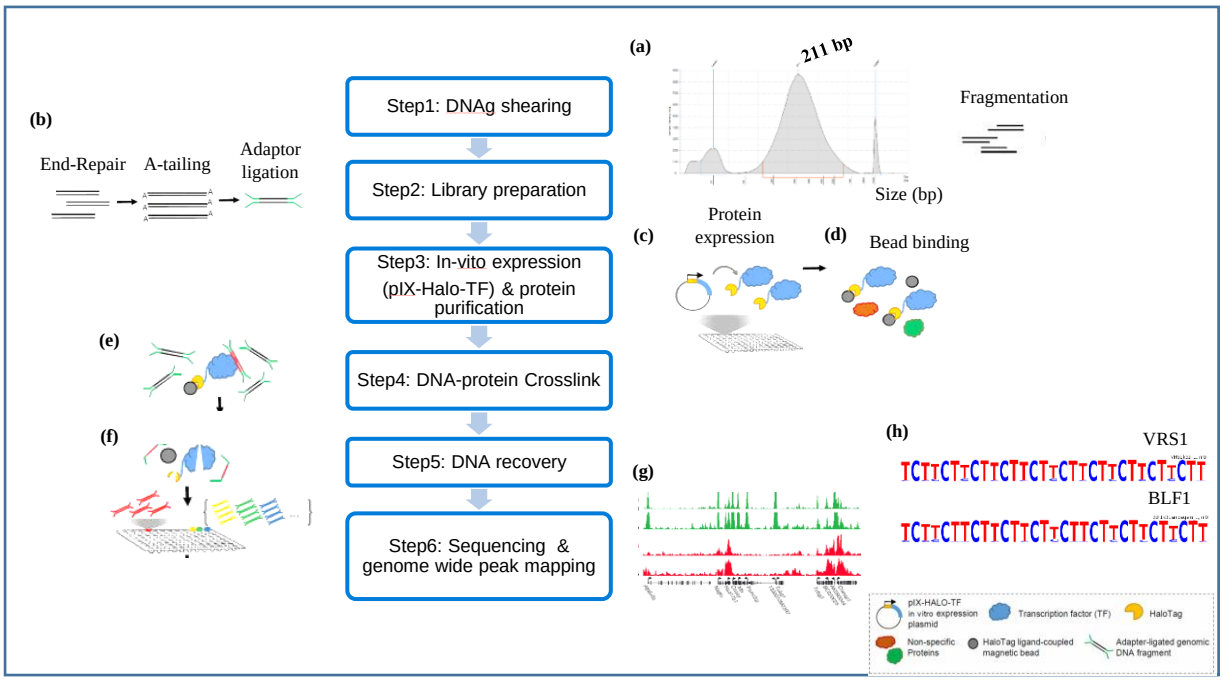

Figure 4. Flow-chart of the DAP-seq protocol & main results obtained in this study.
An adapter-ligated DNA library is prepared by shearing native genomic DNA into ~200 bp fragments **(a)** and ligating Illumina-based sequencing adapters onto the repaired ends **(c). (d)** Transcription factor (TF) ORF clones fused to the Halo affinity tag are expressed *in vitro* and bound to ligand-coupled beads. **(e)** HaloTag-TF fusion proteins are incubated with adapter-ligated genomic DNA library, and unbound DNA fragments are washed away. TF-bound DNA are eluted by sample heat-treatment and the recovered DNA is PCR amplified to attach indexed sequencing primers **(f)**. Purified DNA libraries are sequenced using next-generation sequencing and the resulting genome-wide binding events are analyzed **(g).** Peaks shown **(g)** are barley DAP-seq peaks viewed in the Integrative Genomics Viewer. **(h)** sequence motifs identifying by peak calling of Dap-seq reads.
Figure adapted from Barlett *et al.* (2017).

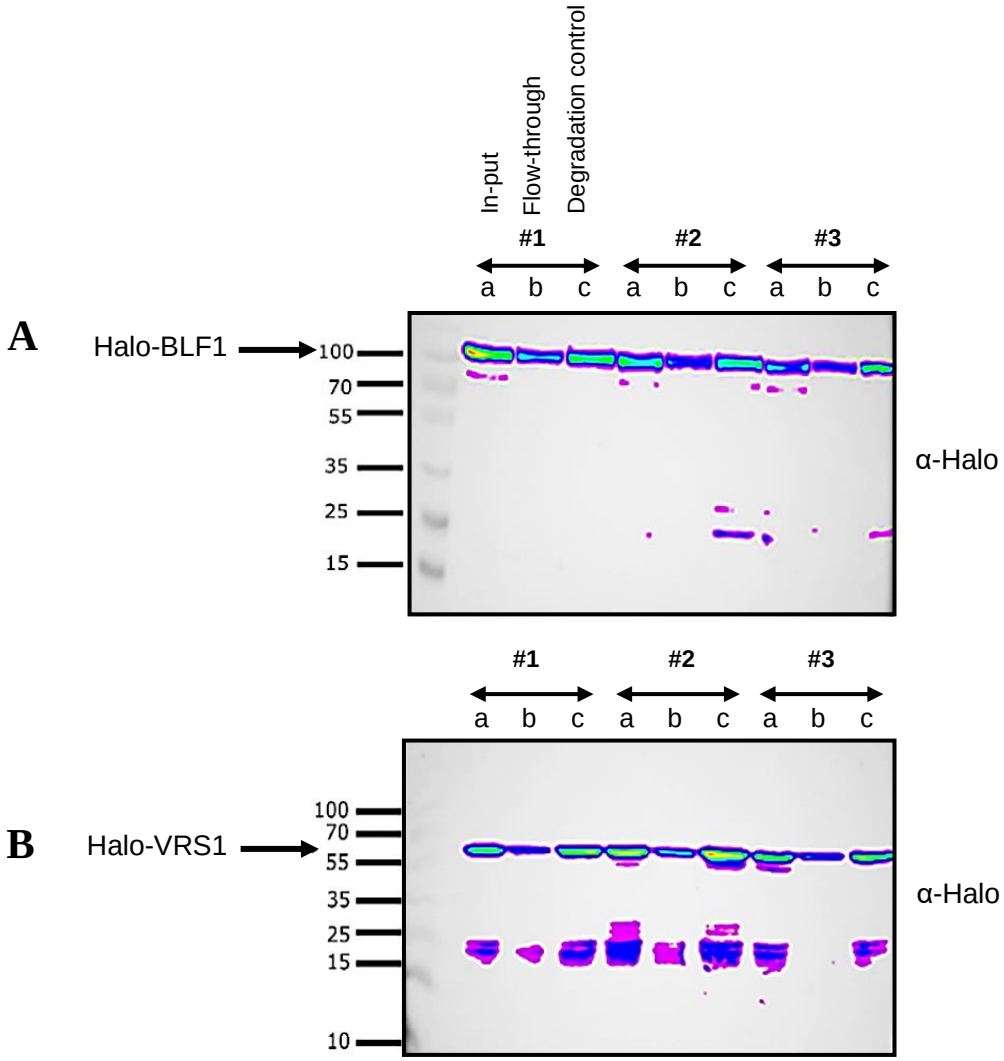

Figure 5. controls for fusion protein expression and bead binding.
Binding of Halo-tagged BLF1 **(A)** and VRS1 **(B)** to ligand-coupled beads and Western blot (WB) analysis with Halo antibody.
(a) "Input" =10% of the expression reaction used for bead binding and
(b) "FT" = indicates 10% of the supernatant after protein binding.
(c) "Degradation control" = the same input sample as in (a) but treated similarly to FT (by incubation at room temperature for 2 hours).

Three replicates for each TF (#1, #2, #3) are shown.

2.2 Identifying BLF1 interacting protein using yeast-two-hybrid library screen

As a complementary approach, the yeast-two-hybrid system was chosen to isolate proteins that interact with BLF1. This system has previously been used successfully to isolate protein-protein interactions in plants (Zhao *et al*., 2017). The cDNA library was generated from developing inflorescences, in which BLF1 is expressed (Jöst *et al*. 2016) and was cloned in prey vectors (pDEST22-cDNA) by the group of Prof. Sarah McKim at the University of Dundee. The principle of the yeast-two-hybrid system is as follows: the cDNA library was transformed into the MaV103 strain with a transformation efficiency of 1.62×10^4 cfu/µg. The library is then mated with the MaV203 yeast strain pretransformed with pDEST32-BLF1 (same Bait construct from the targeted Y2H assay of Part1), and a mating efficiency of 5% was achieved (Table 2, Fig. 6A). The major advantage of this system is that the library transformation is performed only once for multiple screens. This saves time and avoids library amplification in *E. coli* in case the amount of library is limited.

An auto-activation test for pDEST32-BLF1 (Bait-BLF1) was not required for this experiment, as our data from the yeast-two hybrid-assay in Part1 showed that the negative control expressing BLF1 and EV is not able to grow on selective media, indication that BLF1 by its own is not able to activate the GAL4 promoter and induce the expression of the reporter genes.

The yeast-two-hybrid screen was performed as described in Material and Methods. The results are shown in Table 13. From a total number of 5.75 million of screened clones, 432 positive colonies were selected on SD/-LTH (+ 10 mM 3-AT).

To decrease the number of false positives, single colonies of the best-growing positive clones were picked and restreaked on SD/-LTH (+ 10 mM 3-AT) and on SD/-LTU deficient plates (Fig. 6B). A filter lift assay was also performed on these positive colonies to test for activation of the *LacZ* reporter gene in the presence of 20 µg X-gal substrate, and the blue colouring observed for almost all colonies is an indicator of the activated *LacZ* gene (Fig. 6B). The grown positive colonies were characterised by two different approaches. First, by colony PCR using primers flanking the insert followed by two restriction digests of the PCR product with *Alu*I and *Hpa*II to identify the different interacting groups showing similar digestion patterns between the colonies (data not shown). Secondly, by plasmid extraction from each colony followed by the same restriction digestion procedure to confirm the previously identified interacting groups (Fig. 6C, D).

Six groups with identical digestion patterns for each enzyme could be distinguished (Fig. 6C, D). Representative prey plasmids for each of these groups and insert sequences were further analysed using the basic local alignment search tool (nBLAST) of the National Center for Biotechnology Information (NCBI), nBLAST search against a barley genome database (apex.ipk-gatersleben.de, Barley CDS HC May 2016 database). The attained protein sequence was further pBLAST searched against the *Arabidopsis* proteome (blast.ncbi.nlm.nih.gov) and UniProt databases to find protein homologs. This revealed five potential interactors (Table 13).

Among them we found (1) a Vps51 superfamily domain protein involved in the vesicular transport and Golgi retrograde transport in *Arabidopsis*, (2) PKc_DYRK_like domain kinase

(herein called kinase for simplification) involved in apoptosis and growth control in *Arabidopsis*, (3) RING/U-Box and TRAF-like domain E3 ligase and (4) BTB/POZ & MATH domain substrate adaptor (herein called BTB/POZ for simplification), both involved in the regulation of protein ubiquitylation and proteasomal degradation, (5) Phragmoplast Orienting Kinesin POK1, the ortholog of POK1 in *Arabidopsis*, characterized as a cell division plane orienter by modelling the cytoskeleton organisation and (6) microtubule end binding protein, the ortholog of EB1A in *Arabidopsis*, which has been associated with directional organ growth through microtubule bundling and organization. Proteins related to ubiquitylation and proteasomal degradation were found in two independent groups, which makes the hypothesis that BLF1 is regulated through ubiquitylation more plausible.

The yeast-two hybrid interactions were confirmed by plasmid isolation from positive colonies from each identified group, re-transformation of these plasmids into MaV103 cells and mating them with the pDEST32-BLF1 MaV203 transformants (Fig. 7). The same positive and negative controls used for the targeted yeast-two-hybrid assay in Part1 were also used in here. Diploidy of mated cells, including the positive and negative controls, was assayed by plating on SD/-LT. To test for protein interactions, mated cells were grown on triple-drop-out media selecting for activation of the *HIS3* and *URA1* reporter genes, as well as a filter lift assay with X-gal solution to test for activation of the LacZ reporter genes. Growth on SD/-LTH plates was detected for all protein combinations except for the negative control. The SD/-LTU medium is known to select for strongly interacting proteins and this was obvious with our strong positive control showing the strongest growth among all tested protein combinations. Compared to the medium strength positive control, BLF1 showed stronger interaction almost with all the selected candidate proteins except for the BTB/POZ protein where a very weak growth was observed. No growth was detected for the negative control. The blue colouring of the cell prints on the filter lift assay was detected for all protein combination, with a very weak intensity for the medium positive control. No blue colouring was detected for the negative control.

To verify the specificity of interactions observed between BLF1 and each of the candidate proteins, an auto-activation assay was performed for the candidate proteins by mating MaV103 cells and MaV203 cells carrying pDEST22-candidate gene and pDEST32-EV constructs, respectively (Fig. 8). Diploidy of mated cells was confirmed for all protein combinations by growth on SD/-LT plates. Activation of the *HIS3* reporter gene, was only observed for the medium and strong positive control, but not for the candidate proteins x EV combinations. Also, for *URA1* and *LacZ* reporter gene activation was only observed for the strong positive control, suggesting that none of the candidate proteins is auto-activating.

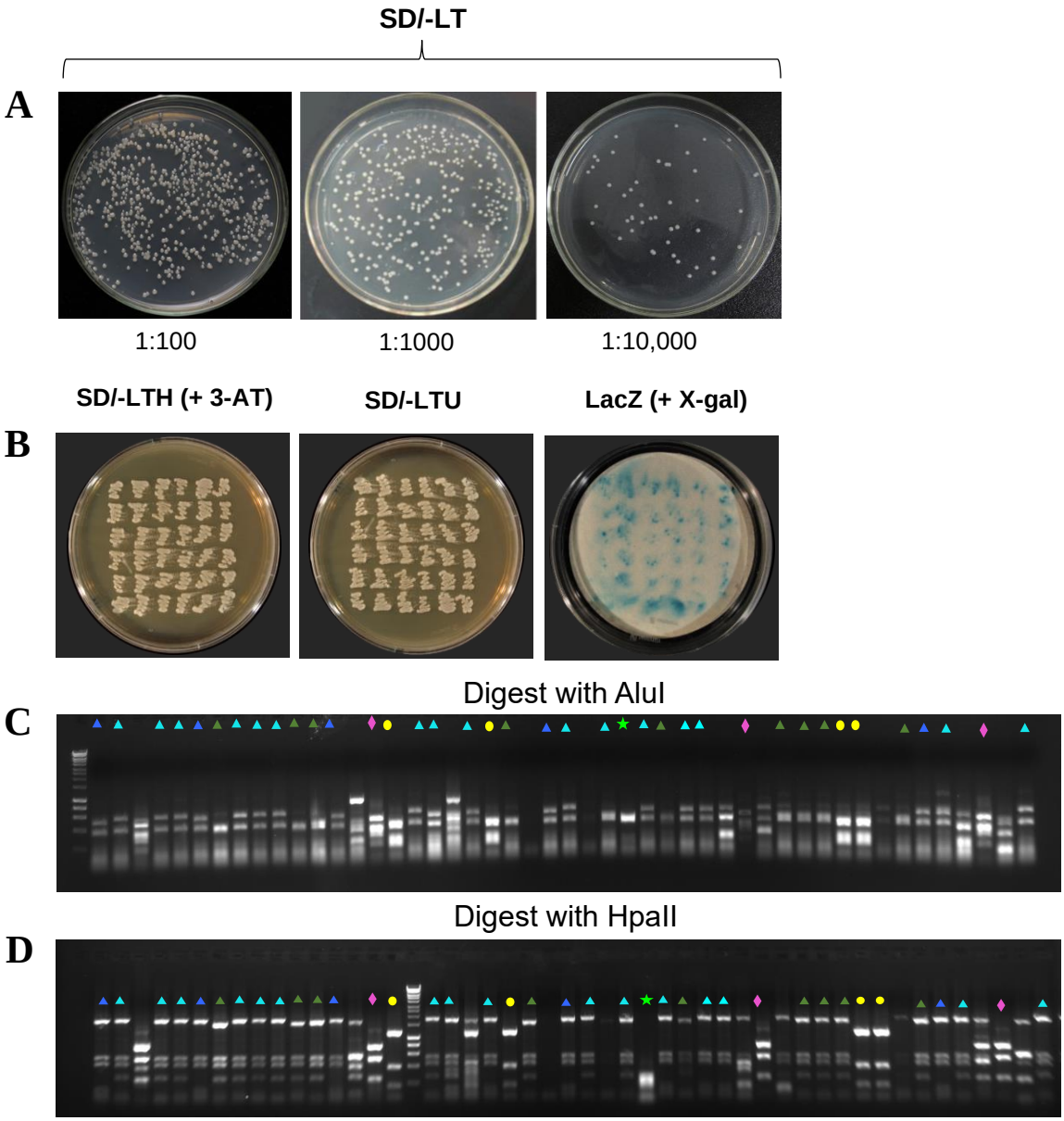

Figure 6. Characterisation of positive clones obtained by yeast-two-hybrid library screening.

(A) quantification of library mating efficiency by plating a dilution series (1:100 to 1:10,000) of mated cells on DDO (SD/-LT). **(B)** Restreaked positive colonies assayed for activity of the HIS3 reporter gene using SD/-LTH + 10 mM 3-AT medium, URA1 reporter gene using SD/-LTU TDO medium, and LacZ reporter gene using a filter lift assay with 40 µg/mL X-gal for a blue-white screening. **(C, D)** Digestion patterns of PCR products from isolated plasmids from each positive colony with **(C)** AluI and **(D)** HpaII. The different symbols indicate separate groups.

Table 13: Blast results of BLF1 interacting proteins

Group	Interacting gene/protein	Nbr of colonies	Localization	Predicted function
1	HORVU2Hr1G052050.6/ Vps51 superfamily domain	243	Nucleus [At]	vesicular transport & Golgi retrograde transport[At]
2	HORVU1Hr1G071160.1/ kinase superfamily (PKc_DYRK_like domain)	21	Nucleus [At]	Apoptosis & growth arrest[At]
3	HORVU6Hr1G082920.1/ E3 ligase (RING/U-Box and TRAF-like domain)	17	Nucleus [At]	Ubiquitylation and protein degradation[At]
4	HORVU1Hr1G020270.1/ E3 ligase (BTB/POZ & MATH domain)	23	Nucleus [At]	Ubiquitylation and protein degradation[At]
5	HORVU2Hr1G026850.26/ Phragmoplast-Orienting Kinesin-1 (POK1)	15	Cytoplasm[At]	Cytoskeleton organisation & cell division plane orientation[At]
6	HORVU1Hr1G044890.1/ microtubule end binding protein (EB1A)	3	Cytoplasm [At]	Microtubule bundling and organization, directional organ growth[At]

[At] – data from *Arabidopsis* homolog in uniprot database

Protein localization determined according to LOCALIZER1.04 browser.

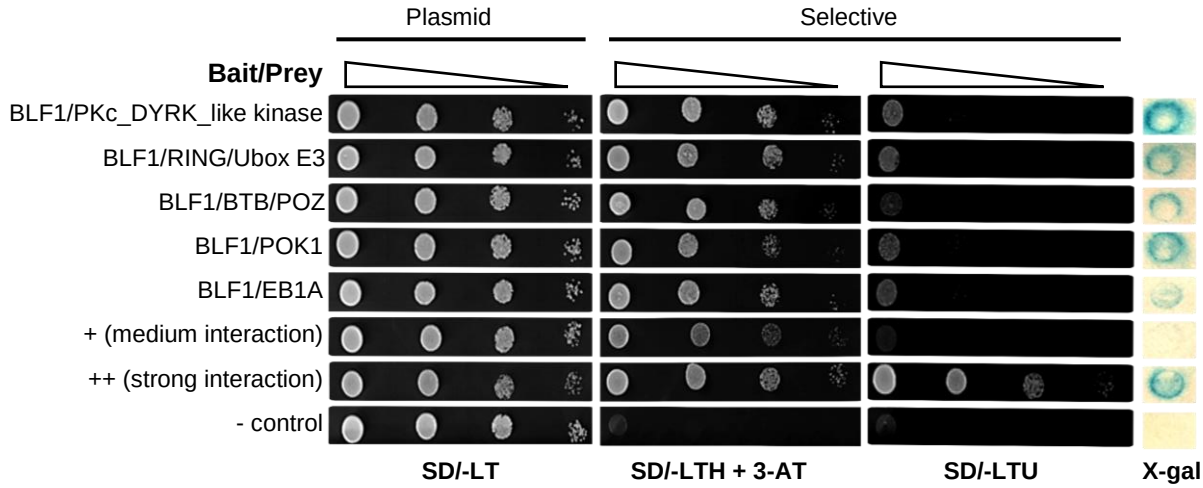

Figure 7. Confirmation of BLF1 and the candidate protein interactions by targeted yeast-two-hybrid assay.

Diploid cells carrying pDEST32-BLF1 (Bait) and pDEST22-candidate protein (Prey) were spotted onto a non-selective medium lacking Trp and Leu (SD/-LT; control) or a stringent selection medium lacking Trp, Leu and His (SD/-LTH) with 10 mM 3-AT to select for medium interacting proteins or Trp, Leu and Ura (SD/-LTU) to select only for strongly interacting proteins. LacZ activity was first assayed with a filter-lift assay containing 20 μg/mL X-α-gal. Positive controls for strong and medium protein-protein interactions in yeast were supplied by Prof. Sarah McKim. pDEST32-BLF1 x pDEST22-EV was used as a negative control.

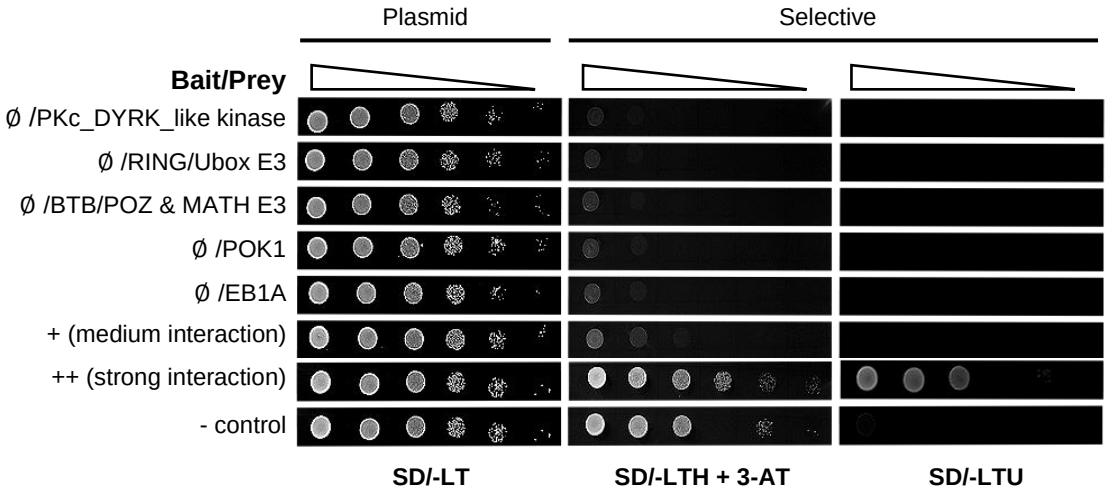

Figure 8. Self-activation detection of the prey vector pDEST22-library by mating with pDEST32-EV.

Diploid cells carrying pDEST32-EV (Ø, Bait) and pDEST22-candidate protein (Prey) were spotted onto a non-selective medium lacking Trp and Leu (SD/-LT; control) or a stringent selection medium lacking Trp, Leu and His (SD/-LTH) with 10 mM 3-AT to select for medium interacting proteins or Trp, Leu and Ura (SD/-LTU) to select only for strongly interacting proteins. Positive controls for strong and medium protein- protein interactions in yeast were supplied by Prof. Sarah McKim. pDEST32-BLF1 x pDEST22-EV was used as a negative control.

2.3 Confirmation of BLF1/candidate proteins interactions in planta

2.3.1 Ratiometric Bimolecular Fluorescence Complementation assay (rBiFC)

In order to confirm these interactions between BLF1 and the five selected candidate proteins *in planta*, we used a Ratiometric Bimolecular Fluorescence Complementation (rBiFC) assay.

The principle of the rBiFC system is as follows: BLF1 was fused to the N-terminus of the YFP fluorescent protein (nYFP-BLF1), and each of the candidate proteins was fused to the C-terminus of YFP (cYFP-proteinX), and both proteins are expressed from the same T-DNA of a binary vector called 2-in-1 developed by Grefen and Blatt (2012) (Fig. 9A). Both fusion proteins were transiently co-expressed in young leaves of *N. benthamiana* (Fig. 9B). Confocal analysis was performed to analyse protein-protein interactions (PPIs) by detecting YFP signal. We chose NPR1 as a negative control for this experiment, as it has been identified as a transcription factor associated with the systemic acquired resistance (SAR) immune response in *Arabidopsis* (Cao *et al*., 1997), and we assumed that it won´t interact with BLF1 as it has acts through a different regulatory pathway.

rBiFC has successfully been used in numerous studies for the detection of PPIs (Grefen *et al*., 2015). The major advantages of this approach are: (1) the ease with which proteins can be transiently expressed in tobacco cells without the need to create stable transformants, which might be tedious and time consuming, (2) the expression of both florescent protein fragments on the same T-DNA which guarantees equal gene dosage of both nonfluorescent fusion proteins, and (3) the inclusion of a soluble RFP marker to provide a readout for ratiometric analysis and transformation control of the cells under study. However, the output of this system tends to be binary and entails the risk of false positives. Indeed, reassembly of the fluorescent proteins is irreversible, which promotes and stabilizes weak or transient interactions, but thereby also can cause artifactual results even in the absence of a true interaction (Horstman *et al*., 2014).

RFP signal, used as an internal marker for *Agrobacterium* mediated transformation and protein expression, was detected in the nucleus after transforming with all the different 2-in-1 combination plasmids, including the negative control and at similar intensities (Fig. 9B, red pannel). YFP signal however, was not present in all protein combinations and its intensity and sub-localisation varied between samples (Fig. 9B, green pannel). Co-expression of BLF1 with the kinase produced intense YFP fluorescence in the nuclei. BLF1 and the RING/U-Box E3 ligase also produced a strong YFP signal in the nucleus, but interestingly a much more pronounced signal was detected in the nucleolus. A medium YFP signal was detected for BLF1 and EB1A and a weak one for BLF1 and BTB/POZ. No interaction was detected between BLF1 and POK1, nor between BLF1 and NPR1 (negative control). The resulting fluorescent signals were systematically quantified for comparison to the negative control. In the statistical analysis, YFP signals were always significantly higher than the negative control with a p-value < 0.001 or < 0.0001 (Fig. 9C). Overall, these results confirmed the interaction between BLF1 and the kinase, RING/U-Box E3, BTB/POZ and EB1A *in planta* and gave a better insight on how strongly these proteins interact with BLF1.

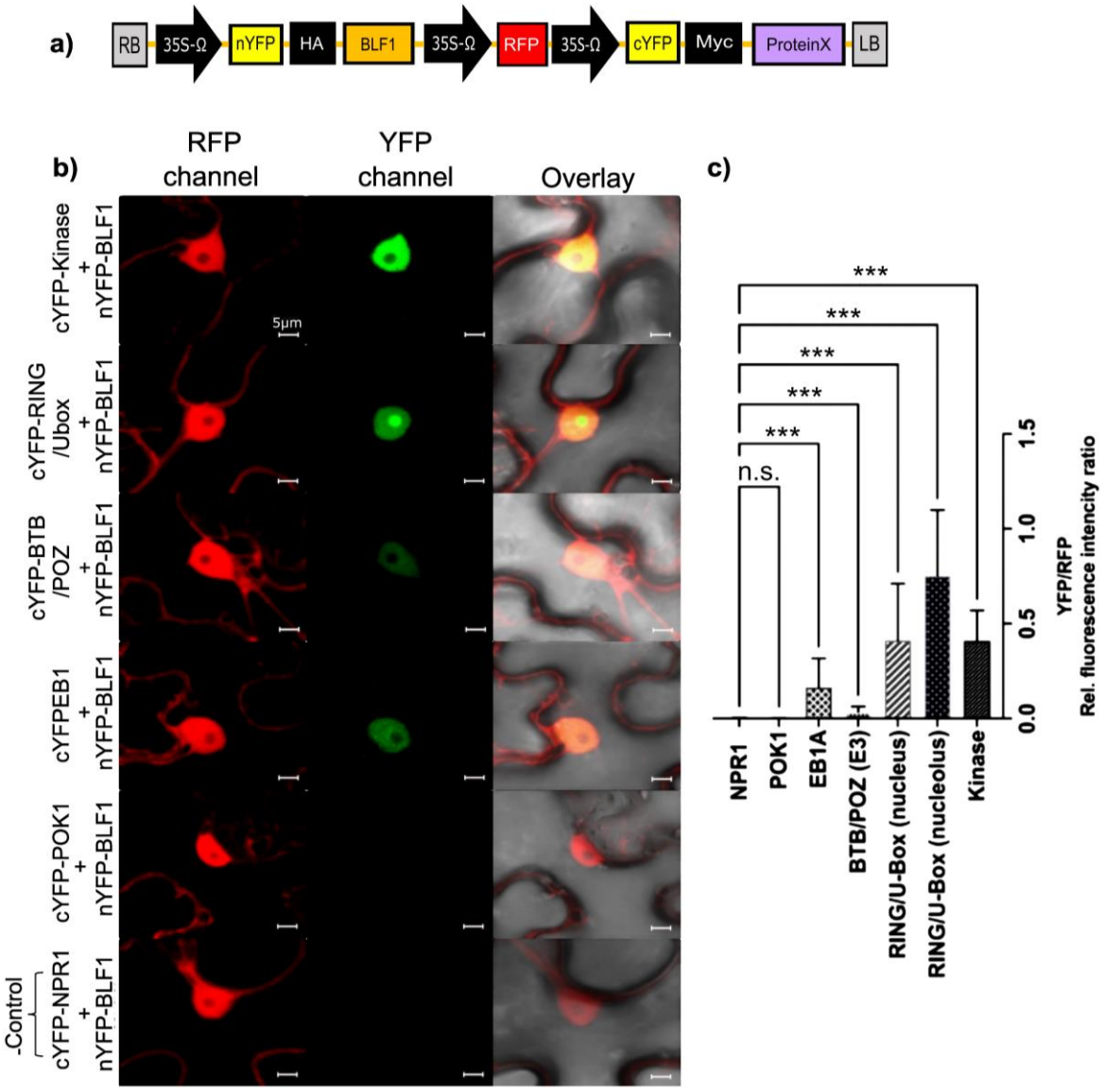

Figure 9. Ratiometric Bimolecular Fluorescence Complementation (rBiFC) assay.
(A) T-DNA cartoon illustrating the vector plasmid used for rBiFC analysis in B and C. RB, Right border of T-DNA; LB, left border of T-DNA. **(B)** Confocal images of *N. bethamiana* epidermal cells expressing rBiFC constructs with nYFP-BLF1 and different cYFP-ProteinX. The first column shows the RFP signal (red), used an internal marker for transformation and protein expression. The second column shows the YFP signal (green) used as an indicator of interaction by reconstitution of the YFP halves. The third column is an overlay image of the YFP and RFP channels and the bright field. Plants co-transfected with plasmids containing nYFP-BLF1 and cYFP-NPR1 are used as negative control. Bars = 5 µm. **(C)** Bar chart showing the mean fluorescence intensity ratios of complemented yellow fluorescent protein (YFP) to red fluorescent protein (RFP) signal averaged over 20 cells per analysed protein. Asterisks indicate significant differences after Student's t-test at $p<0.001$ (***) and $p<0.0001$ (****) or not significant (ns).

2.3.2 Co-Immunoprecipitation (Co-IP)

To gain additional evidence for the interaction of BLF1 and the selected candidate proteins *in planta*, we carried out a *semi-in vivo* Co-IP assay in *N. benthamiana*. As described in Figure 10, we used the same 2-in-1 binary vector from the previous rBiFC assay, carrying the full-length cDNA of BLF1 and the candidate proteins, to transiently co-express the proteins in the epidermal cells of *N. benthamiana*. For a more efficient pull-down of the epitope-tagged proteins, the plasmid was modified by replacing the HA-tag fused to BLF1 and the Myc-tag fused to the protein partner with the Halo-tag and the 3xFLAG tag, respectively (Fig. 10A). Based on our previous findings from the rBiFC, where all interactions between BLF1 and the candidate proteins occurred in the nucleus, the Co-IP was performed on proteins from enriched nuclei (Fig. 10B, Step3). Additionally, as BLF1 might be regulated by ubiquitylation and proteasomal degradation, the tobacco plants were treated with a proteasome inhibitor (MG132) 12h before collecting samples, in order to block the proteasomal degradation system (Fig. 10B, Step2).

POK1 was excluded from the analysed candidate proteins as it did not interact with BLF1 when co-expressed in *N. benthamiana* cells in the rBiFC assay. So, as we are using the same system for Co-IP we assume that no interaction would be found between the two proteins.

Western blots were performed on total nuclei protein extracts (also called Input) using anti-Halo and anti-FLAG antibodies to verify the expression of the proteins of interest. As shown in Figure 11A, specific bands at about ~82 kDa, ~42 kDa, ~46 kDa, ~50 kDa and ~67 kDa, corresponding to the 3xFLAG:kinase, 3xFLAG:RING/U-Box E3, 3xFLAG:BTB/POZ, 3xFLAG:EB1A and 3xFLAG:NPR1 (negative control) fusion proteins, respectively, were detected with anti-FLAG antibody. Given the very small size of the 3xFLAG (~2.9 kDa) protein, used as negative control, no band was detected for it with the anti-FLAG antibody. Input analysis using anti-halo antibody revealed a specific band at around ~88 kDa for all analysed samples corresponding to the size of Halo:BLF1 fusion protein, with ~54 kDa for BLF1 and ~33 kDa for Halo-tag (Fig. 11A). The BLF1 protein was then purified using the magne-halo beads (Fig. 10B, Step4), and analysed by western blot using anti-FLAG antibody (Fig. 10B, Step6) to identify its bound proteins. As shown in Figure 11B, bands with sizes corresponding to each of the candidate proteins were detected, whereas no band was detected for the negative control (3xFLAG:NPR1). This result confirmed both specificity and strength of the physical interaction between BLF1 and the four candidate proteins.

Taking in consideration that these interactions might result from an interaction of the candidate proteins with the Halo-tag rather than with BLF1, we performed an additional Co-IP assay following the same experimental setup used in the previous one, where only the protein combinations were modified (Fig. 11C, D). In this trial, Halo:BLF1 was replaced with simply the Halo-tag. The same negative controls (3xFLAG:NPR1 and 3xFLAG) were used, and as a positive control we co-expressed Halo:BLF1 with 3XFLAG:BTB/POZ shown previously to interact together. The input analysis via Western blot using the anti-FLAG antibody managed to detect specific bands with similar sizes to the candidate proteins and to the negative control NPR1 fused to 3xFLAG. As for the previous trial, no band was detected for the – controls

3xFLAG protein given to its extreme small size (Fig. 11C). The input analysis with anti-Halo antibody revealed a specific band corresponding to Halo-tag protein at around ~33 kDa for all the tested protein combinations and a band at ~88 kDa corresponding to the Halo:BLF1 for the positive control. Pull down analysis of the Halo-tagged protein followed by immunoprecipitation using the anti-FLAG antibody were performed. None of the candidate proteins interacted with the Halo-tag, whereas a specific band at ~46 kDa corresponding to 3XFLAG:BTB/POZ was detected in the presence of BLF1 (Fig. 11D). These results came in accordance with the ones from the previous Co-IP assay, confirming the strong and specific interaction of BLF1 and the four mentioned candidate proteins.

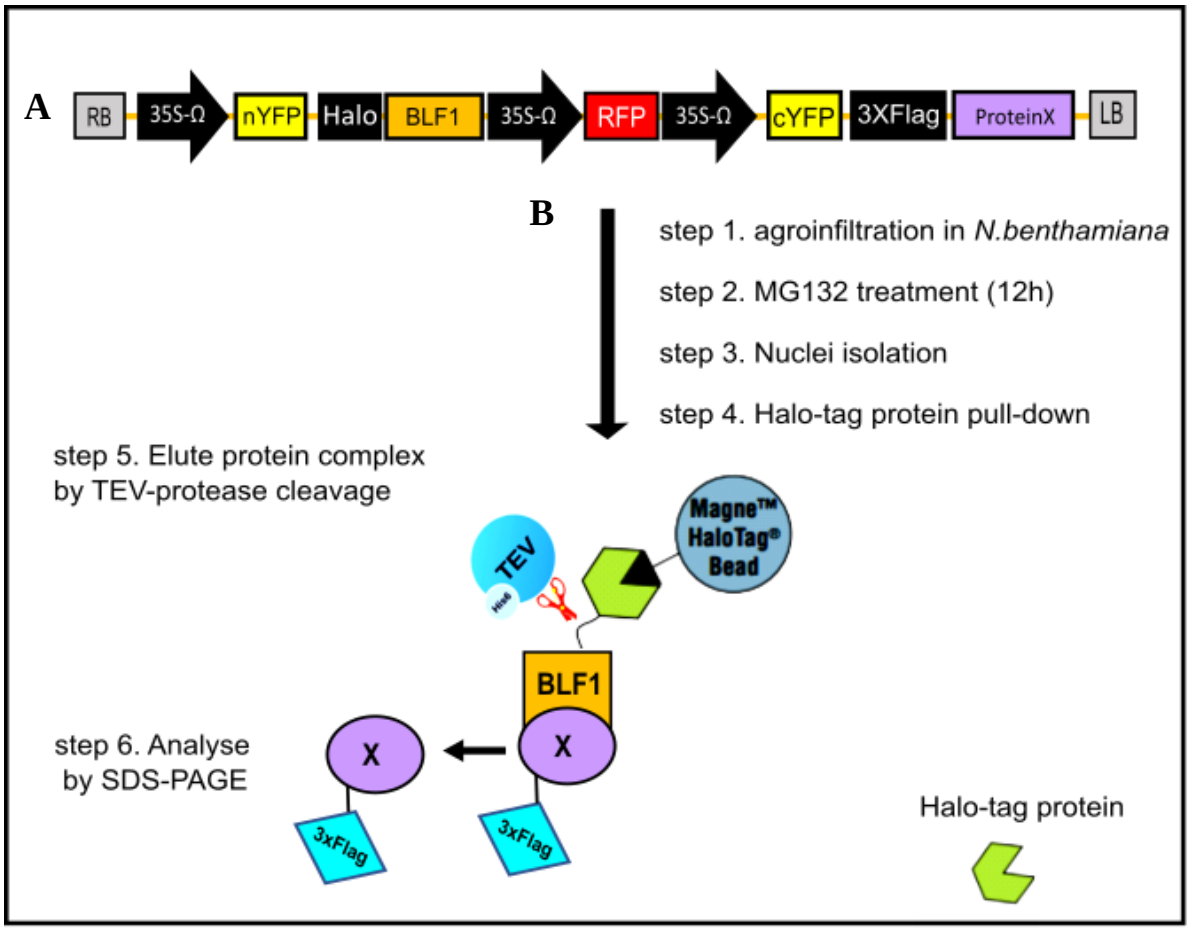

Figure 10. Flow-Chart of the Co-IP system established in this study.
(A) Cartoon illustrating the rBiFC 2-in-1 destination vector carrying the two independent cloning cassettes used to transiently co-express BLF1 and its protein partner in epidermal cells of N. bethamiana. (**B)** Experimental setup of Co-IP includes: *Agrobacteria* mediated transformation of tobacco cells, MG132 treatment to inhibit proteasomal degradation of proteins (12h before sample harvesting), nuclei isolation and protein extraction, Halo-tag fusion protein purification using Magne Halo beads, cleavage of the protein complex using TEV-protease and analysis of the protein complex by SDS-PAGE using the appropriate antibodies.

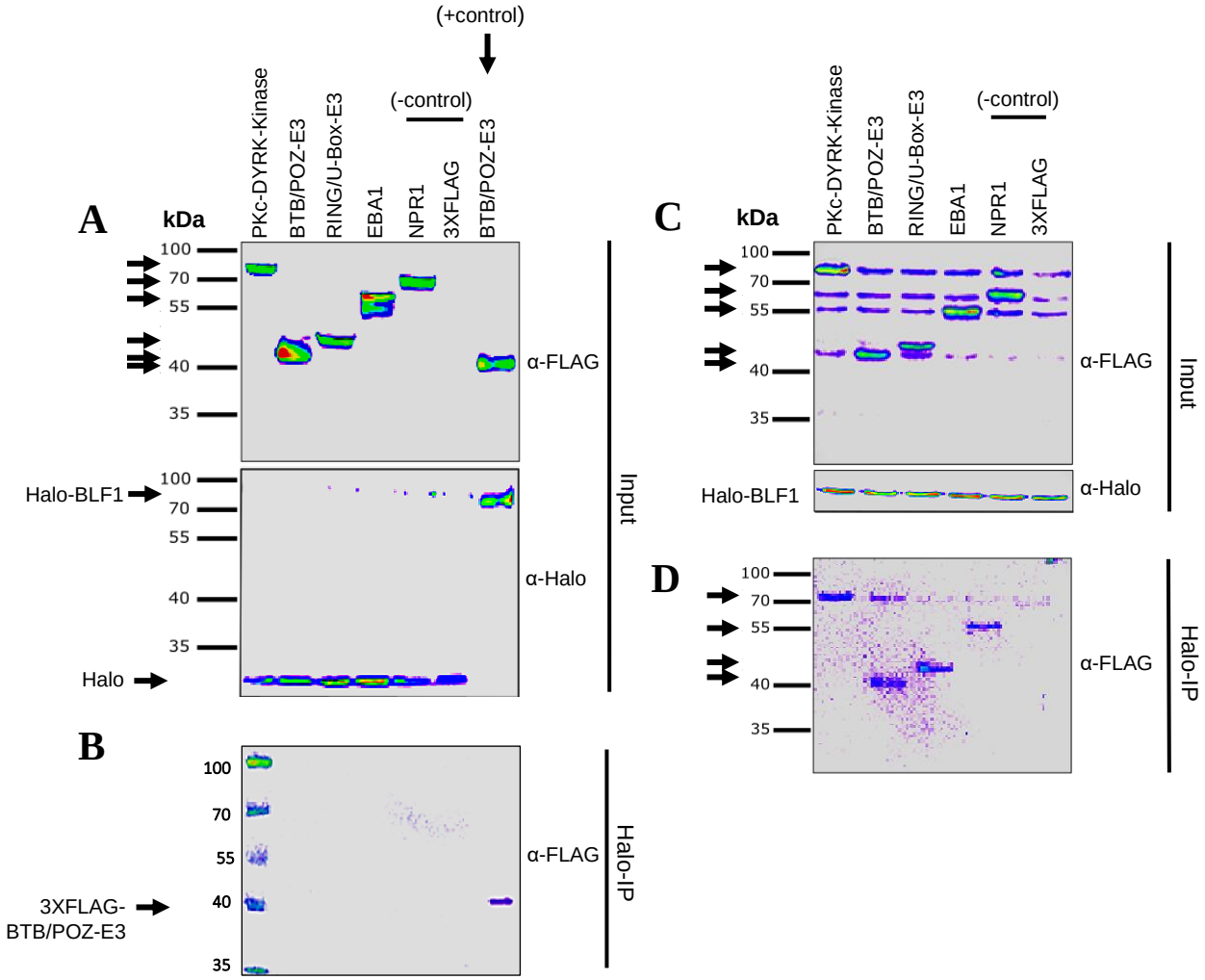

Figure 11. validation of interaction between BLF1 and the candidate proteins using Co-IP.
(A, C) Input subjected to western blot analysis with anti-FLAG and anti-Halo antibodies. Purified Halo:BLF1 **(B)** or only the Halo-tag **(D)** using magne Halo beads were subjected to immunoblotting using anti-FLAG antibody. Input, total protein before immunoprecipitation.

2.4 Functional characterization of the BLF1 interacting proteins

In order to further characterize the BLF1 and RING/U-Box, and BLF1 and BTB/POZ interactions, their physical and genetic interactions were analyzed as described in the following section.

2.4.1 How closely does BLF1 interact with the E3 ligase related proteins?

To determine whether BLF1 and the BTB-POZ/MATH or the RING/U-BOX protein interact directly we used a highly sensitive Förster resonance energy transfer (FRET) approach. The major advantage of this approach is that it exploits the physical phenomenon of resonance energy transfer between the donor and acceptor to study protein interactions. A prerequisite is an overlap of the donor emission with the excitation spectrum of the acceptor. FRET only occurs if donor and acceptor are in close enough proximity of 10 nm or less (Ishikawa *et al*., 2012; Bucherl *et al*., 2014). Such resolution of molecular distances is more than a magnitude lower than the diffraction limit of light microscopy at 200 nm, allowing distinction of protein co-localization from interaction.

For this assay, we used the 2-in-1 pFRETgc-2-in-1-NN plasmid, in which BLF1 was fused to the donor fluorophore (mEGFP) and each of the RING/U-Box or BTP/POZ E3 was fused to the acceptor fluorophore (mCherry) (Fig. 12a). Plants were treated with MG132 to see the impact of the drug treatment on both interaction and enrichment of the analyzed proteins. As a negative control, BLF1-mEGFP was co-expressed with NPR1-mCherry. FRET analysis was performed by the acceptor photobleaching method (Fig. 12b, purple panel) (see "material & methods").

Confocal analysis showed that photobleaching of RING/U-Box-mCherry resulted in an increase in the GFP signal mainly after MG132 treatment (Fig. 12b, green panel). This increase in GFP fluorescence indicates that before bleaching mCherry a part of the excitation energy had been transferred from GFP to mCherry. This observation was further confirmed by the FRET efficiency analysis (Fig. 12c), where the combination of BLF1 and RING/U-Box yielded a FRET signal that was significant in the mock control treatment samples and more significant in the MG132 treated samples when compared with the negative control. This result provided more solid evidence about the direct interaction between BLF1 and RING/U-Box E3, by showing that two the proteins are within several nanometers of each other, distances sufficiently close for bimolecular interactions to occur.

In contrast, no increase in the GFP signal was observed after BTB/POZ-mCherry photobleaching, in both MG132 treated and untreated cells (Fig. 12b, green panel). Similarly, no significant FRET was detected for the BLF1 and PTB/POZ neither in the presence nor in the absence of MG132 treatment (Fig. 12c), proving that the two proteins do not interact directly and arguing against our previous findings from Y2H, rBiFC and Co-IP assays. As expected for the negative control, no increase in the GFP signal was observed after NPR1-mCherry photobleaching and no efficient FRET was detected, confirming the robustness and high sensitivity of this approach.

One further advantage of the FRET system is that it allows separate quantification of the donor and acceptor signal from two independent fluorophores. We exploited this option to study the impact of the MG132 treatment on the enrichment of BLF1 in the presence of the candidate E3 ligases. Average fluorescence quantification of mEGFP-BLF1 (Donor) from 30 different cells, showed a significant increase in the GFP signal after MG132 treatment when BLF1 was co-expressed with the mCherry-RING/U-Box E3 acceptor. In contrast, no significant change in the GFP signal was detected after the MG132 treatment when BLF1 was co-expressed with BTB/POZ. Comparison of the non-treated samples between the two different protein combinations revealed a slight decrease of GFP signal with the RING/U-Box E3, yet this decrease was not significantly different from the signal observed with BTB/POZ (Fig. 13A). Additionally, average fluorescence intensities were calculated for the two acceptors mCherry-RING/U-Box E3 and mCherry-BTB/POZ. MG132 treatment induced a highly significant increase in the mCherry signal for the two E3 ligases (Fig. 13B). Analysis of the mEGFP/mCherry relative fluorescence ratio produced similar results to those obtained from the direct quantification of GFP, with almost a 2-fold increase for the BLF1/ RING/U-Box E3 ratio for MG132 treated cells compared to the non-treated ones, and a nonsignificant change in the BLF1/ BTB/POZ ratio between the treated and non-treated cells (Fig. 13C).

To confirm that this observed variation in the amount of BLF1 protein is specifically related to the presence of the RING/U-Box E3, a stability test was required to verify the stability of the BLF1 protein when transiently expressed on by its own in tobacco cells. For that, we used the same FRET 2-in-1 vector to transiently co-express mEGFP-BLF1 as a donor and only the mCherry fluorophore (mCherry-∅) as an acceptor, in M132 treated and non-treated cells (Fig. 13D). Following that, we quantified the GFP signal to estimate the amount of BLF1 present in cells. Interestingly, no significant change in the GFP signal was observed between the treated and non-treated samples, confirming that BLF1 is stable in tobacco cells and does not undergo proteasomal degradation. Thus, the decrease in BLF1 observed in the presence of the RING/U-Box E3 ligase, and the increase of the protein level observed after inhibition of the proteasomal degradation can be attributed to the BLF1 degradation mediated by the RING/U-Box E3 ligase.

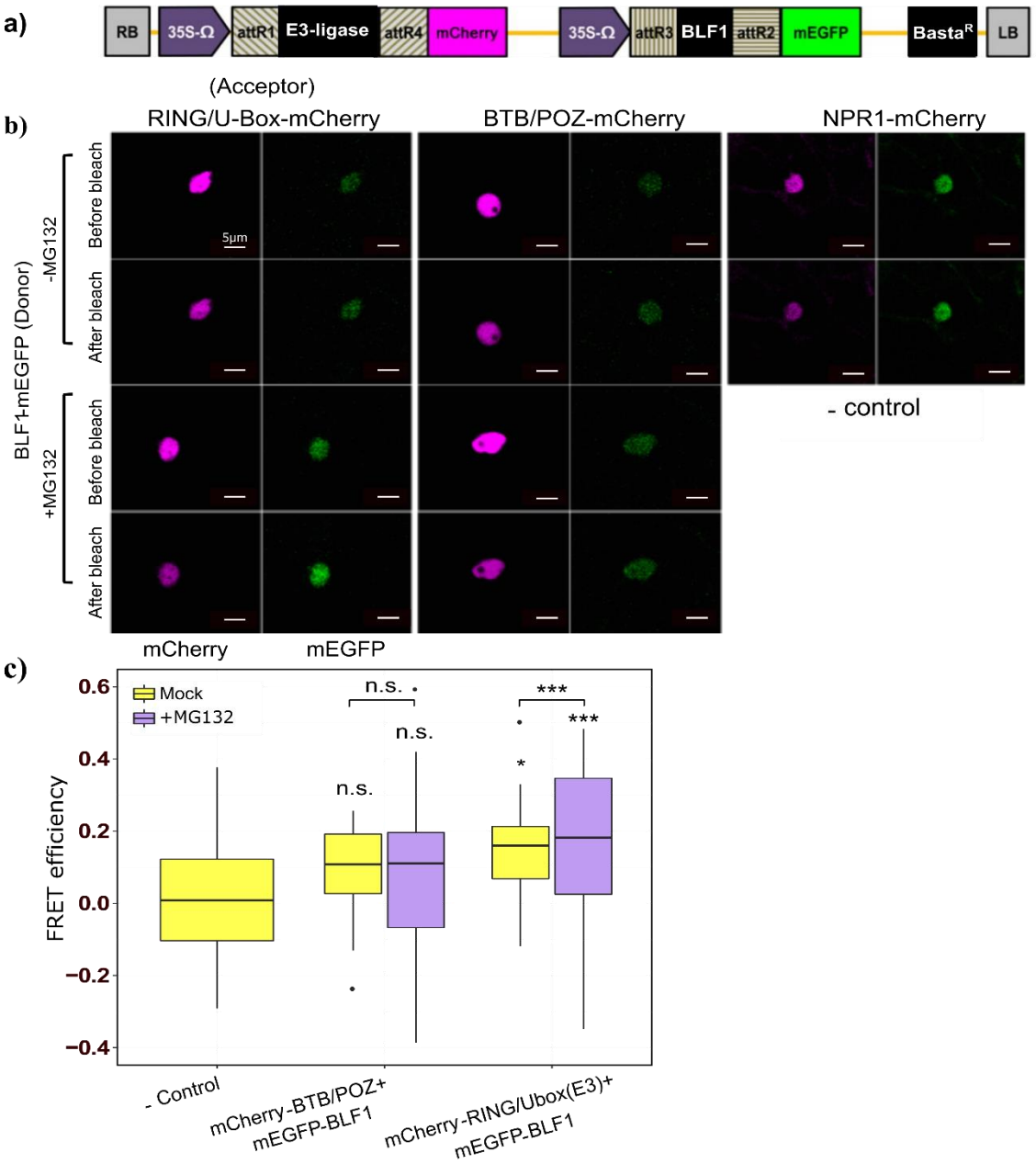

Figure 12. Confirmation of the BLF1–RING/U-Box and BLF1–BTB/POZ interactions by FRET. **(a)** Schematic illustrating the pFRETgc-2-in-1-NN plasmid used for each FRET setup. **(b)** Confocal images of nuclei of *N. benthamiana* expressing the indicated fusion proteins before and after photobleaching of the acceptor, with or without 100 µM MG132 treatment. Fluorescence of the fusion proteins RING/U-Box-, BTB/POZ-MATH- or NPR1-mCherry (acceptor; left panels) and BLF1-mEGFP (donor; right panels) is shown. Bars = 5 µm. **(c)** FRET efficiency analysis of BLF1 and candidate-protein interactions in MG132 treated cells (+ MG132, mauve boxes) and control cells (mock, yellow boxes). FRET efficiency was determined from 30 independently quantified cells. The horizontal line within each box plot represents the median. First and third quartile are represented by the lower and upper hinges. The whiskers extending until the maximum or minimum values are in the 1.5 interquartile ranges. Values beyond this range were considered as outliers and indicated as a dot. Box plots were generated using the ggplot2 package implemented in Rsoftware (Wickham H., 2016). Asterisks indicate significant differences at $p<0.001$ (***) and or not significant (ns) after Student's t-

test relative to the negative control (above the boxes) or after comparing mock- and MG132-treated cells (above the horizontal lines at the top).

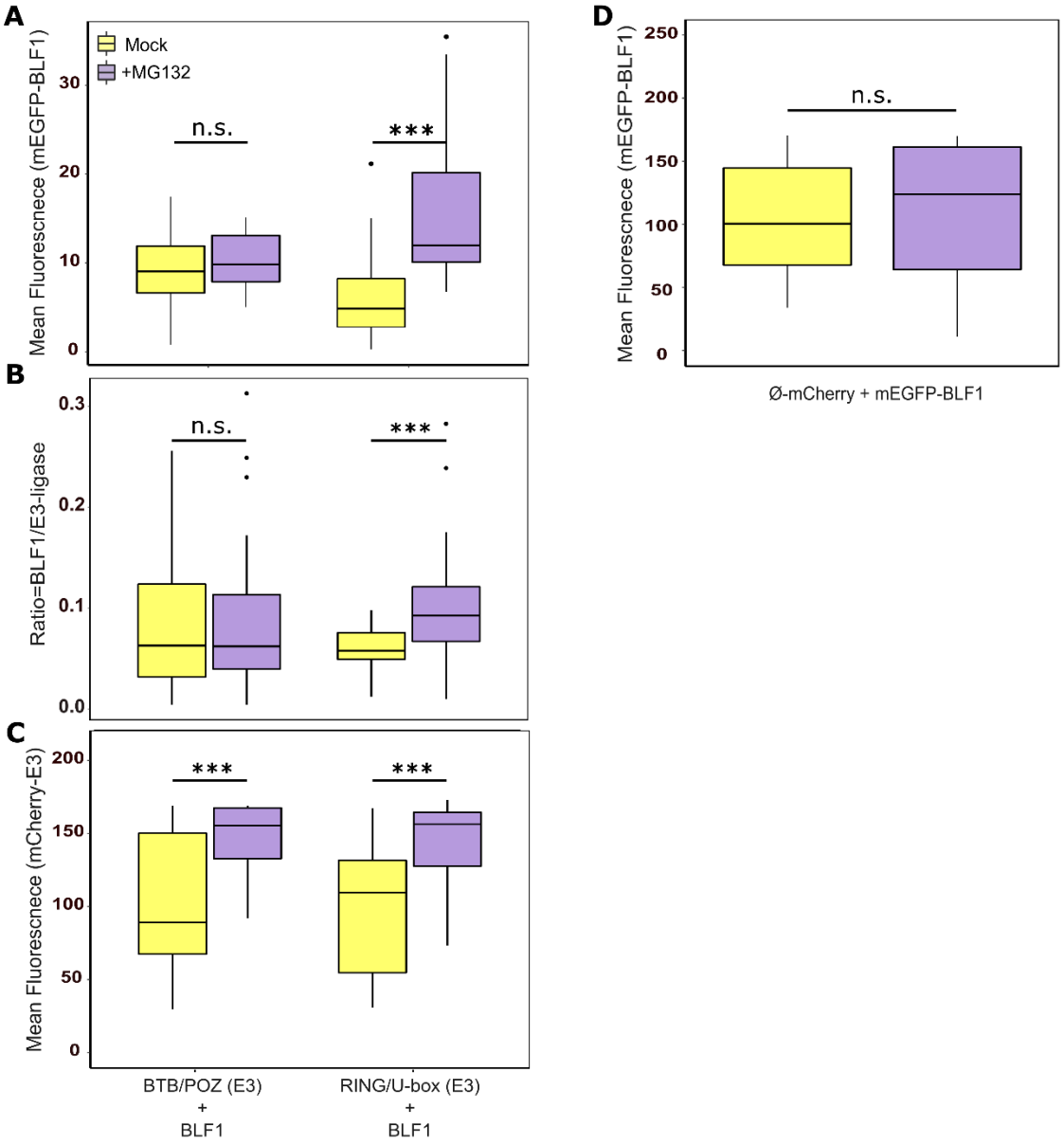

Figure 13. Quantification of the donor and acceptor signals before photobleaching from MG132 treated (+ MG132, mauve boxes) and untreated cells (-MG132, yellow boxes).
(A, D) Box plots showing mean fluorescence intensity of mEGFP-BLF1 (donor) in the presence **(A)** or absence **(D)** of E3 ligases, in **(B)** mean fluorescence intensity of mCherry-BTB/POZ and mCherry-RING/U-Box E3 (acceptor) and in **(C)** mean fluorescence intensity ratio of mEGFP/mCherry, quantifications are averaged over 30 different cells with the median as the horizontal line within each box. Asterisks indicate significant differences after Student's t-test at $p<0.001$ (***) or not significant (ns). **(A-C)** share the same legend for x-axes.

2.4.2 Reconstitution of BLF1 ubiquitination cascade in Bacteria

To determine whether either of the two identified E3 ligases could ubiquitinate BLF1, we used a recently developed system by Prag *et al.* (2012) that allows reconstituting the entire eukaryotic ubiquitylation cascade in bacteria and subsequently allows to test whether a putative E3 ubiquitin-ligase can ubiquitinate a substrate protein (Fig. 14). In this system, the ubiquitylation apparatus is expressed from two compatible plasmids; pGEN that expresses His6–Ub, E1-activating enzyme and E2-conjugating enzyme, and pCOG that carriers a selected substrate for ubiquitylation fused to the GST-tag, and its cognate E3 ligase fused to the MBP-tag. First, we adapted the system to express the required barley enzymes and ubiquitin substrate. For that, we used HvUba2 as E1, HvUbc11 as E2, MBP-HvRING/U-Box or HvBTB/POZ as E3s, and GST-BLF1 or only the GST-tag as a ubiquitin substrate (Fig. 15c-f). As a positive control, we used the ubiquitin receptor from yeast Rpn10 considered as an example that validates the authenticity of this bacterial system, by faithfully recapitulating the ubiquitylation of Rpn10 as observed *in vivo* in yeast (Prag *et al*. 2012). Bacterial lysates co-expressing the different protein combinations were purified using GSH beads to isolate the GST-tagged Ub-targets which were then subjected to immunoblotting using the anti-GST or anti-Ub antibodies. Figure 15a shows the Western blot analysis of purified Rpn10 using anti-GST antibody. Rsp5-dependent ubiquitylation of Rpn10 is clearly evident in the Ubc4 lane. This is translated by an increase in the size of GST-Rpn10 fusion protein at ~100 kDa compared to its original size (~70 kDa). Attachement of Ub molecules on Rpn10 by Ubc5 is confirmed by Western blot analysis using anti-Ub antibody (Fig. 15b).

Similarly, purified GST-BLF1 from two different bacterial extracts were subjected to immunoblotting (Fig. 15c-f). For the first tested protein combination, BLF1 was co-expressed with of HvUBA2 (E1), HvUBC11 (E2) and HvRING/U-Box (E3). Western blot analysis with anti-GST antibody revealed an increase in GST-BLF1 fusion protein at about ~130 kDa compared to its original size (~80 kDa), only in the presence of the three required enzymes (Fig. 15c). Interestingly, no increase in the GST-tag protein size (~24 kDa) was observed (Fig. 15c). For the second protein combination, BLF1 was co-expressed with HvUba2, HvUbc11 and HvBTB/POZ. No change in the GST-BLF1 fusion protein size was observed even when all required enzymes for ubiquitylation are present (Fig. 15d). To verify that the increase in the GST-BLF1 fusion protein size observed with HvRING/U-Box E3 is due to ubiquitylation of BLF1, we performed a Western blot using anti-Ub antibody. HvRING/U-Box E3-dependent ubiquitylation of BLF1 is clearly evident in the HvUbc11 lane from Figure 15e, where the Ub-GST-BLF1 band detected in figure 15c is nicely reflected in the blot, whereas no band was detected neither when GST-tag was used as Ub target nor in the absence of HvUbc11 (Fig. 15e). Given the difference in size between the GST-BLF1 and Ub-GST-BLF1 proteins, we assume that BLF1 undergoes a polyubiquitylation. The absence of ubiquitylation for BLF1 when co-expressed with HvUba2, HvUbc11 and HvBTB/POZ was also confirmed in the Western blot using anti-Ub antibody as no band was detected for the GST-BLF1 fusion protein even in the presence of the three required enzymes (fig. 15f).

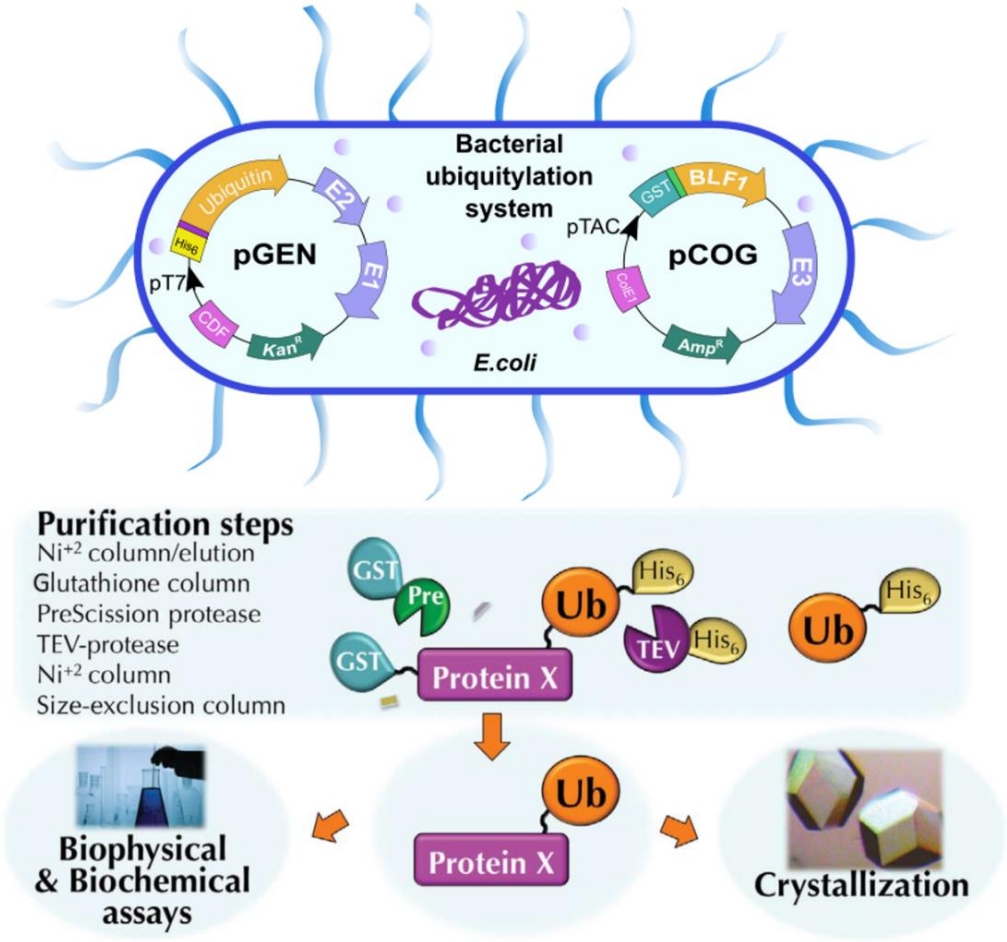

Figure 14. Bacterial system for expression and purification of ubiquitylated proteins.
A scheme describing the ubiquitylation system and the steps for purifying ubiquitylated proteins from *E. coli*. Figure adapted from Keren-Keren *et al*. (2012).

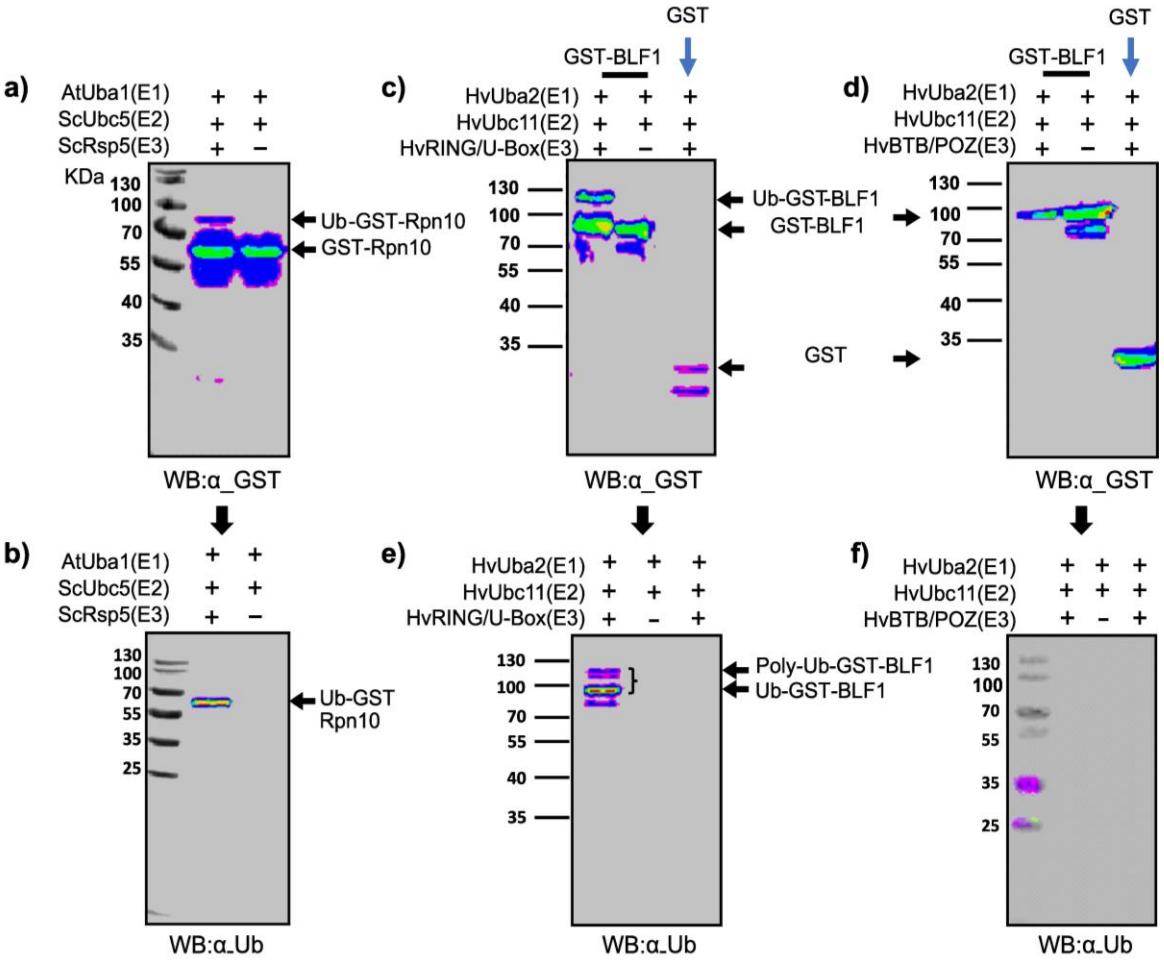

Figure 15. Reconstitution of the BLF1 ubiquitylation in *E. coli.*

(a, b) Bacterial lysates co-expressing MBP–Rsp5 and GST–Rpn10 (expressed from pCOG5) and His6–Ub, AtUba1, with or without ScUbc5 (expressed from pGEN4), were purified on GSH beads. The purified proteins were resolved on SDS–PAGE and subjected to western blot with anti-GST (A) or anti-Ub (B) antibodies as indicated.

(c-f) Bacterial lysates co-expressing MBP–RING/U-Box E3 or MBP–BTB/POZ E3 and GST–BLF1 or only GST-tag (expressed from pCOG5) and His6–Ub, HvUba2, with or without HvUbc11 (expressed from pGEN4), were purified on GSH beads.

The purified proteins were resolved on SDS–PAGE and subjected to western blot with anti-GST **(c, d)** or anti-Ub **(e, f)** antibodies as indicated. Rpn10 ubiquitylation was used as positive control for the specificity and fidelity of the ubiquitylation system in bacteria. As a negative control, we used the GST-tag as a Ub target or a protein combination lacking the E2 conjugating enzyme.

2.4.3 Verification of BLF1 proteasomal degradation in barley

Having found evidence suggesting that BLF1 can be regulated through ubiquitin-mediated proteasomal degradation in tobacco and *E. coli* cells, the question arose whether this can also be observed in barley.

To test this hypothesis, we blocked the 26S proteasome with different proteasome inhibitors in transgenic barley expressing a functional BLF1-vYFP fusion protein driven by the endogenous *Blf1* promoter. Since BLF1 is expressed throughout the shoot apical meristem (SAM) and young leaf primordia of developing shoot apices, we chose to use the shoot apices from 7-day-old seedlings to address the control of BLF1 by protein degradation. As the barley shoot apices are not accessible to the application of drugs, we cut the basal part of the shoots including roots to allow a better infiltration of the drug into the desired tissues. As a negative control we used non transgenic barley plants (wt). As a positive controls we used a previously generated *Arabidopsis* line expressing an auxin signalling reporter named R2D2 carrying the *pRPS5A:DII-3xVenus* construct (Liao *et al*., 2015), a fusion of the auxin-dependent degradation domain II proved to be regulated via proteasome-mediated degradation (Liao *et al*., 2015; Aranda *et al*., 2017). As suggested by Liao *et al*. (2015), we used the root system to assess the protein degradation for the positive control.
Samples were collected from 16 hours pre-treated plants, followed by dissection of shoot apices, tissue fixation with formaldehyde and Clearsee treatment to optimise the confocal imaging of the desired protein. To detect a possible accumulation of the fluorescent protein after drug treatment, we opted for quantification of the fluorescence signals in planta as a highly sensitive detection assay.

First, we attempted to detect a possible accumulation of BLF1-YFP after treatment with 100 µm MG132 and 50 nM epoxomicin. However, we were not able to detect any difference in the YFP signal between the treated and untreated plants (data not shown). By contrast, treatment with bortezomib led to 33% and 50% higher BLF1-YFP levels than in untreated plants, in the SAM and veins, respectively (Fig. 16 a, b, g). The signal was more concentrated in the veins and was expressed in larger zones of the SAM, mainly at the junction where young leaf primordia are initiated. The treatment also induced some autofluorescence in the negative control, mainly in the cell walls of the basal and central parts of the shoot apices (Fig. 16 c), but not in the SAM, leaf primordia or veins where BLF1 is expressed (Jöst *et al*., 2016). Additionally, the fluorescence profile from BLF1-YFP is different from that of the autofluorescence, as BLF1 has a nuclear localisation, which makes it easy to distinguish between the two types of fluorescence while quantifying the real YFP signal. After bortezomib treatment, the DII-3xVenus displayed a 61% higher signal in the treated *Arabidopsis* roots compared to the untreated ones (Fig. 16 e, f, h). The signal was more concentrated in root cortex and epidermis cells, and was expressed in larger zones of the root apical meristem. This experiment was performed in a blinded manner, where the identity of each analysed sample and its treatment condition were unravelled only after signal quantification, giving us an increased confidence in the observed phenotypes from the different analysed lines. Thus, together the results at this point indicated that the RING/U-Box E3 protein can ubiquitinate

BLF1 and target it for proteasomal degradation and suggested that this contributes to keeping BLF1 levels low in the shoot apex and young leaf primordia in barley.

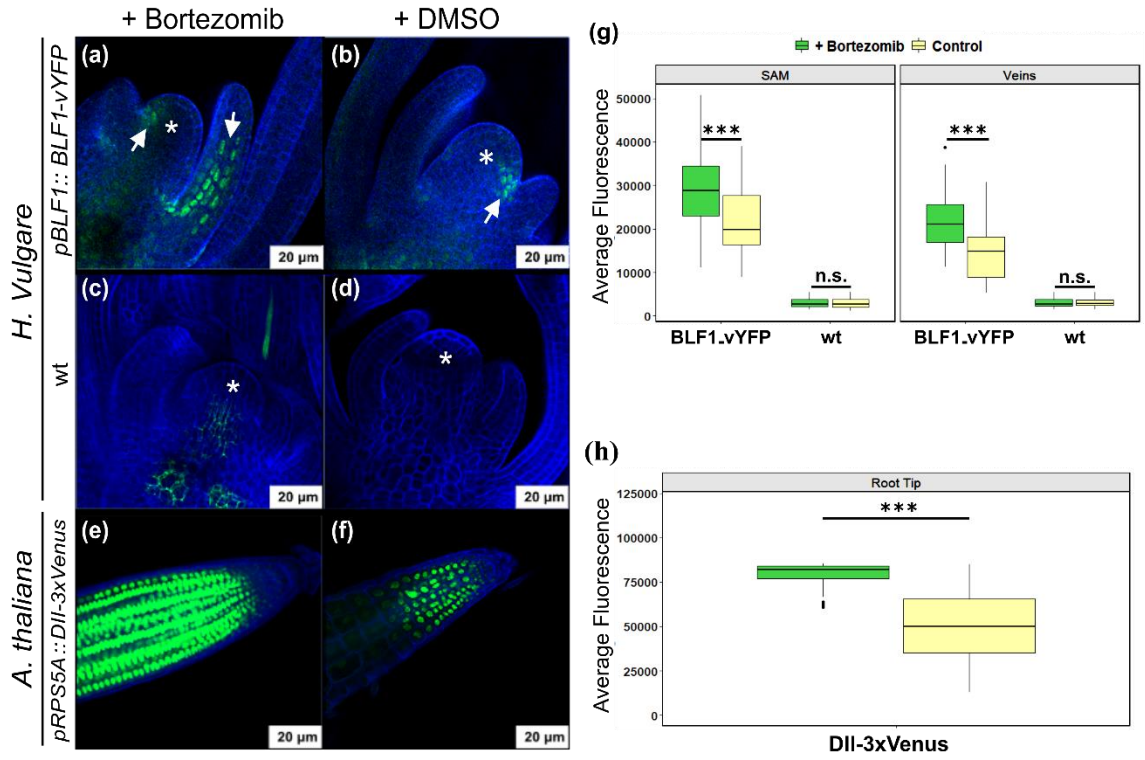

Figure 16. Effects of bortezomib treatments on the expression of *pBLF1:BLF1-vYFP* in barley. Confocal images of shoot apices of barley transgenic line expressing *pBLF1::BLF1-vYFP* **(a, b)**, barley wt plants used as negative control **(c, d)**, root tips of Arabidopsis line over-expressing *pRPS5A:DII-3xVenus* **(e, f)**. 7-day-old barley plants and 14-day-old *Arabidopsis* plants were treated either with 0.1 mM bortezomib or with DMSO for 16 hours before sample collection. Samples were prepared by tissue fixation using formaldehyde, Clearsee treatment, and incubation with propidium iodide to reveal cell periphery. Merged images are shown. Green channel: vYFP signal for *pBLF1::BLF1-Vyfp* and Venus signal for pRPS5A:DII-3xVenus. Scale bars are 20 pm throughout (a-f). Position of shoot apical meristem is indicated (white asterisks). BLF1-vYFP fusion protein is expressed at the basis of developing primordia and along developing veins (white arrows). **(g)** Average quantification of vYFP fluorescence from treated (+ Bortezomib) and untreated (+ DMSO) barley SAM and veins. **(h)** Average quantification of Venus fluorescence from treated (+Bortezomib) and untreated (+ DMSO) Arabidopsis roots. Quantifications were averaged over 30 different cells with the median as the horizontal line within each box. Black asterisks indicate significant differences after Student's t-test at $p<0.001$ (***) and $p<0.0001$ (****) or not significant (ns).

2.4.4 Analysis of genetic interaction of BLF1 and RING/U-Box E3 encoding genes

To determine the functional significance of the BLF1-RING/U-Box protein interaction, we generated genome-edited mutants by CRISPR/Cas9. Specifically, we used a construct with three gRNAs, two against *BLF1* and one against the *RING/U-Box* gene, to generate single and double mutants, so that we could ultimately also study a possible genetic interaction between the two loci (Fig. 17). To validate the desired genetic modifications, DNA from T0 lines was isolated and used for PCR amplifications of the targeted genes. PCR products were then analysed by Sanger sequencing to provide a quantitative assessment of the genome edits. Aligning the sequencing reads against the wt sequence for each gene, succeeded in identifying two independent mutant lines regenerated from two independent transgene-positive calli. One double mutant line (*blf1_a*, *ring-e3_2*) with 6 bp deletion (6 bp-Δ) in the first exon of the *RING-Ubox E3* gene resulting in 2AA deletion (Fig. 17a, c), and a 4 bp-Δ in the second exon of *BLF1* resulting in a premature stop codon (F184*) (Fig. 17b, c). The second transgenic line (*ring-e3_1*) that carries a single mutation in the *RING/U-Box E3* gene with 5 bp-Δ in exon1, resulting in a premature stop codon (L138*) (Fig. 17a, c). T2 populations were generated for each line and a first round of phenotyping with 60 segregating plants per line was performed. Leaf 3 parameters were measured for both T2 populations. While no significant change in leaf width, length or area was observed between the homozygous *ring-e3_2* mutant and the wt (Fig. 18a-c), a slight decrease in the leaf blade area was observed for the *ring-e3_1* mutant (Fig. 19c). A second round of phenotyping of the *ring-e3_1* single mutant line was performed with 200 segregating plants of an T3 population. We determined leaf dimensions for the 3rd and 4th leaves from each plant and genotyped them for the segregating locus. A slight but nonsignificant increase in leaf 3 and leaf 4 width of about 2-3% was observed for the *ring-e3_1* mutants compared to the wt (Fig. 20a). In contrast, a significant decrease in leaf length of the *ring-e3_1* mutants by ~4,6% and ~6% was observed for leaf 3 and leaf 4, respectively (Fig. 20b). Similarly, a significant decrease in leaf blade area was observed for the *ring-e3_1* mutants, mainly for leaf 4 by ~7,2% (Fig. 20c). For the *ring-e3_2 blf1_a* double mutant line, leaf 3 measurements did not show any significant difference in width, length or area in the *ring-e3_2* single mutant plants compared to the wt (Fig. 18a-c). Additionally, no noticeable change in leaf parameters was observed between the single and double mutant plants. In contrast, a significant increase in leaf width and area was observed for the *blf1_a* single mutants and the *ring-e3_2 blf1_a* double mutant plants compared to the wt (Fig. 18a, c).

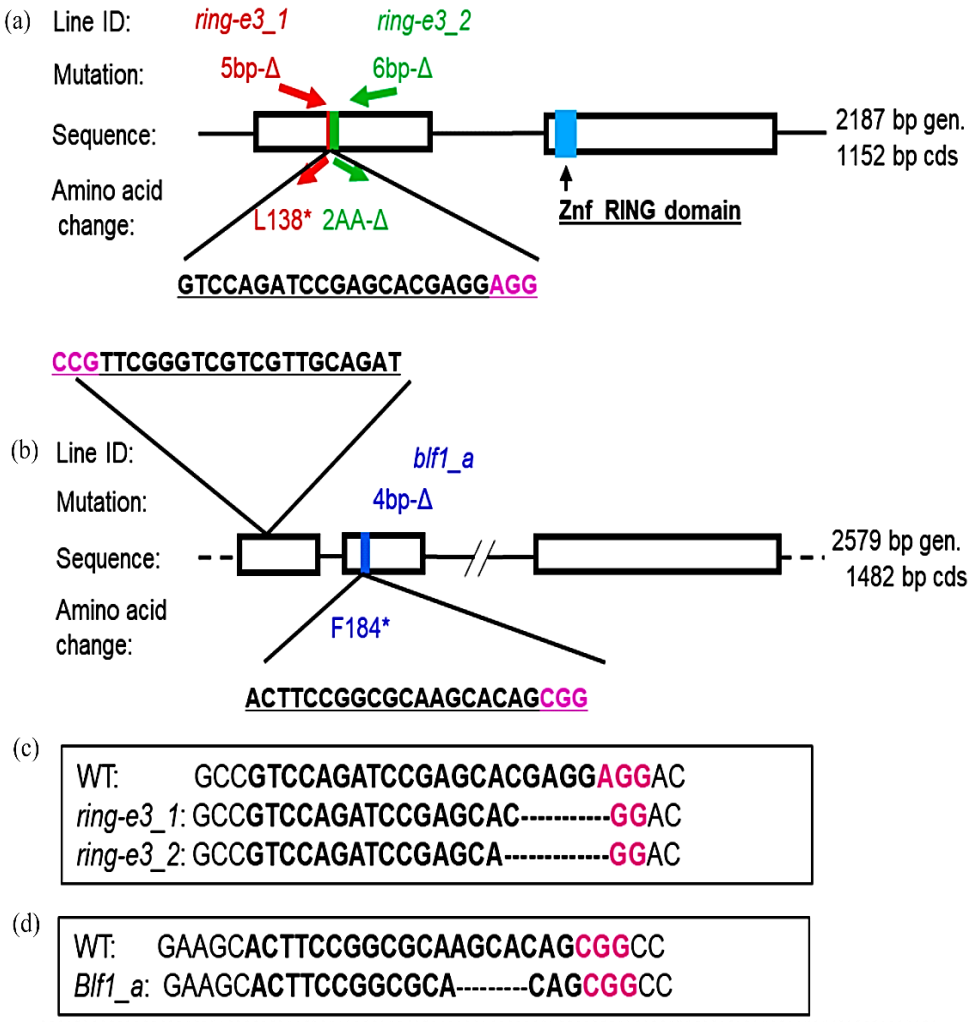

Figure 17. Identification of mutations in the *BLF1* and *RING-E3* genes.
(a, b) Gene structure of *RING/U-Box E3* **(a)** and *BLF1* **(b)** with mutant alleles, Cas9 target sites and predicted effects. For the genes, boxes show exons, lines show introns and dashed lines are UTRs. Underlined sequence was selected for targeting; nucleotides marked in pink represent PAM (protospacer adjacent motif). **(a)** Two editing events at the *RING/U-Box E3* exon 1 that resulted in two stable *Cas9*-free *ring-e3* alleles. One has a 5 bp deletion (named *ring-e3_1*) and the other 6 bp deletion (named *ring-e3_2*) near the PAM site. **(b)** An editing event at the *BLF1* exon 2 with 4 bp deletion near the PAM site that resulted in a stable *Cas9*-free allele (named *blf1_a)*. **(c-d)** The edited sequences from the *BLF1* **(d)** and *RING/U-Box E3* **(c)** at the target sites.

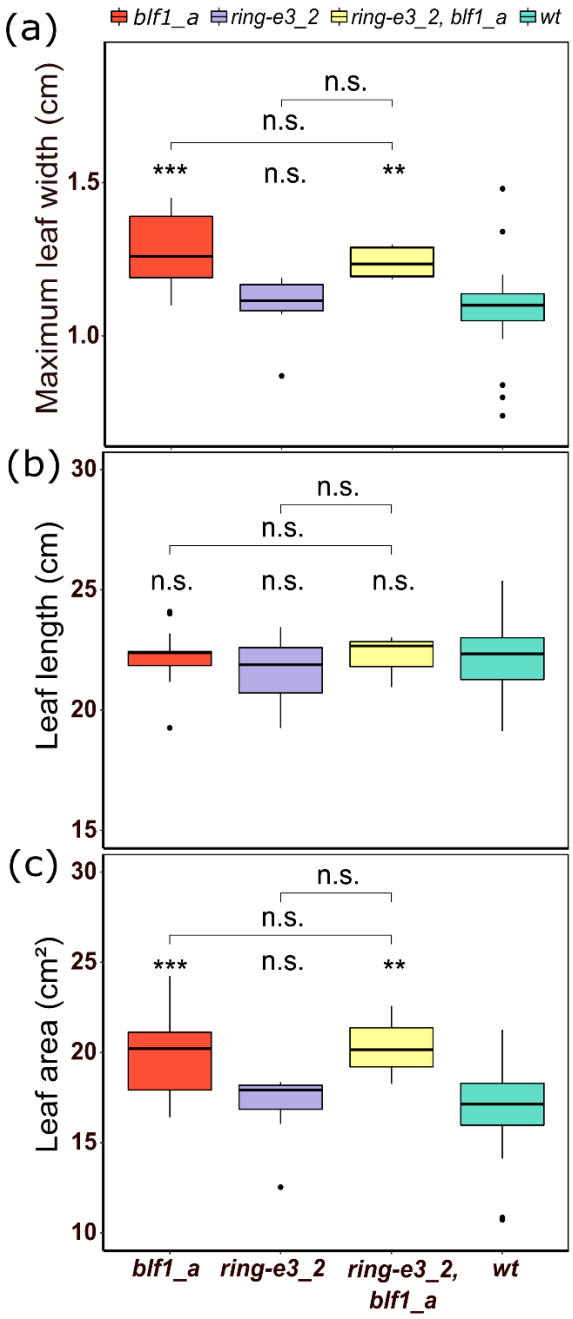

Figure 18. Phenotype of the *ring-e3_2, blf1_a* double mutant.
Maximum width **(a)**, length **(b)** and area **(c)** of mature leaf 3 blades from wt, *blf1_a*, *ring-e3_2 and ring-e3_2 blf1_a* mutants. Green boxes refer to wt, yellow boxes to *blf1_a* mutant, mauve boxes to *ring-e3_2* mutant and orange boxes to *ring-e3_2 blf1_a* double mutant. Legend for x-axes applies throughout **(A-C).** Box plots are mean ± SEM from 3-28 plants with the median as the horizontal line within each box. n = 60 T2 segregating plants. Asterisks indicate significant differences after Student's t-test at $p<0.05$ (*), $p<0.01$ (**) and $p<0.001$ (***) or not significant (ns).

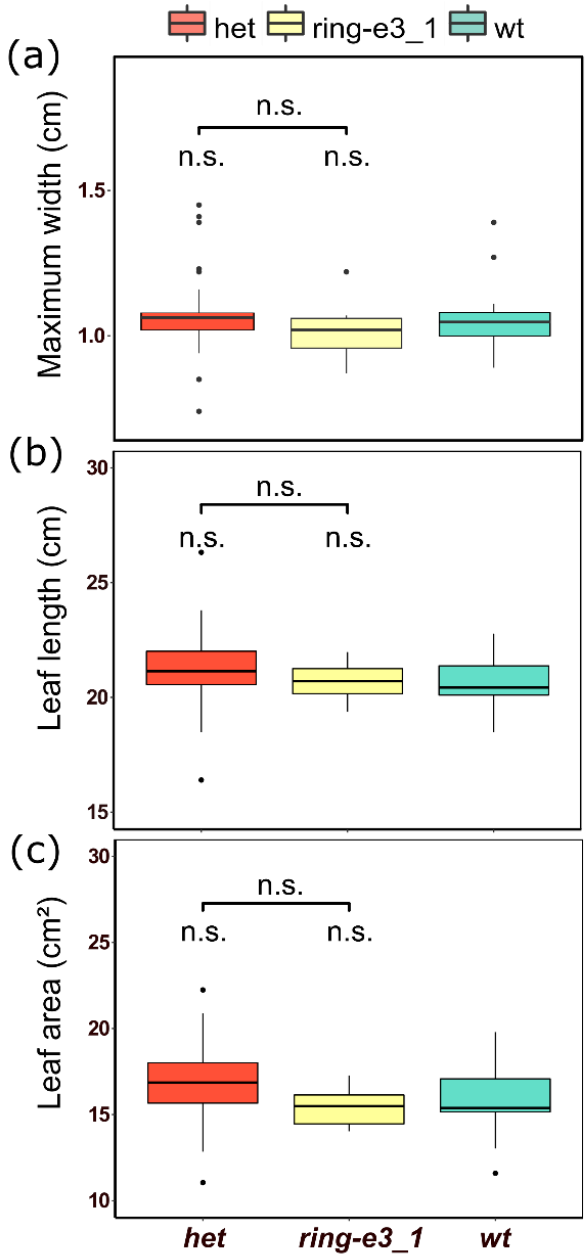

Figure 19. Small scale phenotyping of the *ring-e3_1* mutant.
Maximum width **(a)**, length **(b)** and area **(c)** of mature leaf 3 blades from wt, heterozygous (het) and homozygous (*ring-e3_1*) mutants. green boxes refer to wt, yellow boxes to heterozygous (het) plants and mauve boxes to *ring-e3_1* mutant. Legend for x-axes applies throughout **(a-c).** Box plots are mean ± SEM from 12-31 plants with the median as the horizontal line within each box. n = 60 F2 segregating plants. Asterisks indicate significant differences after Student's t-test relative to the wt at $p<0.05$ (*), $p<0.01$ (**) and $p<0.001$ (***) or not significant (ns).

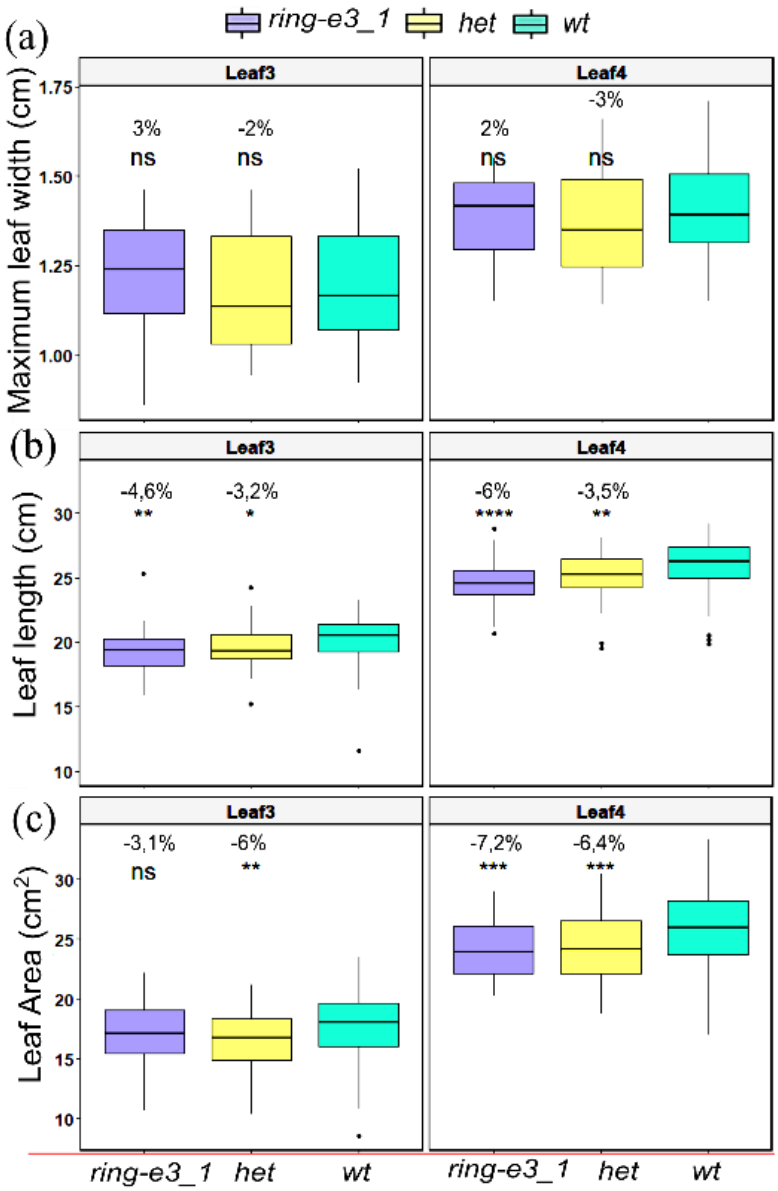

Figure 20. Large scale phenotyping of the *ring-e3_1* mutant.
Maximum width **(a)**, length **(b)** and area **(c)** of mature leaf 3 and leaf 4 blades from wt, *ring-e3_1* / + heterozygous (het) and *ring-e3_1* homozygous mutant plants. Legend for x-axes applies throughout (a-c). Box plots are as defined in Figure 4. Measurements are from 64 wild-type, 100 heterozygous and 35 *ring-e3_1* homozygous mutant plants identified by genotyping from 200 segregating T3 plants. Asterisks indicate significant differences after Student's t-test at $p<0.05$ (*), $p<0.01$ (**), $p<0.001$ (***) or not significant (ns).

Part3. Identifying additional factors acting together with *BLF1* in leaf-shape control by exploiting induced mutations and natural genetic variation

To identify natural modifiers acting together with *BLF1* in leaf width control, we crossed the *blf1* mutant line BW58 (in cultivar Bowman) to 20 genetically diverse barley landraces from the IPK Gatersleben germplasm collection and obtained hybrid F1 seeds for 13 of these crosses. From these, we generated F2 populations and for four of the F2s we grew 100 plants each in the greenhouse, measured their leaf 3 width and genotyped them for the *blf1* allele (Fig. 21). The frequency distributions of leaf 3 width among the wt and *blf1* mutant plants from each cross were analysed (Fig. 22 A-D). The homozygous mutant phenotype was clearly visible in all of the F2 populations. In the family resulting from the cross of Landrace1 (HOR_182.1) with *blf1* (Fig. 22A), the phenotype distribution amongst the homozygous *blf1* mutants presented a kind of bimodal distribution with two subgroups segregating in classical Mendelian ratios; with 1/3 for plants with narrower leaves compared to the *blf1* phenotype and 3/4 for plants with the original *blf1* phenotype. This suggested potentially a polygenic modulation of the phenotype. However, for the other crosses of *blf1* with landrace 2 (HOR_337.2), landrace 11 (HOR_4463.11) and landrace12 (HOR_4469.12), we did not detect a clear single-locus modifier in any of them, which would have been visible by a clear segregation of leaf width amongst the homozygous *blf1* mutants (Fig. 22 B-D). All of the 3 crosses represented a normal distribution of the *blf1* phenotype. Due to time constraints, it was not possible to pursue the phenotypic analysis of the F2 population from the other 9 crosses.

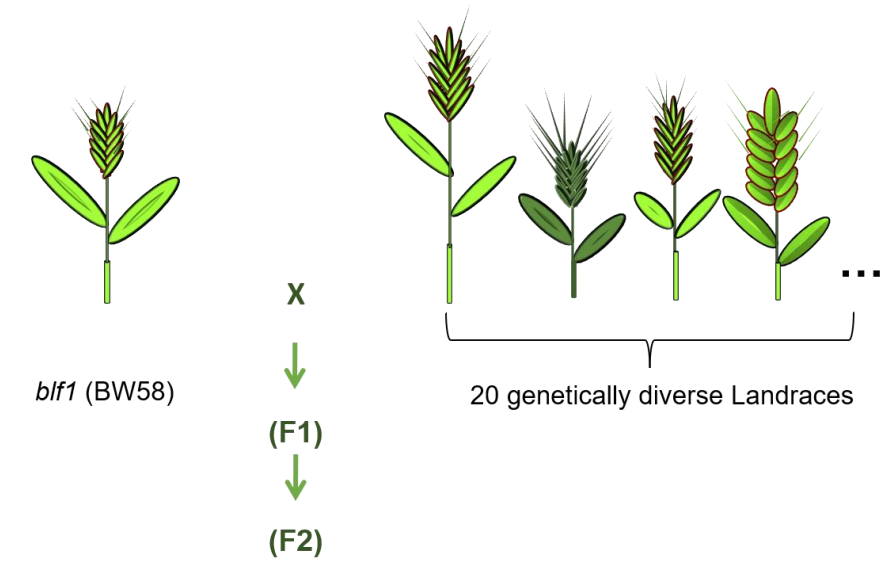

Figure 21. Schematic diagram of the experimental setup used to identify additional factors acting together with *BLF1* in leaf shape control.
blf1 mutant BW58 obtained in cultivar Bowman was crossed to 20 genetically very diverse barley landraces from the IPK Gatersleben germplasm collection. An F2 population was generated for each cross, genotyped to identify *blf1* mutants then phenotyped for leaf 3 width.

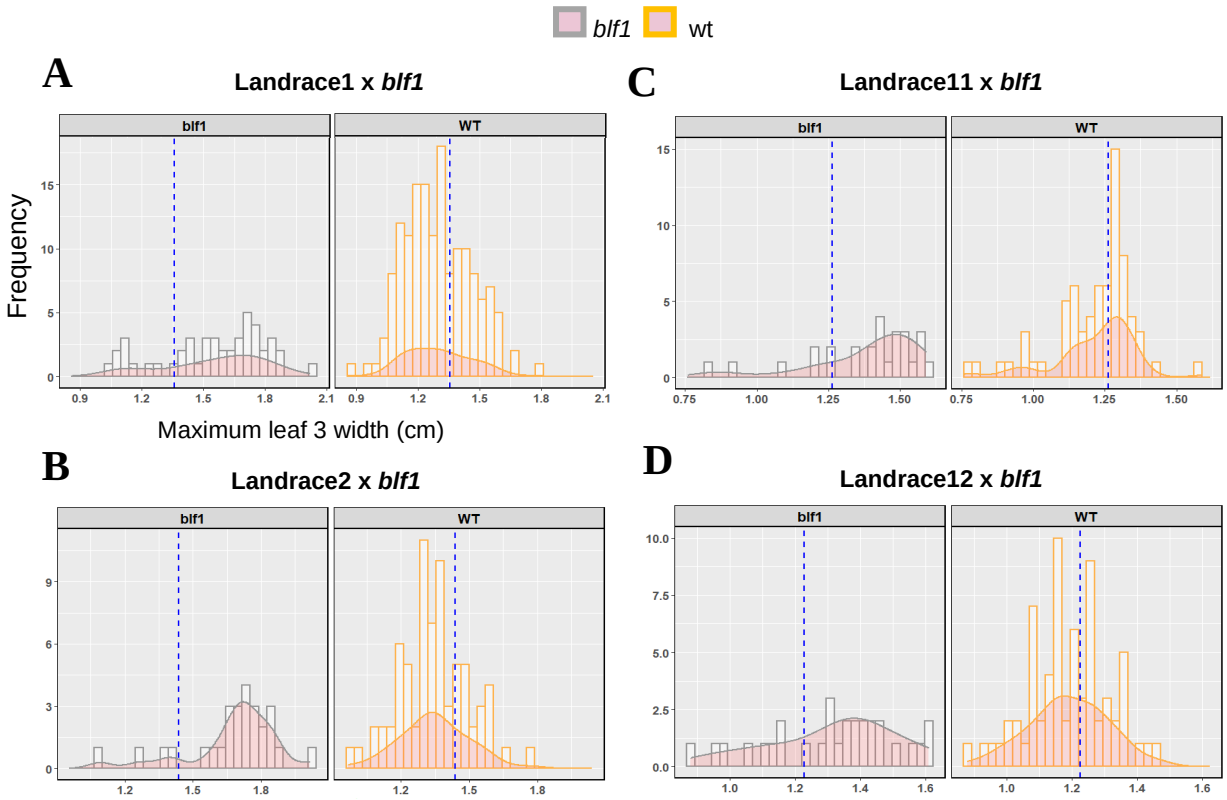

Figure 22. Frequency distribution analysis of leaf 3 width phenotype in Landrace x *blf1* crosses. **(A-D)** Frequency distribution of the leaf 3 width data for different F2 population for wt and *blf1* mutants. Histograms represent the observed distribution. Charts with orange outlines represent the wt population, those with grey outlines represent the *blf1* population. Dotted lines represent the mean value for each population, with n=100 plants analysed per cross.

4. DISCUSSION

4.1 Test for physical and genetic interactions between *Blf1* and *SLN1*

BLF1 has been described as an IDD family protein that limits lateral growth of leaves by inhibiting cell division in the width direction during primordia outgrowth. Concerning the molecular mode of action of IDD proteins, a model is beginning to emerge that has IDD proteins interacting with transcriptional co-regulators of the GRAS family and thus providing a DNA-binding platform for these factors (Yoshida *et al*., 2014; Yoshida and Ueguchi- Tanaka, 2014). Such an IDD/GRAS interaction has first been shown for AtIDD10/JKD and the GRAS proteins SHORTROOT and SCARECROW in root development (Welch *et al*., 2007); more recently five AtIDD proteins including AtIDD1 and AtIDD3 have been demonstrated to bind to the DELLA repressors of gibberellic-acid (GA) signalling and the SCL3 protein, a positive regulator of GA signalling, all of which belong to the GRAS family (Yoshida *et al*., 2014). The latter observation suggests that IDD proteins fine-tune GA signalling by a co-factor exchange model involving positive and negative regulators (Yoshida & Ueguchi-Tanaka, 2014). However, less is known about this interaction in monocots. In contrast to *A. thaliana* and other dicotyledonous plants, the rice and barley genomes encode only a single DELLA protein termed SLENDER RICE1 (SLR1) or SLENDER1 (SLN1), respectively (Ikeda *et al*., 2001; Chandler *et al*., 2002).

During this study the targeted yeast-two-hybrid system was used to test the physical interaction between the BLF1 and SLN1 proteins. BLF1 was shown to not interact with SLN1. Separately, each of these proteins was able to interact positively with other partners, GID1 and cDNA library coding proteins (see above, part2), for SLN1 and BLF1, respectively. Interaction between GID1 and SLN1 is in accordance with previous data from *Arabidopsis* and maize, suggesting that GID1´s function is also conserved in barley. Indeed, in the presence of bioactive GA, GID1 undergoes conformational changes in the N-terminal region (Murase *et al*., 2008). Consequently, the GA–GID1 complex can bind to the TVHYNP motif of the DELLA protein, which results in a new conformational modification that further stabilizes the GA–GID1–DELLA complex (Murase *et al*., 2008; Ueguchi-Tanaka *et al*., 2007). Upon complex formation, the GRAS domain of the DELLA protein also undergoes structural changes to allow its recognition and binding with F-box proteins (Gomi *et al*., 2004; Sasaki *et al*., 2003). These F-box proteins are responsible for the recruitment of DELLAs to the SCF (SKP1, CULLIN, F-box) E3 ubiquitin–ligase complex to be polyubiquitinated and subsequently degraded by the 26S proteasome (Lechner *et al*., 2006). Thus, this interaction between SLN1 and GID1 indicated that SLN1 was successfully expressed in our yeast-two-hybrid system and supported our conclusion that there is no physical interaction between BLF1 and SLN1.

It has been documented that GRAS proteins have been actively diversified during speciation of dicots and monocots, similar to the pattern observed in IDD evolution (Cenci & Rouard, 2017). This was further confirmed by a recent phylogenic analysis, performed by Prochetto & Reinheime (2020), studying the diversity of IDD members in grasses based on their conserved features: N-terminal nuclear localization signal (NLS), four zinc finger domains comprising two CCHH and two CCHC residues, and a C-terminal coiled-coil domain (Coelho *et al.*, 2018).

Through this analysis, BLF1 was found to be genetically distant from AtIDD1, AtIDD3 and AtIDD10 and located on a completely different clade. Hence, this lack of physical interaction between the barley proteins SLN1 and BLF1 might be due to a change in the conserved motif mediating this interaction. This hypothesis is further supported by a study of Hirano *et al.* (2017) showing that IDD proteins interact with the GRAS domain protein SHR via the SRBM binding motif at the end of ZF4. Interestingly, this motif is conserved in all IDDs except in the *K. nitens* IDD sequence and SG5 lineage. This suggests modification or lack of interaction between such proteins. Furthermore, the physical interactions between IDDs and members of the DELLA GRAS subfamily were impaired when motifs MGC-M16 (SATAL) and MGM-M17 were absent. This might be also the case for BLF1 and SLN1 in barley, where interaction is impaired due the subsequent diversification of IDD lineages.

To complement these physical interaction studies, we asked whether BLF1 and SLN1 interact genetically. Double mutants between a strong *blf1* loss-of-function allele and the *Sln1d* dominant gain-of-function allele (Chandler *et al*., 2002) were generated and analyzed relative to the single mutants. Leaf dimensions for the 3rd and 4th leaves from the F3 population were measured. *blf1* mutant plants presented wider and slightly shorter leaf blades compared to the wt. Histological analysis performed by Jöst *et al.* (2016) on the classical barley mutant *blf1-1* indicated that this increase is due to more cell division in the width direction during primordia outgrowth. Due to compensation of the extra width growth by the reduction in length, no significant change was observed in the overall leaf blade area of *blf1*.

By contrast, *Sln1d* mutants presented slightly narrower but significantly shorter leaves compared to wt, resulting in a significant decrease in the overall leaf blade area. *SLN1* is characterised as a negative regulator of GA responses in aleurone cells. The dominant dwarf allele *Sln1d* results in aleurone cells that are less sensitive to GA. Additionally, *Sln1d* mutants were shown to have greatly reduced contents of SLN1 protein, and large changes in the amounts of bioactive GAs, and of their metabolic precursors and catabolites (Chandler *et al*., 2002). Hence the significant reduction in *Sln1d* leaf length could be due to the impaired dynamic interactions between SLN1 protein and GA content in determining leaf elongation rate. However, combination of the *blf1* with the *Sln1d* allele only resulted in additive phenotypes, indicating independent effects of the two loci on leaf growth.

One possible explanation for this could be attributed to the differential expression of these two genes in time and space. According to Chandler *et al.* (2002), SLN1 protein was localized in highest amounts in the basal part of the Elongation Zone (EZ), declining progressively toward the distal end of the EZ, whereas BLF1 protein is known to be localized in the SAM and at the basal part of young leaf primordia (Jöst *et al*., 2016). Hence, although both genes are proved to be involved in the regulation of cell proliferation, their expression could be coordinated over time, and as such, their regulatory networks are linearly organized in the barley leaf. Indeed, serval molecular factors regulating cell proliferation are shown to act via independent networks. For example, *OsNAL1* in rice, promotes cell proliferation through regulation of auxin-transport (Qi *et al*., 2008), whereas *HvHNT1*, the *NAL1* ortholog in barley, positively

regulates cell division through interaction with HvPPIas to stabilize protein folding (Ye *et al*., 2019).

Although several IDD proteins have a conserved function between monocot and dicot species, such as the *ZmID1, AtIDD8* (*NUC*) *and OsID1* (*RID1*) (reviewed by Prochetto & Reinheimer, 2020) all shown to regulate the transition to flowering in maize, *Arabidopsis* and rice, respectively, it is still hard to determine one-to-one orthologous relationships between the *Arabidopsis* and grass *IDD* gene family members due to the divergence times between these two lineages.

4.2 Dissecting the molecular mechanism of the *BLF1* gene in leaf shape control

The aim of this part was to identify which molecular mechanism is deployed by BLF1 to regulate leaf width in barley. As a member of the IDD protein family, BLF1 contains four zinc finger domains responsible for DNA binding and a coiled-coil domain mediating protein-protein interaction. In principle, two complementary strategies to address the molecular mechanism of BLF1 function in an unbiased manner are required: a DNA-protein interaction method to identify the BLF1 targeted genes, and a protein-protein interaction method to identify its interacting proteins.

The DAP-seq system was used with the aim of identifying target genes of BLF1. All steps and quality control check points of this approach were performed successfully as indicated by Bartlett *et al*. (2017).

VRS1, a homeodomain-leucine zipper (HD-Zip) TF, was used as a positive control to assess the successfulness of the DAP-seq approach. Thus, the absence of any plausible VRS1-bound sequences should have technical causes, such as the large size and the high repetitiveness of the barley genome. In fact, the only species other than *Arabidopsis* where DAP-seq was used successfully is maize and only very few papers on this are available. This may suggest that this method is not so robust when using large-genome species.
Which alternative screening strategies could be chosen to isolate the potential targets?

First, one could use ChIP-seq (Chromatin immunoprecipitation sequencing) on our transgenic barley line expressing *pBLF1::BLF1-vYFP* to identify relevant DNA sequences targeted by BLF1. To this end DNA-protein complexes could be affinity-purified and the bound DNA fragments within these complexes identified by Next generation Sequencing. However, the limited amount of starting material due to the restricted zones where BLF1 is expressed, including SAM, leaf primordia, and inflorescence meristem (Jöst *et al*., 2016), and the overall low protein level of BLF1 in barley plants make this approach impossible, unless one could develop an anti-BLF1 antibody to increase the specificity of the assay and allow for a better enrichment of the protein, which might be a costly option. We attempted to generate a peptide-specific antibody against BLF1 in collaboration with the local Antibody Technology group at the University of Potsdam. While the antiserum could detect recombinant BLF1 protein, it failed to detect a band in extracts of barley plants (data not shown). In previous trials, some preliminary experiment (data not shown) had suggested that the BLF1-YFP protein could be

detected by GFP antibodies in protein extracts of shoot apices. However, this could not be replicated in further repeats of the blot. Additionally, an attempt to enrich for the protein was performed by immunoprecipitation with the μMACS GFP isolation kit and this was checked by Western blot with anti-GFP antibody. Even under these conditions, we could not detect the protein (data not shwon). Therefore, we had to abandon the search for target genes by ChIP-seq.

As an alternative approach and to circumvent the low abundance of the BLF1 protein in plants, we used DAP-seq as an *in vitro* method (Bartlett *et al*., 2017). This approach is supposed to present a large-scale analysis of the IDD family, providing a rich resource of cis-regulatory regions controlling many crucial pathways in plant development such as leaf differentiation, transition to flowering, seed germination and maturation, root development, disease resistance and stress tolerance. Surprisingly, we observed no differences in the sequence motifs identified by peak calling from the DAP-seq reads between the BLF1 and the VRS1 screens. Both sequences identified for each transcription factor were corresponded to repetitive sequences from the barley genome (Fig. 4h). Many reasons can explain this inefficiency of the DAP-seq approach in identifying specific targets for barley transcription factors. First of all, it is plausible that with such a large genome size of 5.1 Gbp where more than 80% is formed of repetive elements (reviewed by Sato (2020)), the transcription factor-bound matrix is swamped by non-specific DNA fragments, resulting in excessively high background. The interpretation that DAP-seq may not be easily transferrable to species with larger genomes is supported by personal communication with Steve Kelly from Oxford University, whose lab has invested considerable time and resources into applying DAP-seq to grass genomes, but could not achieve any consistent results, and by the observation that since the original publication of DAP-seq there have only been few publications using the method in species with larger genomes, such as maize (Bartlett *et al*., 2017). Secondly, although we used a wheat based *in vitro* protein expression system to generate our affinity-tagged proteins, this still can not fully mimic the *in vivo* expression environment in barley. Indeed, its likely that transcription factors that require the formation of complexes or posttranslational modifications to bind to DNA, are not suitable for DAP-seq approach. All these given reasons could be good explanations for our DAP-seq results.

As a complimentary approach, the yeast-two-hybrid system was used to identify proteins that bind to BLF1. All screens were performed to saturation as indicated by library transformation and mating efficiency as well as the number of interacting proteins identified. However, it might still be possible that not all proteins involved in the BLF1 regulatory pathway were accessible mainly because some proteins interact within multi-subunit complexes or require posttranslational modifications to bind to other proteins. Both requirements are usually not met in the yeast screening system.

Other complementary screening strategies could be chosen to isolate BLF1 interacting proteins. One could suggest a biochemical approach such as Immunoprecipitation on epitope tagged BLF1 protein expressed under *in vivo* conditions. The output from this approach might seem more pertinent than that from the yeast-two-hybrid screen. However, the levels of BLF1-YFP

in the transgenic plants were too low for immunoprecipitation. For that, the yeast-two-hybrid system was the best option for us to search for BLF1 interacting proteins.

The screen resulted in six main interacting proteins describes as follows: (1) one with a very broad function involved in the Golgi retrograde transport, (2) kinase protein member of the DYRK-like superfamily involved in signalling pathways that are important in regulating a variety of cellular events such as cell proliferation and the regulation of gene expression (Furuya *et al*., 2021), (3) RING-U-Box E3 ligase mediating ubiquitylation and proteasomal degradation, (4) BTB/POZ & MATH domain substrate adaptor required for the formation of Ub-E3-substrate complexes, (5) EB1 modulating microtubule dynamics and cytoskeleton arrangements, and (6) POK1 involved in the orientation of mitotic cytoskeletal arrays and placing cell walls. Given the functional characterization of these selected proteins and their possible relatedness to the BLF1 regulatory pathway we excluded the first protein from all further analysis and focused on the remaining ones. These findings led to two hypotheses concerning the BLF1 regulatory pathways: (1) that BLF1 might be involved in the orientation of the cell division plane, (2) that BLF1 protein is regulated via ubiquitylation and proteasomal degradation. These two hypotheses needed to be further characterised in order to draw firm conclusions out of them. For that, the rBiFC assay was used to confirm the specific binding of the candidate proteins to BLF1 *in planta.* The output from this approach confirmed the interaction of BLF1 with all candidate proteins, except POK1. This finding was completely expected given the fact that these two proteins are known to be localized in two different cellular compartments, as BLF1 is localized in the nucleus whereas POK1 is known to have cytoplasmic localization. Indeed, phenotypic characterization of POK1 orthologs in *Arabidopsis* and maize showed their involvement in the orientation of mitotic cytoskeletal arrays and cell-wall positioning (Müller *et al*., 2006). Although no positive interaction was detected between BLF1 and POK1 in the rBiFC system, these two proteins could still interact at early stages of the cell cycle before the nuclear membrane forms, and POK1 could still regulate BLF1 function by re-orienting cell division toward length direction during primordia outgrowth which explains the extra cell files formed in width direction observed in *blf1* (Jöst *et al*., 2016).

Additionally, comparison of the YFP signal intensity among all analysed protein combinations, revealed a weak interaction between BLF1 and the BTB/POZ. This latter is identified as a substrate-specific adapter of an E3 ubiquitin-protein ligase complex (CUL3-RBX1-BTB) which mediates the ubiquitination and subsequent proteasomal degradation of target proteins in animal, human and plant cells (Pintard *et al*., 2003; Weber *et al*., 2005), suggesting that BLF1 and BTB/POZ probably interact indirectly. As it has already been discussed above, rBiFC analysis can detect the presence of proteins within the same macromolecular complex even without a direct contact between the proteins fused with cYFP/nYFP (Kerppola, 2013). We assume that the interactions between BLF1 and PTB/POZ is indirect. This was further confirmed by several studies showing that a notable feature of E3s is their tendency to exist as multi-subunit assemblies (O'Connor & Huibregtse, 2017), which explains the huge variety in the mechanisms of substrate recognition by RING-type E3s that occur in the context of networks of interactions that often include a cullin, a RING protein, and a substrate receptor,

and adaptor proteins that bridge the substrate receptor to the cullin protein (Sarikas *et al*., 2011). In *Arabidopsis*, AtCUL3a and AtCUL3b assemble with BTB/POZ and AtRBX1 proteins to form functional E3 ligases (Weber *et al*., 2005), suggesting that targeting BLF1 for ubiquitylation might also be mediated by an E3 ligase complex that deploys the BTB/POZ as a substrate adaptor.

Similarly, a medium YFP signal was detected for BLF1 and EB1A. Actually, interaction of these two proteins was unexpected, given their different subcellular localizations. In *Arabidopsis*, EB1A is identified as a plus-end-tracking protein (+ TIP) that localizes to microtubule plus ends where it modulates their dynamics and interactions with intracellular organelles (Vitre *et al*., 2008) and plays a key role in orienting the division plane (Chan *et al*., 2005). For that, EB1A has a cytoplasmic localisation, whereas BLF1 is present in the nucleus, which makes the interaction between these two proteins not possible under the rBiFC conditions. However, as discussed previously for POK1, BLF1 and EB1A could still interact at early stages of the cell cycle before the nuclear membrane forms, and EB1A could still regulate BLF1 function by re-orienting cell division toward length direction during primordia outgrowth.
Besides, this assay confirmed the interaction of BLF1 with the E3 ligase and the E3 substrate adaptors, RING/U-Box and BTB/POZ, respectively, leading to the hypothesis that BLF1 might be regulated via ubiquitylation and proteasomal degradation. This hypothesis is further supported by the low level of the BLF1 protein in barley as well as the plant sterility caused by BLF1 overexpression.

To provide stronger evidence for the interaction of BLF1 and the identified candidate proteins, we used Co-IP as a complementary biochemical approach. To this end and based on our previous findings from the yeast-two-hybrid screen and rBiFC, we established a new experimental set in which we combined proteasome inhibitor treatment and nuclei protein isolation of transiently expressed proteins in tobacco cells, to allow a better enrichment of the studied proteins. A first attempt to immunoprecipitate epitope tagged BLF1 from total protein extracts of tobacco leaves without any proteasome inhibitor treatment did not detect any interacting protein (data not shown). Only after including the MG132 treatment and nuclei protein isolation steps it was possible to co-immunoprecipitate the putative interactors with Halo-tagged BLF1. No precipitation of the interactors was achieved when expressing the Halo-tag alone. This finding supports the idea that all four proteins can specifically and strongly interact with BLF1 in a heterologous plant system.

Both the rBiFC and Co-IP assays indicated that BLF1 could interact with the four candidate proteins. However, both approaches are in disagreement regarding the strength and specificity of the protein interactions, particularly the BLF1 and PTB/POZ interaction. At this point, it is hard to draw a firm conclusion about how closely and specifically these two proteins interact together. This required further characterisations using more pertinent approaches.
To this end, two complementary approaches that deeply study the physical and genetic interaction of proteins were used to shed light on the mechanism through which the RING/U-Box and PTB/POZ E3 ligases control the BLF1 function.

FRET was used to determine whether BLF1 and the BTB/POZ substrate adaptor or the RING/U-Box E3 proteins interact directly. No significant FRET was detected between BLF1 and BTB/POZ, even after MG132 treatment: Although this finding might disagree with our previous ones from the Y2H, rBiFC and Co-IP assays, showing that BLF1 interacts with BTB/POZ, the absence of FRET between the two proteins may be explained by several reasons. First, although yeast has been extensively used as a model to unravel the interactions of plant proteins, it still lacks the complexity of the *in vivo* system of higher organisms (Nagy, 2008). Thus, data from a Y2H approach studying plant protein interactions might not be very reliable. Additionally, diploid yeast cells carrying BLF1 and BTB/POZ plated on SD/-LTU media, used to select for strongly interacting proteins, grew very weakly and had a growth profile similar to that of the medium positive control, suggesting that even in yeast, interaction of the two proteins was not considered strong. Secondly, according to our rBiFC data BLF1 and BTB/POZ presented the weakest interaction compared to the other candidate proteins. Additionally, one major disadvantage of the rBiFC approach is that the reassembly of the YFP halves is irreversible, this might cause artifactual results even in the absence of a true interaction (Hecker *et al*., 2015). Thus, the weak interaction detected between BLF1 and BTB/POZ could be simply an artifact. For this reason, we opted for FRET as an alternative, more reliable and rigorous technique than Y2H and rBiFC to study PPIs.

Additionally, a more plausible explanation for the absence of FRET signal between BLF1 and BTB/POZ can be simply that the two proteins do not interact directly, but instead they interact within a protein complex. This in fact is in accordance with our previous hypothesis, suggesting that BTB/POZ is part of the E3 protein complex that mediates BLF1 degradation. Indeed, as mentioned previously, some E3 ligases associate with an adaptor that plays a key role in the substrate recruitment. For example, for SCF ligases the cullin, CUL1, binds the RING protein, the RING protein recruits the E2, and the substrate receptor proteins (F-box proteins) recruit the substrate. SKP1 serves as an adaptor that connects the cullin to the F-box protein (O'Connor & Huibregtse, 2017). Hence, binding of substrates by these E3s may occur indirectly, which explains the absence of FRET between BLF1 and the candidate BTB/POZ.

In contrast, a clear FRET signal was detected between BLF1 and RING/U-BOX E3 after MG132 treatment, suggesting that RING/U-Box E3 ligase directly interacts with BLF1 to mediate its ubiquitylation and proteasomal degradation. This hypothesis was further confirmed by two more findings: (1) the decrease of the BLF1 level detected in tobacco cells when co-expressed with the RING/U-Box E3, and (2) the enrichment of BLF1 quantified proteins after inhibition of the proteasomal degradation when co-expressed with RING/U-Box, but not when alone or with BTB/POZ. This change in the protein level is specifically related to the presence of RING/U-Box E3 ligase, as in the absence of this latter the BLF1 protein level is stable in tobacco cells.

The efficiency of the protein expression system and the drug treatment in studying the enrichment of the transiently expressed proteins was confirmed by the increase in the amount of the two E3s after blocking the proteasomal degradation. Apart from targeting a protein substrate and canalizing its ubiquitylation; E3s often mediate their own ubiquitylation and protein turn-over (Kim *et al*., 2011; Keren *et al*., 2012), such stabilization is often seen for E3s.

These findings up to now are in line with the previous hypothesis suggesting that BLF1 is regulated through ubiquitylation and proteasomal degradation to maintain a low protein level in barley plants.

To determine whether either of the two E3 ligases could ubiquitinate BLF1, we used a recently developed system by Keren *et al.* (2012) that reconstitutes the eukaryotic ubiquitination cascade in *E. coli* and allows testing whether a putative E3 ubiquitin-ligase can ubiquitinate a substrate protein. The main advantages of using *E. coli* as an expression system are: (1) the absence of deubiquitylating enzymes, which renders the modified product fully stable. As a result, the system yields large amounts of ubiquitylated proteins that can be easily purified (Keren *et al*., 2012). (2) It allows to study the protein ubiquitylation under *in vivo* conditions which provides more reliable data than the *in vitro* systems. First, we evaluated the functionality of this bacterial system by testing the ubiquitination of the Ubiquitin receptor from yeast Rpn10 by its cognate E3 ligase ScRsp5 and E2 ScUbc5, and an E1 from plants AtUba1. As shown by Keren *et al*. (2012), the system succeeded to faithfully recapitulate the ubiquitylation of Rpn10 only when all the ubiquitination cascade components are present. Then, we adapted the system to express BLF1 as substrate, RING/U-Box or BTB/POZ as E3 ligases, and E1 and E2 also from barley. This demonstrated that the RING/U-Box E3 protein can ubiquitinate a GST-BLF1 fusion protein by associating a poly-Ub chain linkage on the protein, and that this requires the presence of its cognate E2 (HvUbc11), indicating that it represents the activity of a canonical ubiquitination pathway.

In the ubiquitylation process, particular protein–protein interactions govern several levels of specificity, including the interactions of E1:E2, E2:E3 and E3: substrate. For that, we assessed the substrate specificity of the RING/U-Box E3 in this bacterial system, and we found that RING/U-Box E3 could not ubiquitinate the GST-tag alone. Similar results proving the E3:substrate specificity were shown by Keren *et al*. (2012) with Rsp5-dependent ubiquitylation of Cps1, where co-expression of Uba1, Ubc4, Rsp5 and the Cps1–GST fusion in the bacterial system was sufficient for the ubiquitylation of Cps1p. In contrast, GST alone was not ubiquitylated. Next, we assessed the requirement for E2 in the ubiquitylation process by showing that RING/U-Box E3 is not able to ubiquitylate the GST-BLF1 fusion protein when the cognate E2 enzyme HvUbc11 was missing. This is also consistent with our findings with Rpn10, showing that deletion of the E2 enzyme from the bacterial system inhibits the substrate ubiquitylation, and that only when all components are co-expressed, ubiquitylation is observed. This system managed to faithfully reconstitute the BLF1 ubiquitylation cascade in bacteria and proved that RING/U-Box E3 and HvUbc11 can mediate this process. In contrast, the BTB-POZ had no effect on GST-BLF1 fusion protein. This finding supports our previous hypothesis which has been discussed above, suggesting that the BTB-POZ acts as an E3 adaptor that helps to stabilize the E3-substrate complex which, in turn, mediates the substrate ubiquitylation. Hence, the BTB/POZ adaptor by itself is not able to induce the substrate ubiquitylation in the bacterial system. This would also explain the weak interactions observed in the Y2H and rBiFC, and the absence of FRET between BLF1 and BTB/POZ.

Following up, as all our previous findings are obtained from different organisms that are evolutionary distant from barley, we wanted to determine whether the barley endogenous BLF1

protein is degraded via the proteasome pathway. For that, we tested whether the potent proteasomal inhibitor bortezomib (PS-341), which binds to the N-terminal Thr residue of the b1 subunit within the 26S proteasome (Richardson *et al*., 2003), results in increased BLF1 accumulation in a barley transgenic line expressing BLF1-YFP under the control of the endogenous BLF1 promoter. While MG132 and epoxomicin treatments did not result in a statistically significant increase in BLF1-YFP levels, treatment with bortezomib led to ~50% higher BLF1-YFP levels in the SAM and veins than in untreated plants. Indeed, bortezomib was shown to have a higher efficiency in *Arabidopsis* and to be metabolically more stable in human cells than MG132 and epoxomicin and thus might represent a better agent to block 26S proteasome activity *in planta* (Gladman *et al*., 2016; Purras- *et al*., 2021). The increase in BLF1-YFP protein after bortezomib treatment indicated that BLF1 expression might be regulated post-translationally by the 26S proteasome. This is consistent with the low level of the BLF1 protein in barley as well as the plant sterility caused by BLF1 overexpression, suggesting that proteasome degradation contributes to keeping BLF1 levels low in the shoot apex and young leaf primordia in barley to maintain the growth balance and functional homeostasis. Results from the positive control confirmed the efficiency of the deployed bortezomib treatment. The treated *Arabidopsis* plants displayed higher DII-3xVenus signal compared to the untreated ones. Similar results from Brunoud *et al*. (2012), using the same reporter line, showed that MG132 treatment resulted in an enrichment in the DII-VENUS protein.

To determine the functional significance of the BLF1 and RING/U-Box protein interaction, we generated genome-edited mutants by CRISPR/Cas9. Ideally, two independent strong loss-of-function alleles for the *RING/U-BOX* gene would be required to be able to draw firm conclusions about the functional relationship between genes based on phenotypic readouts. Yet, despite screening several hundred plants with the CRISPR/Cas9 construct, we were only able to identify two mutant lines. While the 5 bp deletion in the first exon of the *RING/U-BOX* gene resulted in a frameshift and early stop codon, likely abolishing the activity of the gene, the effect of the 6 bp deletion also in exon1 is likely to be more subtle. The line with the 6 bp deletion also carries a 4 bp deletion in the *BLF1* gene resulting in premature stop codon.

Our first round of phenotyping showed a clearly visible phenotype with the expected wider leaves for the homozygous *blf1_a* mutant of the T2 population generated from selfing the *ring-e3_2 blf1_a* double mutant line. However, it did not uncover a statistically significant change in leaf width for the two *RING/U-BOX* mutant alleles (*ring-e3_1* and *ring-e3_2*), even though there was a slight tendency to reduce the overall blade area for the 5 bp deletion line. Therefore, we repeated this experiment with a larger number of plants from the *ring-e3_1* line to test whether a significant effect on leaf size will be found.

Phenotypic characterization of 200 T3 plants segregating for the *ring-e3_1* (5 bp-Δ) mutant allele showed no significant change in leaf width, versus a highly significant decrease in leaf length and blade area mainly for leaf 4 of the homozygous mutants. This suggests that the *RING/U-BOX* gene is involved in the control of leaf growth by promoting its longitudinal growth. These findings are further supported by previous studies focusing on the role of *RING-type E3* genes in the control of both vegetative organs and seed growth in monocot and dicot

species. Among these, is the RING-type E3-ligase TaBAH1 that mediates the ubiquitination and proteasomal degradation of its substrate TaSAHH1 in response to vernalization, in order to promote primordia development (Kim *et al*., 2021). In rice, the *DSG1* gene encoding a U-box E3 ubiquitin ligase positively regulates cell division and elongation of roots, internodes, panicles, and seeds (Nan *et al*.,2017). In *Arabidopsis*, the RING-type E3-ligase TEAR1 was shown to regulate leaf development by promoting the degradation of TIE1, an important repressor of TCP transcription factors, which are key regulators for leaf development. Additional analysis showed that TEAR1 is colocalized with TIE1 in nuclei and negatively regulates TIE1 protein levels (Zhang *et al*., 2017).

Although the *blf1* mutant also exhibits defects in leaf width and length, it is hard to confirm at this level whether *BLF1* and *RING/U-BOX* genes both act within the same functional pathway to regulate leaf growth in barley. In the simplest scenario, if we consider that *BLF1* acts as a negative regulator of cell proliferation in the width direction during primordia outgrowth, and that the RING/U-BOX E3 ligase negatively regulates its protein levels, we would expect an enrichment of the BLF1 protein upon knock-out of the *RING/U-BOX* gene. This should presumably be translated in a phenotype similar to that of the *BLF1* over-expressing line previously described by Jöst *et al.* (2016), and shown to exhibit narrower leaves than the wt, but no significant changes in leaf length were observed between the two genotypes. Oppositely, our data showed no significant change in leaf width between the wt and the *ring-e3_1* mutant line. Instead, *ring-e3_1* presented significantly shorter leaves than the wt. Thus, at this point it is hard to draw a firm conclusion about the genetic interaction of these two genes. Ideally, a phenotypic characterisation of a double mutant line carrying two strong loss-of-function alleles for the *RING/U-BOX* and *BLF1* genes is required for that.

Yet, it is important to consider that identifying a clear phenotype for an E3 ligase mutant allele was always a hard task given their known functional redundancy. Indeed, in *Arabidopsis*, where about 6% of the genome or about 1600 genes encode RING/U-box E3 ligases, *At*PUB59 and *At*PUB5960, are shown to function redundantly in the regulation of plant innate immunity (Monaghan *et al*., 2009). Additionally, many of the ~230 putative RING/U-box E3 ligases identified in the barley genome remain relatively uncharacterized and identification of E3 ligase substrates is notoriously difficult (Uniprot; Ryu *et al*., 2019). However, our data managed to identify a clear impact of our *RING/U-BOX in* barley leaf size control by promoting growth in the length direction and increasing the overall blade area. In accordance with these data, *TaGW2* in wheat, ortholog of *OsGW2* and *ZmGW2* genes encoding RING/U-BOX E3 ligases in rice and maize, respectively, has also been identified as a positive regulator of cell division. As downregulation of *TaGW2* resulted in a decrease in the endosperm cell number and the final grain size (Zombori *et al.*, 2020). In contrast, previous investigations showed that genes encoding RING/U-BOX E3 ligases in *Arabidopsis AtDA2,* rice *OsGW2,* maize *ZmGW2-CHR4* and *ZmGW2-CHR5,* and barley *HvYrg1* and *HvYrg2,* all negatively regulate the vegetative and seed growth by inhibition of cell proliferation and/or elongation (Shu & Yang, 2017). This occurs through regulation of the cell cycle progression by proteolysis of the cell cycle regulatory proteins via ubiquitylation, which ensures the irreversibility of the cycle progression.

4.3 Identifying additional factors acting together with *BLF1* in leaf-shape control by exploiting natural genetic variation

The use of genetic modifiers to identify novel loci interacting with a gene of interest represents a very powerful, unbiased approach to isolate novel factors influencing a biological process (Griffiths *et al.*, 2015). Traditionally, the search for such modifiers was mostly based on second-site mutagenesis screens of the focal mutant. An alternative approach is to exploit the cryptic genetic variation that occurs naturally within populations. Such cryptic genetic variation that only becomes phenotypically expressed when the system is perturbed by a mutation at the focal locus appears to be ubiquitous in natural populations (Paaby and Rockman, 2014). In light of this and given the enormous genetic variation present in barley landraces evident from their phenotypic differences, it is very plausible that naturally occurring genetic modifiers for a gene of interest can be isolated from this germplasm resource.

Therefore, we searched for novel factors involved in leaf growth control that interact genetically with *BLF1*; by looking for naturally occurring genetic modifiers of the *blf1* phenotype in F2 populations generated by crossing the *blf1* homozygous line to four barley landraces with enormous genetic variation evident from their phenotypic differences. In the cross *blf1* x Landrace1 the phenotype distribution amongst the homozygous *blf1* mutants appeared rather broad with a ¾ ratio for the original *blf1* phenotype and ¼ for the attenuated blf1 phenotype, suggesting potentially the presence of a recessive modifier of the phenotype. This was the simplest scenario we expected, the presence of a modifier allele is visible as a clearly attenuated *blf1* phenotype amongst the genotypically *blf1* homozygous mutants in classical Mendelian ratios. This finding can be followed up by genetic fine mapping approach to identify the locus encoding for this modifier.

However, for the other crosses frequency distribution analysis did not detect a clear single-locus modifier in any of them, which would have been visible by a clear segregation of leaf width amongst the homozygous *blf1* mutants. This might be explained by the presence of more subtle modifiers that can be detected by comparing the coefficient of variation between the *blf1* homozygous mutant and wt plants from the same F2, where a *blf1* modifier would result in a higher coefficient of variation amongst the former than the latter cohort. However, it is relevant to admit that this type of modifiers is more difficult to pursue. More complex scenarios involving more than one locus are also conceivable in this scenario and they would be also very difficult to follow up.

5. CONCLUSION AND OUTLOOK

Many genetic and molecular factors controlling leaf architecture have been identified in the dicotyledonous species thanks to extensive researches on the model plant *Arabidopsis thaliana.* However, although researches on monocotyledonous species have been growing heavily in the last few decades, our knowledge is still fragmentary for these species (Townsley and Sinha 2012; Hepworth & Lenhard, 2014).

Barley has been successfully used as a model organism to study and understand the genetic basis of spike architecture and floral development in grasses (Koppolu *et al.*, 2013; Digel *et*

al., 2015; Poursarebani *et al.,* 2015). Compared to the wide variety of leaf mutants described in maize (Neuffer *et al.,* 1997), barley leaf mutants are not so well characterized. In a previous characterization of the classical barley mutant *blf1-1,* this latter exhibited wider but slightly shorter leaves due to more cell division in the width direction during primordia outgrowth (Jöst *et al.,* 2016). Fine mapping analysis identified BLF1 as a novel member of IDD transcription factor (TF) family, that regulates a variety of development processes and abiotic stresses in plants. During this work, we aimed to dissect the molecular function of the *BLF1* gene using variable molecular and genetic approaches. Several IDD proteins in *Arabidopsis* have been shown to serve as DNA binding platforms for GRAS domain proteins such as DELLA and SCL3, to regulate the GA signalling (Yoshida & Ueguchi-Tanaka, 2014). Based on this model, we first tested the interaction of BLF1 and the only DELLA protein in barley SLN1 at the physical and genetic levels. Our yeast two hybrid assay revealed that there is no physical interaction between the two proteins. Combination of the two mutant alleles *blf1* and *Sln1d* resulted in additive phenotypes, indicating independent effects of the two loci on leaf growth.

Given the high complexity and repetitiveness of the barley genome, DAP-seq. approach, was unable to identify any clear target genes of the BLF1 protein. On the other hand, a yeast two hybrid library screen was performed to identify the BLF1 interacting proteins. This resulted in five main protein candidates. The BLF1 and the candidate proteins interactions were further confirmed using different approaches: by reconstruction of the yeast two hybrid positives, rBiFC and Co-IP assays. Two of the interactors (EB1, POK1) are linked to the tubulin cytoskeleton and possibly to control of the cell division orientation; one is a kinase that may be involved in modulating BLF1 activity; and two proteins could act in ubiquitin-mediated degradation of BLF1 and/or other substrates. The RING/U-Box E3 appeared to bind strongly to BLF1 and suggested several obvious follow-up experiments to ask whether they might regulate BLF1 stability by ubiquitin-mediated degradation.

FRET experiment revealed a clear signal for the RING/U-BOX and BLF1 proteins, showing how close the interaction between the two proteins is. Also, combining BLF1 with the RING/U-BOX protein appeared to lead to lower levels of the BLF1 protein. Further investigations by inhibition of the proteasomal degradation with MG132 resulted in an increase in BLF1 levels and a stronger FRET signal, suggesting that the RING/U-BOX protein can trigger proteasomal degradation of BLF1. Additionally, co-expression of BLF1-GST fusion protein with the RING/U-BOX E3 ligase, HvUba2(E1), HvUbc11(E2), and AtUb in bacteria managed to reconstitute the BLF1 ubiquitylation cascade and proved that RING/U-BOX E3 interacts with BLF1 to mediate its ubiquitylation and proteasomal degradation. Furthermore, enrichment of the endogenous BLF1-vYFP fluorescent protein upon treatment with bortezomib to inhibit proteasomal degradation was further evidence that the ubiquitin-mediated proteasomal degradation of BLF1 also occurs in barley. Further characterisation of the BLF1 ubiquitylated protein by Mass Spectrometry would be useful to map the ubiquitilation sites**.**

On the other hand, phenotypic analysis of *ring-e3_1* (5 bp-Δ) mutant line showed a significant decrease in leaf 3 and leaf 4 length compared to the wt, suggesting that the *RING/U-BOX* gene also plays a role in the regulation of leaf growth in barley. Further histological analysis with longitudinal and transversal sections of the *ring-e3_1* mutant leaves are required to identify

which cellular mechanisms underlie the observed defects in length. A follow-up experiment to characterize the phenotype of a double mutant line carrying the *ring-e3_1 and blf1_a* loss-of-function alleles is also required to determine the functional significance of the *BLF1* and *RING/U-BOX* genetic interaction. Additionally, a quantitative proteomic analysis of BLF1 in the *ring-e3_1* and *wt* plants, either by using an anti-BLF1 antibody or by crossing the *ring-e3_1* mutant line to the *BLF1-vYFP* transgenic line, would allow to further confirm the enrichment of the BLF1 protein upon knock-out of the *RING/U-BOX* gene.

To sum-up, the two main novel insights obtained from this work are (1) the finding that *BLF1* does not appear to be involved in the GA pathway in barley, arguing against a recently proposed model for IDD-protein function in growth control, and (2) the observation that BLF1 protein can be ubiquitinated by a novel RING/U-BOX protein and that its protein levels in barley plants are kept low in part via ubiquitin/proteasome-mediated degradation.

Acknowledgements

This thesis was made possible with the support and help of many people to whom I would like to express my gratitude.

Special thanks and appreciation go to my main supervisor Michael Lenhard for the opportunity to work on this exciting topic, as well as for his guidance, helpful discussions, and valuable advice in my research project. I am also indebted to Michael and the whole AG Genetik for their guidance and support when first I arrived in Germany.

I would also like to thank Moritz Jöst for invaluable help during all stages of this project ranging from excellent advice to hands-on work in the lab.

I thank Sarah McKim and Laura Rossini for taking the time reviewing this thesis, as well as Michael Lenhard for proof reading.

I would like to express my appreciation to our collaborators at the IPK in Gatersleben, especially Götz Hensel, Jochen Kumlehn and Nils Stein my co-supervisor, making this work at all possible.

I am grateful to Elke Dittmann and her lab members for help and assistance with the bacterial protein extractions along my work.

Thanks go also to Christian Kappel for image analysis, Otto Baumann for assistance with confocal microscopy making my work much easier, and the whole AG Genetik for a truly inspiring and friendly working atmosphere.

This work was supported by a grant from the Deutsche Forschungsgemeinschaft (DFG).

Last but not least I deeply thank my parents for believing in me and always encouraging me to fulfill my dreams.

References

Andrews, S. (2010). FastQC: A Quality Control Tool for High Throughput Sequence Data [Online].

Andriankaja, M., Dhondt, S., DeBodt, S., Vanhaeren, H., Coppens, F., DeMilde, L., Mühlenbock, P., Skirycz, A., Gonzalez, N., Beemster, G. T. S. and lnzé, D. (2012). Exit from Proliferation during Leaf Development in Arabidopsis thaliana: A Not-So-Gradual Process. Developmental Cell 22, 64—78.

Aranda, S., Laguna, A., & de la Luna, S. (2011). DYRK family of protein kinases: evolutionary relationships, biochemical properties, and functional roles. FASEB journal: official publication of the Federation of American Societies for Experimental Biology, 25(2), 449–462.

Arite, T., Umehara, M., Ishikawa, S., Hanada, A., Maekawa, M., Yamaguchi, S., & Kyozuka, J. (2009). d14, a strigolactone-insensitive mutant of rice, shows an accelerated outgrowth of tillers. Plant & cell physiology, 50(8), 1416–1424.

Bae, H., Kim, S. K., Cho, S. K., Kang, B. G., & Kim, W. T. (2011). Overexpression of OsRDCP1, a rice RING domain containing E3 ubiquitin ligase, increased tolerance to drought stress in rice (Oryza sativa L.). Plant science, 180(6), 775-782.

Bartlett A, O'Malley RC, Huang SC, Galli M, Nery JR, Gallavotti A, Ecker JR. (2017). Mapping genome-wide transcription-factor binding sites using DAP-seq. Nat Protoc, (8):1659-1672.

Bayer, M.M., Rapazote-Flores, P., Ganal, M., Hedley, P.E., Macaulay, M., Plieske, J., Ramsay, L., Russell, J., Shaw, P.D., Thomas, W., Waugh, R. (2017). Development & evaluation of a barley 50k iSelect SNP array. Front Plant Sci 8, 1–10.

Blatt, M. R., & Grefen, C. (2014). Applications of fluorescent marker proteins in plant cell biology. Methods in molecular biology (Clifton, N.J.), 1062, 487–507.

Brunoud, G., Wells, D. M., Oliva, M., Larrieu, A., Mirabet, V., Burrow, A. H., Beeckman, T., Kepinski, S., Traas, J., Bennett, M. J., & Vernoux, T. (2012). A novel sensor to map auxin response and distribution at high spatio-temporal resolution. Nature, 482(7383), 103–106. https://doi.org/10.1038/nature10791.

Brzovic PS, Rajagopal P, Hoyt DW, King MC, Klevit RE. (2001). Structure of a BRCA1-BARD1 heterodimeric RING-RING complex. Nat Struct Biol 8, 833–837.

Buescher, E. M., Moon, J., Runkel, A., Hake, S., & Dilkes, B. P. (2014). Natural variation at sympathy for the ligule controls penetrance of the semidominant Liguleless narrow-R mutation in Zea mays. G3 (Bethesda, Md.), 4(12), 2297–2306.

Callis, J. (2014). The ubiquitination machinery of the ubiquitin system. The Arabidopsis book/American Society of Plant Biologists, 12.

Cao R, Tsukada Y, Zhang Y. Role of Bmi-1 and Ring1A in H2A ubiquitylation and Hox gene silencing. Mol Cell. 2005; 20:845–854.

Cao, H., Glazebrook, J., Clarke, J. D., Volko, S., & Dong, X. (1997). The Arabidopsis NPR1 gene that controls systemic acquired resistance encodes a novel protein containing ankyrin repeats. Cell, 88(1), 57–63.

Cenci A, Rouard M. (2017). Evolutionary analyses of GRAS transcription factors in angiosperms. Frontiers in Plant Science 8: 1–15.

Ch&ler, P. M., Marion-Poll, A., Ellis, M., & Gubler, F. (2002). Mutants at the Slender1 locus of barley cv Himalaya. Molecular & physiological characterization. Plant physiology, 129(1), 181-190.

Chan, J., Calder, G., Fox, S., & Lloyd, C. (2005). Localization of the microtubule end binding protein EB1 reveals alternative pathways of spindle development in Arabidopsis suspension cells. The Plant cell, 17(6), 1737–1748.

Chandler, P. M., Marion-Poll, A., Ellis, M. and Gubler, F. (2002). Mutants at the Slenderl locus of barley cv Himalaya. Molecular and physiological characterization. Plant Physiology 129, 181-190.

Chen, H.I. and Sudol, M. (1995). The WW domain of Yes-associated protein binds a proline-rich ligand that differs from the consensus established for Src homology 3-binding modules. Proc. Natl Acad. Sci. USA 92, 7819–7823.

Chen, Y. J., Wu, H., & Shen, X.Z. (2016). The ubiquitin–proteasome system & its potential application in hepatocellular carcinoma therapy. Cancer letters, 379(2), 245-252.

Cheng, H., Bao, X., Gan, X., Luo, S., & Rao, H. (2017). Multiple E3s promote the degradation of histone H3 variant Cse4. Scientific reports, 7(1), 8565.

Cheng, M.C., Hsieh, E. J., Chen, J.H., Chen, H.Y., & Lin, T.P. (2012). Arabidopsis RGLG2, functioning as a RING E3 ligase, interacts with AtERF53 and negatively regulates the plant drought stress response. Plant physiology, 158(1), 363-375.

Chuck G., Muszynski M., Kellogg E., Hake S., Schmidt R. J. (2002). The control of spikelet meristem identity by the branched silkless1 gene in maize. Science 298: 1238–1241.

Clark S. E., Jacobsen S. E., Levin J., Meyerowitz E.M. (1996). The CLAVATA & SHOOT MERISTEMLESS loci competitively regulate meristem activity in Arabidopsis. Development 122, 1567–1575.

Clark S. E., Running M.P., Meyerowitz E.M. (1995). CLAVATA3 is a specific regulator of shoot & floral meristem development affecting the same processes as CLAVATA1. Development 121, 2057–2067.

Clark S. E., Williams R.W., Meyerowitz E.M. (1997). The CLAVATA1 gene encodes a putative receptor kinase that controls shoot & floral meristem size in Arabidopsis. Cell 89, 575–585.

Clauw, P., Coppens, F., Korte, A., Herman, D., Slabbinck, B., Dhondt, S., Daele, T.V., De Milde, L., Vermeersch, M., Maleux, K., Maere, S., Gonzalez, N., & Inzé, D. (2016). Leaf growth response to mild drought: natural variation in Arabidopsis sheds light on trait architecture. The Plant Cell, 28(10), 2417-2434.

Cleary, A. L., & Smith, L. G. (1998). The Tangled1 gene is required for spatial control of cytoskeletal arrays associated with cell division during maize leaf development. The Plant cell, 10(11), 1875–1888.

Coelho CP, Huang P, Lee DY, Brutnell TP. (2018). Making roots, shoots, and seeds: IDD gene family diversification in plants. Trends in Plant Science 23: 66–78.

Coelho, C. P., Huang, P., Lee, D. Y., & Brutnell, T. P. (2018). Making Roots, Shoots, and Seeds: IDD Gene Family Diversification in Plants. Trends in plant science, 23(1), 66–78.

Conklin PA, Strable J, Li S, Scanlon MJ. On the mechanisms of development in monocot and eudicot leaves. New Phytol. 2019 Jan;221(2):706-724. doi: 10.1111/nph.15371. Epub 2018 Aug 14. PMID: 30106472.

Conklin, P. A., Strable, J., Li, S., & Scanlon, M. J. (2019). On the mechanisms of development in monocot and eudicot leaves. The New phytologist, 221(2), 706–724.

Conlon, I., & Raff, M. (1999). Size control in animal development. Cell, 96(2), 235-244.

Cui, D., Zhao, J., Jing, Y., Fan, M., Liu, J., Wang, Z., Xin, W., & Hu, Y. (2013). The Arabidopsis IDD14, IDD15, & IDD16 cooperatively regulate lateral organ morphogenesis & gravitropism by promoting auxin biosynthesis & transport. PLoS genetics, 9(9), e1003759.

Cui, D., Zhao, J., Jing, Y., Fan, M., Liu, J., Wang, Z., Xin, W., & Hu, Y. (2013). The Arabidopsis IDD14, IDD15, and IDD16 cooperatively regulate lateral organ morphogenesis and gravitropism by promoting auxin biosynthesis and transport. PLoS genetics, 9(9), e1003759.

Dawson I.K., Russell, J., Powell, W., Steffenson, B., Thomas, W.T.B., Waugh, R. (2015). Barley: a translational model for adaptation to climate change. New Phytologist 206, 913–931.

De Jager, S. M., Maughan, S., Dewitte, W., Scofield, S., & Murray, J.A. (2005, June). The developmental context of cell-cycle control in plants. Seminars in cell & developmental biology, 16(3), 385-396.

Derbyshire P., Byrne M. E. (2013). MORE SPIKELETS1 is required for spikelet fate in the inflorescence of Brachypodium. Plant Physiol. 161: 1291–1302.

Derbyshire, P., Byrne, M.E. (2013). MORE SPIKELETS1 is required for spikelet fate in the inflorescence of Brachypodium. Plant Physiol,161(3):1291-302.

Digel, B., Pankin, A. and von Korff, M. (2015). Global Transcriptome Profiling of Developing Leaf and Shoot Apices Reveals Distinct Genetic and Environmental Control of Floral Transition and Inflorescence Development in Barley. The Plant Cell 9, 2318-2334.

Digel, B., Tavakol, E., Verderio, G., Tondelli, A., Xu, X., Cattivelli, L., Rossini, L., & von Korff, M. (2016). Photoperiod-H1 (Ppd-H1) controls leaf size. Plant physiology, 172(1), 405-415.

Dobrovolskaya, O., Pont, C., Sibout, R., Martinek, P., Badaeva, E., Murat, F., Chosson, A., Watanabe, N., Prat, E., Gautier, N., Gautier, V., Poncet, C., Orlov, Y.L., Krasnikov, A.A., Bergès H., Salina, E., Laikova, L., & Salse, J. (2015). FRIZZY PANICLE drives supernumerary spikelets in bread wheat. Plant Physiology, 167(1), 189-199.

Doebley, J. F., Gaut, B. S., & Smith, B. D. (2006). The molecular genetics of crop domestication. Cell, 127(7), 1309–1321.

Donnelly, P. M., Bonetta, D., Tsukaya, H., Dengler, R. E. and Dengler, N. G. (1999). Cell cycling and cell enlargement in developing leaves of Arabidopsis. Developmental Biology 215, 407—419.

Dreher, K., & Callis, J. (2007). Ubiquitin, hormones & biotic stress in plants. Annals of botany, 99(5), 787-822.

Druka, A., Franckowiak, J., Lundqvist, U., Bonar, N., Alex&er, J., Houston, K., Radovic, S., Shahinnia, F., Vendramin, V., Morgante, M., Stein, N., Waugh, R. (2011). Genetic dissection of barley morphology & development. Plant Physiol 155, 617–627.

Fiorani, F. and Beemster, G. T. S. (2006). Quantitative analyses of cell division in plants. Plant Molecular Biology 60, 963—979.

Fleming, A. (2006). Metabolic aspects of organogenesis in the shoot apical meristem. Journal of experimental botany, 57(9), 1863-1870.

Fleming, A. J. (2005). The control of leaf development. New Phytologist, 166(1), 9-20.

Fletcher, J.C., Br&, U., Running, M.P., Simon, R., Meyerowitz, E.M. (1999). Signallingof cell fate decisions by CLAVATA3 in Arabidopsis shoot meristems. Science 283, 1911 – 1914.

Förster T. (2012). Energy migration and fluorescence. 1946. Journal of biomedical optics, 17(1), 011002

Fournier, C., Dur&, J.L., Ljutovac, S., Schäufele, R., Gastal, F., & &rieu, B. (2005). A functional–structural model of elongation of the grass leaf & its relationships with the phyllochron. New Phytologist, 166(3), 881-894.

Furuya, T., Shinkawa, H., Kajikawa, M., Nishihama, R., Kohchi, T., Fukuzawa, H., & Tsukaya, H. (2021). A plant-specific DYRK kinase DYRKP coordinates cell morphology in Marchantia polymorpha. Journal of plant research, 134(6), 1265–1277.

Galli, M., Khakhar, A., Lu, Z., Chen, Z., Sen, S., Joshi, T., Nemhauser, J. L., Schmitz, R. J., & Gallavotti, A. (2018). The DNA binding landscape of the maize AUXIN RESPONSE FACTOR family. Nature communications, 9(1), 4526. https://doi.org/10.1038/s41467-018-06977-6

Garnett, T., Appleby, M.C., Balmford, A., Bateman, I.J., Benton, T.G., Bloomer, P., Burlingame, B., Dawkins, M., Dolan, L., Fraser, D., Herrero, M., Hoffmann, I., Smith, P., Thornton P.K., Toulmin, C., Vermeulen, S.J., & Godfray, H. C. J. (2013). Sustainable intensification in agriculture: premises & policies. Science, 341(6141), 33-34.

Garrett, S., & Broach, J. (1989). Loss of Ras activity in Saccharomyces cerevisiae is suppressed by disruptions of a new kinase gene, YAKI, whose product may act downstream of the cAMP-dependent protein kinase. Genes & development, 3(9), 1336–1348.

Gladman, N. P., Marshall, R. S., Lee, K. H., & Vierstra, R. D. (2016). The Proteasome Stress Regulon Is Controlled by a Pair of NAC Transcription Factors in Arabidopsis. The Plant cell, 28(6), 1279–1296.

Gomi, K., Sasaki, A., Itoh, H., Ueguchi-Tanaka, M., Ashikari, M., Kitano, H., & Matsuoka, M. (2004). GID2, an F-box subunit of the SCF E3 complex, specifically interacts with phosphorylated SLR1 protein and regulates the gibberellin-dependent degradation of SLR1 in rice. The Plant journal: for cell and molecular biology, 37(4), 626–634.

Govind, G., Rutten, T., Sakuma, S., Tagiri, A., Wolde, G. M., Youssef, H. M., Battal, A., Ciannamea, S., Fusca, T., Nussbaumer, T., Pozzi, C., Börner, A., Lundqvist, U., Komatsuda, T., Salvi, S., Tuberosa, R., Uauy, C., Sreenivasulu, N., Rossini, L. and Schnurbusch, T. (2015). The genetic basis of composite spike form in barley and 'miracle-wheat'. Genetics 201, 155-165.

Grbic, B. and Bleecker, A.B. (2000). Axillary meristem development in Arabidopsis thaliana. Plant J. 21: 215–223.

Green, P. B. (1976). Growth and Cell Pattern Formation on an Axis: Critique of Concepts, Terminology , and Modes of Study Author (s): Paul B . Green Published by: The University of Chicago Press Stable URL : http://www.jstor.org/stable/2473850. Botanical Gazette 137, 187-202.

Griffiths, J., Murase, K., Rieu, I., Zentella, R., Zhang, Z. L., Powers, S. J., Gong, F., Phillips, A. L., Hedden, P., Sun, T. P., & Thomas, S. G. (2006). Genetic characterization and functional analysis of the GID1 gibberellin receptors in Arabidopsis. The Plant cell, 18(12), 3399–3414.

Guo Y, Mahony S, Gifford DK (2012) High Resolution Genome Wide Binding Event Finding and Motif Discovery Reveals Transcription Factor Spatial Binding Constraints. PLoS Comput Biol 8(8): e1002638.

Haas, A. L., Warms, J.V., Hershko, A., & Rose, I.A. (1982). Ubiquitin-activating enzyme. Mechanism & role in protein-ubiquitin conjugation. Journal of Biological Chemistry, 257(5), 2543-2548.

Harper, J.W. and Tan, M.-K.M. (2012). Understanding cullin-RING E3 biology through proteomics-based substrate identification. Mol. Cell. Proteomics 11, 1541–1550.

Hecker, A., Wallmeroth, N., Peter, S., Blatt, M. R., Harter, K., & Grefen, C. (2015). Binary 2-in-1 Vectors Improve in Planta (Co)localization and Dynamic Protein Interaction Studies. Plant physiology, 168(3), 776–787.

Hedges, S.B. (2002). The origin & evolution of model organisms. Nat. Rev. Genet. 3, 838-849.

Hepworth, J. and Lenhard, M. (2014). Regulation of plant lateral-organ growth by modulating cell number and size. Current Opinion in Plant Biology 17, 36—42.

Hirano Y, Nakagawa M, Suyama T, et al. (2017). Structure of the SHR-SCR heterodimer bound to the BIRD/IDD transcriptional factor JKD. Nature Plants 3: 17010.

Horstman, A., Tonaco, I. A., Boutilier, K., & Immink, R. G. (2014). A cautionary note on the use of split-YFP/BiFC in plant protein-protein interaction studies. International journal of molecular sciences, 15(6), 9628–9643.

Iconomou M, Saunders DN. Systematic approaches to identify E3 ligase substrates. (2016). Biochem J. 15;473(22):4083-4101. doi: 10.1042/BCJ20160719. PMID: 27834739; PMCID: PMC5103871.

Ingvardsen, C., & Veierskov, B. (2001). Ubiquitin-& proteasome-dependent proteolysis in plants. Physiologia Plantarum, 112(4), 451-459.

Ishikura, S., Weissman, A.M., & Bonifacino, J.S. (2010). Serine residues in the cytosolic tail of the T-cell antigen receptor α-chain mediate ubiquitination & endoplasmic reticulum-associated degradation of the unassembled protein. Journal of Biological Chemistry, 285(31), 23916-23924.

Itoh, H., Sasaki, A., Ueguchi-Tanaka, M., Ishiyama, K., Kobayashi, M., Hasegawa, Y., Minami, E., Ashikari, M., and Matsuoka, M. (2005). Dissection of the phosphorylation of rice DELLA protein, SLENDER RICE1. Plant Cell Physiol. 46 1392–1399.

Itoh, J.I., Nonomura, K.I., Ikeda, K., Yamaki, S., Inukai, Y., Yamagishi, H., Kitano, H., & Nagato, Y. (2005). Rice plant development: from zygote to spikelet. Plant & cell physiology, 46(1), 23-47.

Iwakawa, H., Takahashi, H., Machida, Y., & Machida, C. (2020). Roles of ASYMMETRIC LEAVES2 (AS2) & Nucleolar Proteins in the Adaxial–Abaxial Polarity Specification at the Perinucleolar Region in Arabidopsis. International Journal of Molecular Sciences, 21(19), 7314.

Jain, A. K., & Barton, M. C. (2009). Regulation of p53: TRIM24 enters the RING. Cell cycle (Georgetown, Tex.), 8(22), 3668–3674.

Jain, A.K. and Barton, M.C. (2009). Regulation of p53: TRIM24 enters the RING. Cell Cycle 8, 3668–3674 doi:10.4161/cc.8.22.9979 62 Harper, J.W. and Tan, M.-K.M. (2012) Understanding cullin-RING E3 biology through proteomics-based substrate identification. Mol. Cell. Proteomics 11, 1541–1550.

Jathish, P. (2022). Repressing a repressor: E3 ligase COP1/SPA promotes seed germination by targeting the DELLA protein RGL2, Plant Physiology, Volume 189, Issue 3, Pages 1192–1193

Jayakodi, M., Padmarasu, S., Haberer, G. et al. The barley pan-genome reveals the hidden legacy of mutation breeding. Nature 588, 284–289 (2020).

Jeong, S., Trotochaud, A.E., Clark, S.E. (1999). The Arabidopsis CLAVATA2 gene encodes a receptor-like protein required for the stability of the CLAVATA1 receptor-like kinase.

Jiang, L., Liu, X., Xiong, G., Liu, H., Chen, F., Wang, L., Meng, X., Liu, G., Yu, H., Yuan, Y., Yi, W., Zhao, L., Ma, H., He, Y., Wu, Z., Melcher, K., Qian, Q., Xu, H. E., Wang, Y., & Li, J. (2013). DWARF 53 acts as a repressor of strigolactone signalling in rice. Nature, 504(7480), 401–405.

Jiang, W., Wang, S., Xiao, M., Lin, Y., Zhou, L., Lei, Q. et al. (2011). Acetylation regulates gluconeogenesis by promoting PEPCK1 degradation via recruiting the UBR5 ubiquitin ligase. Mol. Cell 43, 33–44.

Jiao Y. Wang Y. Xue D. Wang J. Yan M. Liu G. Dong G. Zeng D. Lu Z. Zhu X. Qian Q. Li J. (2010). Regulation of OsSPL14 by OsmiR156 defines ideal plant architecture in rice. Nat. Genet. 42: 541–544.

Jöst, M., Hensel, G., Kappel, C., Druka, A., Sicard, A., Hohmann, U., Beier, S., Himmelbach, A., Waugh, R., Kumlehn, J., Stein, N., & Lenhard, M. (2016). The INDETERMINATE DOMAIN protein BROAD LEAF1 limits barley leaf width by restricting lateral proliferation. Current Biology, 26(7), 903-909.

Joukov V, Chen J, Fox EA, Green JB, Livingston DM. (2001). Functional communication between endogenous BRCA1 and its partner, BARD1, during Xenopus laevis development. Proc Natl Acad Sci U S A. 98, 12078–12083.

Kanelis, V., Rotin, D. & Forman-Kay, J. Solution structure of a Nedd4 WW domain–ENaC peptide complex. (2001). Nat Struct Mol Biol 8, 407–412.

Kazama, T., Ichihashi, Y., Murata, S. and Tsukaya, H. (2010). The mechanism of cell cycle arrest front progression explained by a KLUH/CYP78A5-dependent mobile growth factor in developing leaves of Arabidopsis thaliana. Plant & Cell Physiology 51. 1046—1054.

Keren-Kaplan, T., Attali, I., Motamedchaboki, K., Davis, B. A., Tanner, N., Reshef, Y., Laudon, E., Kolot, M., Levin-Kravets, O., Kleifeld, O., Glickman, M., Horazdovsky, B. F., Wolf, D. A., & Prag, G. (2012). Synthetic biology approach to reconstituting the ubiquitylation cascade in bacteria. The EMBO journal, 31(2), 378–390. https://doi.org/10.1038/emboj.2011.397

Kerppola T. K. (2013). Bimolecular fluorescence complementation (BiFC) analysis of protein interactions in live cells. Cold Spring Harbor protocols, 2013(8), 727–731. https://doi.org/10.1101/pdb.prot076497

Kim, J. H., Khan, I. U., Lee, C. W., Kim, D. Y., Jang, C. S., Lim, S. D., Park, Y. C., Kim, J. H., & Seo, Y. W. (2021). Identification and analysis of a differentially expressed wheat RING-type E3 ligase in spike primordia development during post-vernalization. Plant cell reports, 40(3), 543–558.

Kim, J. S., Park, Y. Y., Park, S. Y., Cho, H., Kang, D., & Cho, H. (2011). The auto-ubiquitylation of E3 ubiquitin-protein ligase Chfr at G2 phase is required for accumulation of polo-like kinase 1 and mitotic entry in mammalian cells. The Journal of biological chemistry, 286(35), 30615–30623.

Kirby, E. J. M., & Appleyard, M. (1987). Development & structure of the wheat plant. Wheat breeding, 287-311.

Komander, D. (2009) The emerging complexity of protein ubiquitination. Biochem. Soc. Trans. 37, 937–953.

Komander, D., Reyes-Turcu, F., Licchesi, J.D.F., Odenwaelder, P., Wilkinson, K.D., Barford, D. et al. (2009) Molecular discrimination of structurally equivalent Lys 63-linked and linear polyubiquitin chains. EMBO Rep. 10, 466–473.

Komatsuda, T., Pourkheirandish, M., He, C., Azhaguvel, P., Kanamori, H., Perovic, D., Stein, N., Graner, A., Wicker, T., Tagiri, A., Lundqvist, U., Fujimura, T., Matsuoka, M., Matsumoto, T., & Yano, M. (2007). Six-rowed barley originated from a mutation in a homeodomain-leucine zipper I-class homeobox gene. Proceedings of the National Academy of Sciences of the United States of America, 104(4), 1424–1429.

Koppolu, R., Anwar, N., Sakuma, S., Tagiri, A., Lundqvist, U., Pourkheirandish, M., Rutten,

Kraft, E., Stone, S. L., Ma, L., Su, N., Gao, Y., Lau, O. S., Deng, X. W., & Callis, J. (2005). Genome analysis and functional characterization of the E2 and RING-type E3 ligase ubiquitination enzymes of Arabidopsis. Plant physiology, 139(4), 1597–1611.

Kraft, E., Stone, S. L., Ma, L., Su, N., Gao, Y., Lau, O.S., Deng, X.W., & Callis, J. (2005). Genome analysis and functional characterization of the E2 and RING-type E3 ligase ubiquitination enzymes of Arabidopsis. Plant physiology, 139(4), 1597-1611.

Kumar, M., Le, D. T., Hwang, S., Seo, P. J., & Kim, H. U. (2019). Role of the INDETERMINATE DOMAIN Genes in Plants. International journal of molecular sciences, 20(9), 2286.

Kumar, M., Le, D. T., Hwang, S., Seo, P. J., & Kim, H. U. (2019). Role of the INDETERMINATE DOMAIN Genes in Plants. International journal of molecular sciences, 20(9), 2286.

Kurepa, J., & Smalle, J. A. (2008). Structure, function & regulation of plant proteasomes. Biochimie, 90(2), 324-335.

Lechner E., Achard P., Vansiri A., Potuschak T., Genschik P. (2006) F-box proteins everywhere. Curr. Opin. Plant Biol. 9: 631–638.

Lee, M., Sharopova, N., Beavis, W. D., Grant, D., Katt, M., Blair, D., & Hallauer, A. (2002). Expanding the genetic map of maize with the intermated B73 x Mo17 (IBM) population. Plant molecular biology, 48(5-6), 453–461.

Lenhard, M., Jürgens, G., & Laux, T. (2002). The WUSCHEL & SHOOTMERISTEMLESS genes fulfil complementary roles in Arabidopsis shoot meristem regulation. Development 129, 3195-3206.

Lewis, M.W., Hake, S. (2016). Keep on growing: Building & patterning leaves in the grasses. Curr Opin Plant Biol 29, 80–86.

Li H. (2013) Aligning sequence reads, clone sequences and assembly contigs with BWA-MEM.

Li, N., & Li, Y. (2016). Signalling pathways of seed size control in plants. Current opinion in plant biology, 33, 23-32.

Li, Q., Li, L., Yang, X., Warburton, M.L., Bai, G., Dai, J., Li, J., & Yan, J. (2010). Relationship, evolutionary fate and function of two maize co-orthologs of rice GW2 associated with kernel size and weight. BMC Plant Biology, 10(1), 1-15.

Li, X., Qian, Q., Fu, Z., Wang, Y., Xiong, G., Zeng, D., Wang, X., Liu, X., Teng, S., Hiroshi, F., Yuan, M., Luo, D., Han, B., & Li, J. (2003). Control of tillering in rice. Nature, 422(6932), 618–621.

Liao, C. Y., Smet, W., Brunoud, G., Yoshida, S., Vernoux, T., & Weijers, D. (2015). Reporters for sensitive and quantitative measurement of auxin response. Nature methods, 12(3), 207–210.

Lim, P. S., Sutton, C. R., & Rao, S. (2015). Protein kinase C in the immune system: from signallingto chromatin regulation. Immunology, 146(4), 508–522.

Lin, H., Wang, R., Qian, Q., Yan, M., Meng, X., Fu, Z., Yan, C., Jiang, B., Su, Z., Li, J., & Wang, Y. (2009). DWARF27, an iron-containing protein required for the biosynthesis of strigolactones, regulates rice tiller bud outgrowth. The Plant cell, 21(5), 1512–1525.

Liu, P. Y., Chen, C. C., Chin, C. Y., Liu, T. J., Tsai, W. C., Chou, J. L., Huang, C. Y., Chen, Y. G., & Chen, Y. C. (2021). E3 ubiquitin ligase Grail promotes hepatic steatosis through Sirt1 inhibition. Cell death & disease, 12(4), 323.

Liu, R., Xia, R., Xie, Q., & Wu, Y. (2021). Endoplasmic reticulum related E3 ubiquitin ligases: Key regulators of plant growth & stress responses. Plant Communications, 100186.

Long, J.A., Moan, E.I., Medford, J.I. & Barton, M. K. (1996). A member of the KNOTTED class of homeodomain proteins encoded by the SHOOTMERISTEMLESS gene of Arabidopsis. Nature 397, 66-69.

Long, S.P., Zhu, X.G., Naidu, S.L., Ort, D.R. (2006). Can improvement in photosynthesis increase crop yields? Plant Cell Environ 29, 315–330.

Lyzenga, W. J., & Stone, S. L. (2012). Abiotic stress tolerance mediated by protein ubiquitination. Journal of experimental botany, 63(2), 599-616.

Maraschin, F., Memelink, J., & Offringa, R. (2009). Auxin-induced, SCF(TIR1)-mediated poly-ubiquitination marks AUX/IAA proteins for degradation. The Plant journal: for cell and molecular biology, 59(1), 100–109.

Mark, K. G., Simonetta, M., Maiolica, A., Seller, C. A., & Toczyski, D. P. (2014). Ubiquitin ligase trapping identifies an SCF(Saf1) pathway targeting unprocessed vacuolar/lysosomal proteins. Molecular cell, 53(1), 148–161.

Mascher, M., Richmond, A.T., Gerhardt, J.D., Himmelbach, A., Clissold, L., Sampath, D., Ayling, S., Steuernagel, B., Pfeifer, M., D'Ascenzo, M., Akhunov, D.E., Hedley, E.P., Gonzales, M.A., Morrell, P.L., Kilian, B., Blattner, R.F., Scholz, U., Mayer, F.X.K., Flavell, J.A., Muehlbauer, J.G., Waugh, R., Jeddeloh, A.J., Stein, N. (2013). Barley whole exome capture: A tool for genomic research in the genus Hordeum & beyond. Plant J 76, 494–505.

Mayer, K.F., Schoof, H., Haecker, A., Lenhard, M., Jürgens, G., & Laux, T. (1998). Role of WUSCHEL in regulating stem cell fate in the Arabidopsis shoot meristem. Cell, 95(6), 805-815.

McSteen, P., Malcomber, S., Skirpan, A., Lunde, C., Wu, X., Kellogg, E., & Hake, S. (2007). barren inflorescence2 Encodes a co-ortholog of the PINOID serine/threonine kinase and is required for organogenesis during inflorescence and vegetative development in maize. Plant physiology, 144(2), 1000–1011.

Metzger, M. B., Pruneda, J. N., Klevit, R. E., & Weissman, A. M. (2014). RING-type E3 ligases: master manipulators of E2 ubiquitin-conjugating enzymes and ubiquitination. Biochimica et biophysica acta, 1843(1), 47–60.

Mir, R., Aranda, L. Z., Biaocchi, T., Luo, A., Sylvester, A. W., & Rasmussen, C. G. (2017). A DII domain-based auxin reporter uncovers low auxin signallingduring telophase and early G1. Plant Physiology, 173(1), 863–871.

Mizukami, Y. (2001). A matter of size: developmental control of organ size in plants. Current opinion in plant biology, 4(6), 533-539.

Monaghan, J., Xu, F., Gao, M., Zhao, Q., Palma, K., Long, C., Chen, S., Zhang, Y., & Li, X. (2009). Two Prp19-like U-box proteins in the MOS4-associated complex play redundant roles in plant innate immunity. PLoS pathogens, 5(7), e1000526.

Müller, S., Han, S., & Smith, L. G. (2006). Two kinesins are involved in the spatial control of cytokinesis in Arabidopsis thaliana. Current biology: CB, 16(9), 888–894.

Muñoz-Amatriaín, M., Cuesta-Marcos, A., Hayes, P. M., & Muehlbauer, G. J. (2014). Barley genetic variation: implications for crop improvement. Briefings in functional genomics, 13(4), 341–350.

Munoz-Amatriain, M., Cuesta-Marcos, A., Hayes, P.M., Muehlbauer, J.G. (2014). Barley genetic variation: Implications for crop improvement. Brief Funct Genomics 13, 341–350.

Murase, K., Hirano, Y., Sun, T. P., & Hakoshima, T. (2008). Gibberellin-induced DELLA recognition by the gibberellin receptor GID1. Nature, 456(7221), 459–463.

Nagy, P.D. (2008) Yeast as a model host to explore plant virus-host interactions. Annual Review of Phytopathology. 46:217-242.

Nardmann, J., Ji, J., Werr, W., & Scanlon, M. J. (2004). The maize duplicate genes narrow sheath1 and narrow sheath2 encode a conserved homeobox gene function in a lateral domain of shoot apical meristems. Development (Cambridge, England), 131(12), 2827–2839.

Nath, U., Crawford, B. C., Carpenter, R. and Coen, E. (2003). Genetic control of surface curvature. Science 299, 1404—1407.

Nelissen, H., Gonzalez, N., & Inze, D. (2016). Leaf growth in dicots & monocots: so different yet so alike. Current opinion in plant biology, 33, 72-76.

Neuffer, M.G., Coe, E.H., Wessler, S.R. (1997). Mutants of maize. Cold Spring Harbor Press, Cold Spring Harbor Laboratory Press, 468.

Ning, Y., Jantasuriyarat, C., Zhao, Q., Zhang, H., Chen, S., Liu, J., Liu, L., Tang, S., Park, C.H., Wang, X., Liu, X., Dai, L., Xie, Q., & Wang, G. L. (2011). The SINA E3 ligase OsDIS1 negatively regulates drought response in rice. Plant Physiology, 157(1), 242-255.

O'Connor, H.F., Huibregtse, J.M. (2017). Enzyme–substrate relationships in the ubiquitin system: approaches for identifying substrates of ubiquitin ligases. Cell. Mol. Life Sci. 74, 3363–3375.

Ogasawara, H., Kaimi, R., Colasanti, J., & Kozaki, A. (2011). Activity of transcription factor JACKDAW is essential for SHR/SCR-dependent activation of SCARECROW & MAGPIE & is modulated by reciprocal interactions with MAGPIE, SCARECROW & SHORT ROOT. Plant molecular biology, 77(4-5), 489.

olá, D. Neuffer, M.G., Coe, E.H., Wessler, S.R.: Mutants of Maize. Biologia Plantarum 40, 640 (1997).

Ordureau, A., Munch, C. and Harper, J.W. (2015) Quantifying ubiquitin signalling. Mol. Cell 58, 660–676.

Ort D.R., Merchant S.S., Alric J., Barkan A., Blankenship R.E., Bock R. (2015). Redesigning photosynthesis to sustainably meet global food and bioenergy demand. Proceedings of the National Academy of Sciences, USA112, 8529–8536.

Park, J.J., Yi, J., Yoon, J., Cho, L.H., Ping, J., Jeong, H.J., Cho,K.S., Kim, W.T., & An, G. (2011). OsPUB15, an E3 ubiquitin ligase, functions to reduce cellular oxidative stress during seedling establishment. The Plant Journal, 65(2), 194-205.

Pederson, T., & Powell, K. (2015). Thoru Pederson: Spotting novel roles for the nucleolus. The Journal of cell biology, 208(4), 384–385.

Philip Machanick and Timothy L. Bailey, "MEME-ChIP: motif analysis of large DNA datasets", Bioinformatics 27(12):1696-1697, 2011.

Pierce, N.W., Kleiger, G., Shan, S.-o. and Deshaies, R.J. (2009) Detection of sequential polyubiquitylation on a millisecond timescale. Nature 462, 615–619.

Pintard L, Willis JH, Willems A, Johnson J-LF, Srayko M, Kurz T, Glaser S, Mains PE, Tyers M, Bowerman B, et al. (2003). The BTB protein MEL-26 is a substrate-specific adaptor of the CUL-3 ubiquitin-ligase. Nature 425, 311–316.

Porras-Yakushi, T. R., Reitsma, J. M., Sweredoski, M. J., Deshaies, R. J., & Hess, S. (2021). In-depth proteomic analysis of proteasome inhibitors bortezomib, carfilzomib and MG132 reveals that mortality factor 4-like 1 (MORF4L1) protein ubiquitylation is negatively impacted. Journal of proteomics, 241, 104197.

Pourkheir&ish, M., Hensel, G., Kilian, B., Senthil, N., Chen, G., Sameri, M., Azhaguvel, P., Sakuma, S., Dhanagond, S., Sharma, R., Mascher, M., Himmelbach, A., Gottwald, S., Nair, S.K., Tagiri, A., Yukuhiro, F., Nagamura, Y., Kanamori, H., Matsumoto, T., Willcox, G., Middleton, C.P., Wicker, T., Walther, A., Waugh, R., Fincher, G.B., Stein, N., Kumlehn, J., Sato, K., Komatsuda, T. (2015). Evolution of the Grain Dispersal System in Barley. Cell,162(3), 527-39.

Pourkheirandish, M., Hensel, G., Kilian, B., Senthil, N., Chen, G., Sameri, M., Azhaguvel, P., Sakuma, S., Dhanagond, S., Sharma, R., Mascher, M., Himmelbach, A., Gottwald, S., Nair, S. K., Tagiri, A., Yukuhiro, F., Nagamura, Y., Kanamori, H., Matsumoto, T., Willcox, G., … Komatsuda, T. (2015). Evolution of the Grain Dispersal System in Barley. Cell, 162(3), 527–539.

Poursarebani, N., Seidensticker, T., Koppolu, R., Trautewig, C., Gawrohski, P., Bini, F.,

Qi, Y., Balem, F., Faloutsos, C., Klein-Seetharaman, J., & Bar-Joseph, Z. (2008). Protein complex identification by supervised graph local clustering. Bioinformatics (Oxford, England), 24(13), i250–i258.

Raghavendra, A.S. (2003). PHOTOSYNTHESIS & PARTITIONING | C3 Plants. Encyclopedia of Applied Plant Sciences, 673-680.

Ramos, J. A., Zenser, N., Leyser, O. & Callis, J. (2001). Rapid degradation of auxin/indoleacetic acid proteins requires conserved amino acids of domain II and is proteasome dependent. Plant Cell 13, 2349–2360.

Ray, D.K., Gerber, J.S., MacDonald, G.K., West, P.C. (2015). Climate variation explains a third of global crop yield variability. Nat Commun 6, 5989.Grassini, P., Eskridge, K. M., & Cassman, K. G. (2013). Distinguishing between yield advances & yield plateaus in historical crop production trends. Nature communications, 4(1), 1-11.

Ren, X., Wang, Y., Yan, S., Sun, D., & Sun, G. (2014). Population genetics and phylogenetic analysis of the vrs1 nucleotide sequence in wild and cultivated barley. Genome, 57(4), 239–244.

Richardson, A. E., Cheng, J., Johnston, R., Kennaway, R., Conlon, B. R., Rebocho, A. B., Kong, H., Scanlon, M. J., Hake, S., & Coen, E. (2021). Evolution of the grass leaf by primordium extension and petiole-lamina remodeling. Science (New York, N.Y.), 374(6573), 1377–1381.

Richardson, P. G., Hideshima, T., & Anderson, K. C. (2003). Bortezomib (PS-341): a novel, first-in-class proteasome inhibitor for the treatment of multiple myeloma and other cancers. Cancer control: journal of the Moffitt Cancer Center, 10(5), 361–369.

Robinson, J., Thorvaldsdóttir, H., Winckler, W. et al. Integrative genomics viewer. Nat Biotechnol 29, 24–26 (2011).

Rotasperti, L., Sansoni, F., Mizzotti, C., Tadini, L., & Pesaresi, P. (2020). Barley's second spring as a model organism for chloroplast research. Plants 9, 803.

Ryu, M. Y., Cho, S. K., Hong, Y., Kim, J., Kim, J. H., Kim, G. M., Chen, Y. J., Knoch, E., Möller, B. L., Kim, W. T., Lyngkjær, M. F., & Yang, S. W. (2019). Classification of barley U-box E3 ligases and their expression patterns in response to drought and pathogen stresses. BMC genomics, 20(1), 326.

Ryu, M. Y., Cho, S. K., Hong, Y., Kim, J., Kim, J. H., Kim, G. M., Chen, Y. J., Knoch, E., Møller, B. L., Kim, W. T., Lyngkjær, M. F., & Yang, S. W. (2019). Classification of barley U-box E3 ligases and their expression patterns in response to drought and pathogen stresses. BMC genomics, 20(1), 326.

Sadanandom, A., Bailey, M., Ewan, R., Lee, J., & Nelis, S. (2012). The ubiquitin–proteasome system: central modifier of plant signalling. New Phytologist, 196(1), 13-28.

San, N. S., Suzuki, K., Soda, K., Adachi, S., Kasahara, H., Yamamoto, T., Ikka, T., Kondo, K., Yamanouchi, U., Sugimoto, K., Nagamura, Y., Hirasawa, T., & Ookawa, T. (2020). Semi-dwarf 1 (sd1) gene enhances light penetration into the canopy through regulating leaf inclination angle in rice. Field Crops Research 246, 107694.

Santiago Prochetto, Renata Reinheimer. (2020). Step by step evolution of Indeterminate Domain (IDD) transcriptional regulators: from algae to angiosperms, Annals of Botany, 126, 85–101.

Sarikas, A., Hartmann, T., & Pan, Z. Q. (2011). The cullin protein family. Genome biology, 12(4), 220.

Sasaki A., Itoh H., Gomi K., et al. (2003). Accumulation of phos-phorylated repressor for gibberellin signaling in an F-boxmutant. Science299, 1896–1898.

Sato K. (2020). History and future perspectives of barley genomics. DNA research: an international journal for rapid publication of reports on genes and genomes, 27(4), dsaa023.

Scanlon, M. J., Schneeberger, R. G., & Freeling, M. (1996). The maize mutant narrow sheath fails to establish leaf margin identity in a meristematic domain. Development (Cambridge, England), 122(6), 1683–1691.

Scanlon, M.J., Schneeberger, R.G., Freeling, M. (1996). The maize mutant narrow sheath fails to establish leaf margin identity in a meristematic domain. Development 122, 1683–1691.

Schnurbusch T. (2019). Wheat and barley biology: Towards new frontiers. Journal of integrative plant biology, 61(3), 198–203.

Schoof, H., Lenhard, M., Haecker, A., Mayer, K. F., Jürgens, G., & Laux, T. (2000). The stem cell population of Arabidopsis shoot meristems is maintained by a regulatory loop between the CLAVATA & WUSCHEL genes. Cell, 100(6), 635-644.

Seo, D. H., Ryu, M.Y., Jammes, F., Hwang, J.H., Turek, M., Kang, B.G., Kwak, J.M., & Kim, W.T. (2012). Roles of four Arabidopsis U-box E3 ubiquitin ligases in negative regulation of abscisic acid-mediated drought stress responses. Plant physiology, 160(1), 556-568.

Shaaf, S., Bretani, G., Biswas, A., Fontana, I. M., & Rossini, L. (2019). Genetics of barley tiller & leaf development. Journal of integrative plant biology, 61(3), 226-256.

Sharman, B. C. (1942). Developmental Anatomy of the Shoot of Zea mays L. Annals of Botany VI, 245-282.

Shimizu, Y., Okuda-Shimizu, Y., & Hendershot, L. M. (2010). Ubiquitylation of an ERAD substrate occurs on multiple types of amino acids. Molecular cell, 40(6), 917-926.

Shimizu, Y., Okuda-Shimizu, Y., & Hendershot, L. M. (2010). Ubiquitylation of an ERAD substrate occurs on multiple types of amino acids. Molecular cell, 40(6), 917–926.

Shu, K., & Yang, W. (2017). E3 ubiquitin ligases: ubiquitous actors in plant development & abiotic stress responses. Plant & Cell Physiology, 58(9), 1461-1476.

Singh, R. K., Gonzalez, M., Kabbaj, M. H., & Gunjan, A. (2012). Novel E3 ubiquitin ligases that regulate histone protein levels in the budding yeast Saccharomyces cerevisiae. PloS one, 7(5), e36295.

Song X.J., Huang W., Shi M., Zhu M.Z. & Lin H.X. (2007). A QTL for rice grain width and weight encodes a previously unknown RING-type E3 ubiquitin ligase. Nature Genetics, 39, 623– 630.

Song, Q., Chu, C., Parry, M. A., & Zhu, X. G. (2016). Genetics-based dynamic systems model of canopy photosynthesis: the key to improve light & resource use efficiencies for crops. Food & energy security, 5(1), 18–25.

Soppa, U., & Becker, W. (2015). DYRK protein kinases. Current biology: CB, 25(12), R488–R489.

Stone, S. L., Hauksdóttir, H., Troy, A., Herschleb, J., Kraft, E., & Callis, J. (2005). Functional analysis of the RING-type ubiquitin ligase family of Arabidopsis. Plant physiology, 137(1), 13–30.

Stone, S. L., Hauksdóttir, H., Troy, A., Herschleb, J., Kraft, E., & Callis, J. (2005). Functional Analysis of the RING-Type Ubiquitin Ligase Family of Arabidopsis. Plant physiology, 137(1), 13-30.

Sun, F., Zhang, W., Xiong, G., Yan, M., Qian, Q., Li, J., & Wang, Y. (2010). Identification and functional analysis of the MOC1 interacting protein 1. Journal of genetics and genomics = Yi chuan xue bao, 37(1), 69–77.

Sun, T. (2010). Gibberellin-GID1-DELLA: A Pivotal Regulatory Module for Plant Growth and Development1. American Society of Plant Biologists.

Swatek, K. N., & Komander, D. (2016). Ubiquitin modifications. Cell research, 26(4), 399–422.

Sylvester, A. A. W., Cande, W. Z. and Freeling, M. (1990). Division and differentiation during normal and liguleless-l maize leaf development. Development 110, 985—1000.

Sylvestersen, K.B., Young, C. and Nielsen, M.L. (2013) Advances in characterizing ubiquitylation sites by mass spectrometry. Curr. Opin. Chem. Biol. 17, 49–58.

T., Seiler, C., Himmelbach, A., Ariyadasa, R., Youssef, H. M., Stein, N., Sreenivasulu, N., Komatsuda, T. and Schnurbusch, T. (2013). Six-rowed spike4 (Vrs4) controls spikelet determinacy and row-type in barley. Proceedings of the National Academy of Sciences of the United States of America (PNAS) 110, 13198—13203.

Takeda, T., Suwa, Y., Suzuki, M., Kitano, H., Ueguchi-Tanaka, M., Ashikari, M., Matsuoka, M., & Ueguchi, C. (2003). The OsTB1 gene negatively regulates lateral branching in rice. The Plant journal: for cell and molecular biology, 33(3), 513–520.

Tilman, D., Balzer, C., Hill, J., & Befort, B. L. (2011). Global food dem& & the sustainable intensification of agriculture. Proceedings of the national academy of sciences, 108(50), 20260-20264.

Townsley, B. T. and Sinha, N. R. (2012). A New Development: Evolving Concepts in Leaf Ontogeny. Annual Review of Plant Biology 63, 535—562.

Tricase, C., Lamonaca, E., Ingrao, C., Bacenetti, J., Giudice, A.L. (2018) A comparative Life Cycle Assessment between organic & conventional barley cultivation for sustainable agriculture pathways. J. Clean. Prod. 172, 3747–3759.

Tsukaya, H. (2013). Leaf development. The Arabidopsis Book 1, e0072.

Ueguchi-Tanaka, M., Ashikari, M., Nakajima, M., Itoh, H., Katoh, E., Kobayashi, M., Chow, T. Y., Hsing, Y. I., Kitano, H., Yamaguchi, I., & Matsuoka, M. (2005). GIBBERELLIN INSENSITIVE DWARF1 encodes a soluble receptor for gibberellin. Nature, 437(7059), 693–698.

Ueguchi-Tanaka, M., Ashikari, M., Nakajima, M., Itoh, H., Katoh, E., Kobayashi, M., Chow, T. Y., Hsing, Y. I., Kitano, H., Yamaguchi, I., & Matsuoka, M. (2005). GIBBERELLIN INSENSITIVE DWARF1 encodes a soluble receptor for gibberellin. Nature, 437(7059), 693–698.

Vierstra, R. D. (2009). The ubiquitin–26S proteasome system at the nexus of plant biology. Nature Reviews Molecular Cell Biology, 10(6), 385-397.

Vitre, B., Coquelle, F. M., Heichette, C., Garnier, C., Chrétien, D., & Arnal, I. (2008). EB1 regulates microtubule dynamics and tubulin sheet closure in vitro. Nature cell biology, 10(4), 415–421.

Waugh, R., Jannink, J.L., Muehlbauer, G.J., Ramsay, L. (2009). The emergence of whole genome association scans in barley. Curr Opin Plant Biol 12, 218–222.

Weber, H., Bernhardt, A., Dieterle, M., Hano, P., Mutlu, A., Estelle, M., Genschik, P., & Hellmann, H. (2005). Arabidopsis AtCUL3a and AtCUL3b form complexes with members of the BTB/POZ-MATH protein family. Plant physiology, 137(1), 83–93.

Welch, D., Hassan, H., Blilou, I., Immink, R., Heidstra, R., & Scheres, B. (2007). Arabidopsis JACKDAW & MAGPIE zinc finger proteins delimit asymmetric cell division & stabilize tissue boundaries by restricting SHORT-ROOT action. Genes & Development, 21(17), 2196-2204.

Whipple, C. J., Kebrom, T. H., Weber, A. L., Yang, F., Hall, D., Meeley, R., Schmidt, R., Doebley, J., Brutnell, T. P., & Jackson, D. P. (2011). grassy tillers1 promotes apical dominance in maize and responds to shade signals in the grasses. Proceedings of the National Academy of Sciences of the United States of America, 108(33), E506–E512.

Wilson, M.D., Benlekbir, S., Fradet-Turcotte, A., Sherker, A., Julien, J.P., McEwan, A., Noordermeer, S.M., Sicheri, F., Rubinstein, J.L., & Durocher, D. (2016). The structural basis of modified nucleosome recognition by 53BP1. Nature, 536(7614), 100-103.

Xia, T., Li, N., Dumenil, J., Li, J., Kamenski, A., Bevan, M. W., Gao, F., & Li, Y. (2013). The ubiquitin receptor DA1 interacts with the E3 ubiquitin ligase DA2 to regulate seed and organ size in Arabidopsis. The Plant cell, 25(9), 3347–3359.

Xia, T., Li, N., Dumenil, J., Li, J., Kamenski, A., Bevan, M.W., Gao, F., & Li, Y. (2013). The ubiquitin receptor DA1 interacts with the E3 ubiquitin ligase DA2 to regulate seed and organ size in Arabidopsis. The Plant Cell, 25(9), 3347-3359.

Xu, L., Liu, F., Lechner, E., Genschik, P., Crosby, W. L., Ma, H., Peng, W., Huang, D., & Xie, D. (2002). The SCFCOI1 ubiquitin-ligase complexes are required for jasmonate response in Arabidopsis. The Plant Cell, 14(8), 1919-1935.

Ye, L., Wang, Y., Long, L., Luo, H., Shen, Q., Broughton, S., Wu, D., Shu, X., Dai, F., Li, C., & Zhang, G. (2019). A Trypsin Family Protein Gene Controls Tillering and Leaf Shape in Barley. Plant physiology, 181(2), 701–713.

Yee, D., & Goring, D.R. (2009). The diversity of plant U-box E3 ubiquitin ligases: from upstream activators to downstream target substrates. Journal of Experimental Botany, 60(4), 1109-1121.

Yoshida, H., and Ueguchi-Tanaka, M. (2014). DELLA and SCL3 balance gibberellin feedback regulation by utilizing INDETERMINATE DOMAIN proteins as transcriptional scaffolds. Plant Signal Behav 9.

Yoshida, H., Hirano, K., Sato, T., Mitsuda, N., Nomoto, M., Maeo, K., Koketsu, E., Mitani, R., Kawamura, M., Ishiguro, S., Tada, Y., Ohme-Takagi, M., Matsuoka, M., & Ueguchi-Tanaka, M. (2014). DELLA protein functions as a transcriptional activator through the DNA binding of the

indeterminate domain family proteins. Proceedings of the National Academy of Sciences, 111(21), 7861-7866.

Yoshida, S., Bartolini, S., & Pellman, D. (2009). Mechanisms for concentrating Rho1 during cytokinesis. Genes & development, 23(7), 810–823.

Yoshida, Y., Saeki, Y., Murakami, A., Kawawaki, J., Tsuchiya, H., Yoshihara, H., Shindo, M., & Tanaka, K. (2015). A comprehensive method for detecting ubiquitinated substrates using TR-TUBE. Proceedings of the National Academy of Sciences of the United States of America, 112(15), 4630–4635.

Yoshikawa, T., Tanaka, S. Y., Masumoto, Y., Nobori, N., Ishii, H., Hibara, K. I., Itoh, J.I., Tanisaka, T., & Taketa, S. (2016). Barley NARROW LEAFED DWARF1 encoding a WUSCHEL-RELATED HOMEOBOX 3 (WOX3) regulates the marginal development of lateral organs. Breeding Science, 16019.

Yu, F., Wang, H., Liu, W., & Lu, L. (2016). Grass carp Ctenopharyngodon idella Fibulin-4 as a potential interacting partner for grass carp reovirus outer capsid proteins. Fish & shellfish immunology, 48, 169–174.

Yu, F., Wu, Y., & Xie, Q. (2016). Ubiquitin–proteasome system in ABA signalling: from perception to action. Molecular plant, 9(1), 21-33.

Zhai, Z., Liu, H., & Shanklin, J. (2017). Phosphorylation of WRINKLED1 by KIN10 Results in Its Proteasomal Degradation, Providing a Link between Energy Homeostasis and Lipid Biosynthesis. The Plant cell, 29(4), 871–889.

Zhang, J., Wei, B., Yuan, R., Wang, J., Ding, M., Chen, Z., Yu, H., & Qin, G. (2017). The Arabidopsis RING-Type E3 Ligase TEAR1 Controls Leaf Development by Targeting the TIE1 Transcriptional Repressor for Degradation. The Plant cell, 29(2), 243–259.

Zhang, J., Wei, B., Yuan, R., Wang, J., Ding, M., Chen, Z., Yu, H., & Qin, G. (2017). The Arabidopsis RING-Type E3 Ligase TEAR1 Controls Leaf Development by Targeting the TIE1 Transcriptional Repressor for Degradation. The Plant cell, 29(2), 243–259.

Zhang, Y., Tang, L., Liu, X., Liu, L., Cao, W., & Zhu, Y. (2017). Modeling the leaf angle dynamics in rice plant. PloS one, 12(2), e0171890.

Zhang, Y., Yang, C., Li, Y., Zheng, N., Chen, H., Zhao, Q., Gao, T., Guo, H., & Xie, Q. (2007). SDIR1 is a RING finger E3 ligase that positively regulates stress-responsive abscisic acid signallingin Arabidopsis. The Plant Cell, 19(6), 1912-1929.

Zhao, B., Li, H., Li, J., Wang, B., Dai, C., Wang, J., & Liu, K. (2017). Brassica napus DS-3, encoding a DELLA protein, negatively regulates stem elongation through gibberellin signalling pathway. TAG. Theoretical and applied genetics. Theoretische und angewandte Genetik, 130(4), 727–741.

Zhu Q. H., Hoque M. S., Dennis E. S., Upadhyaya N. M. (2003). Ds tagging of BRANCHED FLORETLESS 1 (BFL1) that mediates the transition from spikelet to floret meristem in rice (Oryza sativa L). BMC Plant Biol. 3: 6.

Zhu, X.G., Long, S.P., Ort, D.R. (2010). Improving photosynthetic efficiency for greater yield. Annu Rev Plant Biol 61, 235–261.

Zohary, D., Hopf, M., & Weiss, E. (2012). Domestication of Plants in the Old World: The origin & spread of domesticated plants in Southwest Asia, Europe, & the Mediterranean Basin. Oxford University Press on Dem.

Zombori, Z., Nagy, B., Mihály, R., Pauk, J., Cseri, A., Sass, L., Horváth V, G., & Dudits, D. (2020). RING-Type E3 Ubiqitin Ligase Barley Genes (HvYrg1-2) Control Characteristics of Both Vegetative Organs and Seeds as Yield Components. Plants (Basel, Switzerland), 9(12), 1693.

Homepages cited

NordGen.org, Nordic Genetic Resource Center. URL: http://www.nordgen.org, last access: April 5th, 2016.

FAOSTAT 2013, Food and Agriculture Organization of the United Nations (FAO). URL: http://faostat3.fao.org, last access: September 2nd, 2015.

APPENDIX A: Oligonucleotides

Name	Function	Sequence
• **Y2H colony PCR and Prey plasmid sequencing**		
OS_23	GAL4_AD (pDEST22)	CGCGTTTGGAATCACTACAGG
OS_24	Term_yADH1 (pDEST22)	GACCAAACCTCTGGCGAAGA
• **Gateway cloning primers**		
OS_11	For-attB1-BLF1-CDS	GGGGACAAGTTTGTACAAAAAAGCAGGCTTCATGTTGGGTTCTTGCGTGC
OS_12	Rev-attB2-BLF1-CDS	GGGGACCACTTTGTACAAGAAAGCTGGGTCTTAGACAGTGTCCATCGCGG
OS_5	For-attB1-SLN1 (synthetic CDS)	GGGGACAAGTTTGTACAAAAAAGCAGGCTTCATGAAGAGAGAATATCAAGATGGT
OS_6	Rev-attB2-SLN1 (synthetic CDS)	GGGGACCACTTTGTACAAGAAAGCTGGGTCTTACGGAGCAGCCAATCT
OS_7	For-attB1-SLN1(barley CDS)	GGGGACAAGTTTGTACAAAAAAGCAGGCTTCATGAAGCGCGAGTACCAGGACGG
OS_8	Rev-attB2-SLN1(barley CDS)	GGGGACCACTTTGTACAAGAAAGCTGGGTCTTACGGCGCGGCGAGGC
OS_25	For-attB1-GID1-CDS	GGGGACAAGTTTGTACAAAAAAGCAGGCTTCATGGCCGGCAGCGAC
OS_26	Rev-attB2-GID1 -CDS	GGGGACCACTTTGTACAAGAAAGCTGGGTCCTAGCGGAGGTTAAGTTGGACG
OS_100	For-attB1-VRS1 barley CDS	GGGGACAAGTTTGTACAAAAAAGCAGGCTTCATGGACAAGCAGCACCTCTT
OS_101	Rev-attB2-VRS1 barley CDS	GGGGACCACTTTGTACAAGAAAGCTGGGTCCTAAATCAGCCCATACAGGCTAAAC
OS_129	For-attB1- HORVU1Hr1G071160.1 (Kinase)	GGGGACAACTTTGTATAGAAAAGTTGGGTGCTAGCGGAGGTTAAGTTGGACG
OS_133	Rev-attB4- HORVU1Hr1G071160.1	GGGGACAACTTTGTATAGAAAAGTTGGGTGTCAACGATACTTGTGTGAAAACCATC

OS_136	For-attB1-HORVU6Hr1G082920.1 (RING-Ubox)	GGGGACAAGTTTGTACAAAAAAGCAGGCTTAATGGGCGGCAAGAGGAAGAG
OS_137	Rev-attB4-HORVU6Hr1G082920.1	GGGGACAACTTTGTATAGAAAAGTTGGGTGGTATCGGCAAGACGAAGATCATCTGTT
OS_140	For-attB1-HORVU1Hr1G020270.1 (BTB/POZ &MATH)	GGGGACAAGTTTGTACAAAAAAGCAGGCTTAATGAGGACGGCGTCGACGTG
OS_141	Rev-attB4- HORVU1Hr1G020270.1	GGGGACAACTTTGTATAGAAAAGTTGGGTGAATTTTGCGGGACCTTTTTGCCCT
OS_144	For-attB1- HORVU1Hr1G044890.1 (EBA1)	GGGGACAAGTTTGTACAAAAAAGCAGGCTTAATGCCGAGGAGGGCAGAACC
OS_145	Rev-attB4-HORVU1Hr1G044890.1	GGGGACAACTTTGTATAGAAAAGTTGGGTGGGTGAAGCTCATCAACGGTGAGC
OS_116	For-attB1-HORVU2Hr1G026850.26 (POK1)	GGGGACAAGTTTGTACAAAAAAGCAGGCTTAATGTTCACGTTTGATCATGTCGCATG
OS_117	Rev-attB4-HORVU2Hr1G026850.26	GGGGACAACTTTGTATAGAAAAGTTGGGTGTGTACTGCGCAGCGGCC
OS_66	For-attB3-BLF1	GGGGACAACTTTGTATAATAAAGTTGGAATGTTGGGTTCTTGCGTGCC
OS_67	Rev-attB2- BLF1	GGGGACCACTTTGTACAAGAAAGCTGGGTGAGTGTCCATCGCGGCGTGTT
• **Illumina primers**		
OS_102	Y-adapter strand A (Truncated Illumina TruSeq Adapter)	ACACTCTTTCCCTACACGACGCTCTTCCGATCT
OS_103	Y-adapter strand B (Truncated Illumina TruSeq Adapter)	P-GATCGGAAGAGCACACGTC
		TGAACTCCAGTCAC
OS_104	Primer A (Illumina TruSeq Universal Primer)	AATGATACGGCGACCACCGAGATCTACACTCTTTCCCTACACGACGCTCTTCCGATCT
OS_105	Primer B, index1 (Illumina TruSeq Universal Primer)	CAAGCAGAAGACGGCATACGAGATCGTGATGTGACTGGAGTTCAGACGTGTGCTCTTCCG
OS_106	Primer B, index2 (Illumina TruSeq Universal Primer)	CAAGCAGAAGACGGCATACGAGATACATCGGTGACTGGAGTTCAGACGTGTGCTCTTCCG
OS_107	Primer B, index3 (Illumina TruSeq Universal Primer)	CAAGCAGAAGACGGCATACGAGATGCCTAAGTGACTGGAGTTCAGACGTGTGCTCTTCCG
OS_108	Primer B, index4 (Illumina TruSeq Universal Primer)	CAAGCAGAAGACGGCATACGAGATTGGTCAGTGACTGGAGTTCAGACGTGTGCTCTTCCG
OS_109	Primer B, index5 (Illumina TruSeq Universal Primer)	CAAGCAGAAGACGGCATACGAGATCACTGTGTGACTGGAGTTCAGACGTGTGCTCTTCCG
OS_110	Primer B, index6 (Illumina TruSeq Universal Primer)	CAAGCAGAAGACGGCATACGAGATATTGGCGTGACTGGAGTTCAGACGTGTGCTCTTCCG

• **Replace HALO-tag with 3XFLAG in pIX vector**		
OS_154	3XFLAG adapter	ATCATGGACTACAAAGACCATGACGGTGATTATAAAGATCATGACATCGATTACAAGGATGACGATGACAAGGAGCT
OS_155	3XFLAG adapter	CCTTGTCATCGTCATCCTTGTAATCGATGTCATGATCTTTATAATCACCGTCATGGTCTTTGTAGTCCATGAT
• **Construction of pCOG5 carrying BLF1 and RING/U-Box E3 or BTB/POZ E3**		
OS_250	For-insert1 (BLF1 + 25 bp GST)	GTATTTTCAGGGCGCCATGGGATCTATGTTGGGTTCTTGCGTGCC
OS_251	Rev-insert1 (BLF1+25 bp backbone)	ACGTGCCAAGCTTGGTACCGCATGCCTAGACAGTGTCCATCGCGG
OS_252	For-Backbone (pCOG5)	GCATGCGGTACCAAGCTTGGC
OS_253	Rev-Backbone (pCOG5)	AGGATCCATGGCGCCCTGAAAATAC
OS_254	For-insert2 (GST+ 25 bp RING/U-Box)	CAAGACGAAGATCATCTGTTCCTGACTCGACGAGCTCAACTGGGAACA
OS_255	Rev-insert2 (GST+ 25 bp BLF1)	CCATCGGCACGCAAGAACCCAACATAGATCCCATGGCGCCCTGAAAATA
OS_256	For-insert3 (RING/U-Box +20 bp pCOG5)	GTATTTTCAGGGCGCCATGGATCCTATGGTGAAGACGCCGTCTAC
OS_257	Rev-insert3 (RING/U-Box +20 bp pCOG5)	GTGTGAAATTGTTCCCAGTTGAGCTCGTCGAGTCAGGAACAGATGATCTTCGTCTTG
OS_258	For-insert2´ (GST+25bp BTB/POZ & MATH)	GGCAAAAAGGTCCCGCAAAATTTAGCTCGACGAGCTCAACTGGGAACA
OS_259	Rev-insert2´ (GST+25 bp BLF1)	CCATCGGCACGCAAGAACCCAACATAGATCCCATGGCGCCCTGAAAATA
OS_260	For-insert3´ (BTB/POZ & MATH +25 bp pCOG5)	GTATTTTCAGGGCGCCATGGATCCTATGAGGACGGCGTCGACG
OS_261	Rev-insert3´ (BTB/POZ & MATH +25bp pCOG5)	GTGAAATTGTTCCCAGTTGAGCTCGTCGAGCTAAATTTTGCGGGACCTTTTTGCC
• **Construction of pGEN4 carrying HvUbc11 and HvUba2**		
OS_391	For-Insert1_HvUbc11 (E2)-EcoRI	TCAGAGGTGGGTGAGAATTCTAAGGAAATCCATTATGGCATCCAAGCGCATC
OS_392	Rev-Insert1_HvUbc11-AscI	CGGAATTGTGGCGCGCCTCAACCCATGGCGTACTTCT
OS_393	For-Insert2_HvUba2 (E1)-AscI	CGCCATGGGTTGAGGCGCGCCACAATTCCGACAGGAAACAGCTATGCTCCCTCGGAAGCGG
OS_394	Rev-Insert2_HvUba2-BstBI	CAGGCTCTAGATTCGAATCAACGGAAGTAGACAGATACG
• **CRISPR/CAS9 genotyping primers**		
OS_337	For-dCAPS (AgeI digest) ring/U-Box-5bp/6bp_Δ exon 1	CCGGGCGTCGAGGTACCG

OS_338	Rev-dCAPS (AgeI digest) ring/U-Box-5bp/6bp_Δ exon 1	GACGTGCTGCACGCGGG
OS_270	For-dCAPS (BssSI digest) for ring/U-Box-5bp/6bp_Δ exon 1	GGTCGCCCGAGGAAGAAC
OS_271	Rev-dCAPS (BssSI digest) for ring/U-Box-5bp/6bp_Δ exon 1	GCAGCTTCACCTGCTCCTC
OS_640	For-dCAPS (BssSI digest)- ring/U-Box -5bp/6bp_Δ exon1	CTGGTAGATGGGGGGCCTGA
OS_643	Rev-dCAPS (BssSI digest) ring/U-Box -5bp/6bp_Δ exon1	CAAGAGGAAGAGCACCGGG
OS_663	For-dCAPS (Cac8II digest) for blf1-4bp_Δ exon2	TGCACCACGACCCCTC
OS_664	Rev- dCAPS (Cac8II digest) for blf1-4bp_Δ exon2	CCGCAGTCGCAGGAGT
OS_244	For-primer Blf1-exon2	AGATCTGCAACCAGGGGTTCC
OS_245	Rev-primer Blf1-exon2	CAGGTCTTGAGGTGGGCCTT
OS_303	For-INDEL-kinase (200bp_Δ)	GAAAGGGCAGTGCAGAGACT
OS_304	Rev-INDEL-kinase (200bp_Δ)	ACTGTTAGCAGCATCCGTGT
OS_315	For-dCAPS (BsmI digest) for kinase	ACGGAGGTGCTGGATGAATG
OS_316	Rev- dCAPS (BsmI digest) for kinase	TTTCGACAGTCAGGTGCTAGT

APPENDIX B: Plasmid constructs

Code	***E. coli* strain**	**Vector**	**Resistance in *E. coli***
EOS_1	TOP10	pDONR221_P1P4-PKc_DYRK_like Kinase	KanR, Chloram
EOS_2	TOP10	pDONR221_P1P4-CDS_RING/U-Box E3.1	KanR, Chloram
EOS_3	TOP10	pDONR221_P1P4-CDS_BTB/POZ E3	KanR, Chloram
EOS_4	TOP10	pDONR221_P1P4-EB1A	KanR, Chloram
EOS_5	TOP10	pDONR221_P1P4-BLF1	KanR, Chloram
EOS_6	TOP10	pDONR221_P3P2-BLF1	KanR, Chloram
EOS_7	DH5α	pBiFCt-2-in-1-NC	Spect, Chloram, Basta, lacZ
EOS_8	DH5α	pBiFCt-2-in-1-CN	Spect, Chloram, Basta, lacZ
EOS_9	DH5α	pFRETgc-2-in-1-NC	Spect, Chloram, Basta, lacZ
EOS_10	DH5α	pFRETgc-2-in-1-CN	Spect, Chloram, Basta, lacZ
EOS_13	DH5α	pIX-HALO	AmpR
EOS_15	DH5α	pDONR221_BLF1:FLAG	KanR, Chloram
EOS_16	DH5α	pDONR221_SLN1:FLAG	KanR, Chloram
EOS_17	DH5α	pDONR221_GID1:FLAG	KanR, Chloram

EOS_18	DH5α	pIX-HALO-BLF1	AmpR
EOS_19	TOP10	pIX-HALO-VRS1	AmpR
EOS_20	TOP10	pBlue-Slice-KINESIN	AmpR
EOS_21	TOP10	2-in-1-NN-MYC:PKc_DYRK_like Kinase-HA:BLF1	Spect, Chloram, lacZ
EOS_22	TOP10	2-in-1-NN-MYC:RING/U-Box E3-HA:BLF1	Spect, Chloramphenicol, lacZ
EOS_23	TOP10	2-in-1-NN-MYC:BTB/POZ E3-HA:BLF1	Spect, Chloramphenicol, lacZ
EOS_24	TOP10	2-in-1-NN-MYC:EB1A-HA:BLF1	Spect, Chloram, lacZ
EOS_25	TOP10	2-in-1-NN-MYC:NPR1-HA:BLF1	Spect, Chloram, lacZ
EOS_26	TOP10	pDONR221-BLF1	KanR, Chloram
EOS_28	TOP10	pDONR221-p1p2-EV	KanR, Chloram
EOS_32	DH5α	pCOG5-RING/U-Box E3	AmpR
EOS_34	DH5α	pGEN1	KanR
EOS_36	XL1-Blue	pDEST22	KanR
EOS_38	XL1-Blue	pDEST32	AmpR
EOS_40	DH5α	pIX-3X FLAG-BLF1	GentR
EOS_42	TOP10	pDONR221_P1P2-PKc_DYRK_like Kinase	AmpR
EOS_44	TOP10	pDONR221_P1P2-RING/U-Box E3.1	KanR
EOS_46	TOP10	pDONR221_P1P2-BTB/POZ E3	KanR
EOS_48	TOP10	pDONR221_P1P2-EB1A	KanR
EOS_50	TOP10	pGEN4	KanR
EOS_52	TOP10	pCOG5-RING/U-Box E3 #1	kanR
EOS_54	TOP10	pIX-Halo-PKc_DYRK_like Kinase	AmpR
EOS_56	TOP10	pIX-Halo-RING/U-Box E3	AmpR
EOS_58	TOP10	pIX-Halo-BTB/POZ E3	AmpR
EOS_60	TOP10	pIX-Halo-POK1	AmpR
EOS_62	TOP10	pIX-Halo-EB1A	AmpR
EOS_64	TOP10	pCOG5-RING/U-Box E3-BLF1	AmpR
EOS_66	TOP10	pDONR221-p1p2_SLN1	KanR
EOS_68	DH5α	pDEST22-SLN1	AmpR
EOS_70	DH5α	pDEST32-BLF1	GentR
EOS_72	DH5α	pIX-3X FLAG	GentR
EOS_74	DH5α	pGEN4_Ub_E1 (-E2)	kanR
EOS_76	DH5α	pCOG5-RING/U-Box E3-BLF1	AmpR
EOS_78	DH5α	pCOG5 -BTB/POZ E3 -BLF1	AmpR
EOS_80	Rosetta	pCOG5-RING/U-Box E3 + pGEN4 (original)	Amp,kan,chlorom
EOS_82	Rosetta	pCOG5-original + pGEN4 (-E2)	Amp,kan,chlorom
EOS_84	Rosetta	pCOG5-BTB/POZ E3-BLF1 + pGEN4 (original)	Amp,kan,chlorom
EOS_86	Rosetta	pCOG5-BTB/POZ E3-BLF1 + pGEN4 (-E2)	Amp,kan,chlorom

EOS_88	Rosetta	pCOG5-RING/U-Box E3-BLF1 + pGEN4 (original)	Amp,kan,chlorom
EOS_90	Rosetta	pCOG5-RING/U-Box E3-BLF1 + pGEN4 (-E2)	Amp,kan,chlorom
EOS_94	TOP10	2-in-1-NN-Halo-BLF1-3XFLAG-PKc_DYRK Kinase	SpectR
EOS_96	TOP10	2-in-1-NN-Halo-BLF1-3XFLAG-RING/U-Box E3	SpectR
EOS_98	TOP10	2-in-1-NN-Halo-BLF1-3XFLAG-BTB/POZ E3	SpectR
EOS_100	TOP10	2-in-1-NN-Halo-BLF1-3XFLAG-EB1A	SpectR
EOS_102	TOP10	2-in-1-NN-p1p4-ø-p3p2-BLF1	SpectR
EOS_104	TOP10	pDONR221_P1P4	KanR, Chloram
EOS_106	TOP10	pDONR221_P3P2	KanR, Chloram
EOS_108	TOP10	pDONR221_P1P4-PKc_DYRK_like Kinase	KanR, Chloram
EOS_109	TOP10	pDONR221_P1P4-RING/U-Box E3	KanR, Chloram
EOS_110	DH5α	pDEST32-GID1	GentR
EOS_112	XL1-Blue	pGEN4_AtUb_E1(UBA2 *At*)-E2(HvUbc11)	kanR
EOS_114	TOP10	pIX-3XFLAG-CDS-PKc_DYRK_like Kinase	AmpR
EOS_116	TOP10	pIX-3XFLAG-CDS_RING/U-Box E3	AmpR
EOS_118	TOP10	pIX-3XFLAG-CDS_BTB/POZ E3	AmpR
EOS_120	TOP10	pIX-3XFLAG-CDS_EB1A	AmpR
EOS_122	TOP10	pDONR221_P1P2-NPR1	AmpR
EOS_124	TOP10	pIX-3XFLAG-CDS-NPR1	AmpR
EOS_126	TOP10	2-in-1-NN-FRET-p1p4-RING/U-Box E3-p3p2-BLF1	SpectR
EOS_128	TOP10	2-in-1-NN-FRET-p1p4-BTB/POZ E3-p3p2-BLF1	SpectR
EOS_130	Rosetta	pCOG5-RING/U-Box E3-BLF1 + pGEN4 (ubc11_Hv)	AmpR,kanR, Chloram
EOS_134	TOP10	pDONR221_P1P2-Uba2_Hv (E1)	kanR
EOS_136	TOP10	pDONR221_P1P2-Ubc11_Hv (E2)	kanR
EOS_138	TOP10	pDONR221_P1P2-Ub_At	kanR
EOS_140	TOP10	pIX-GST	ampR
EOS_142	XL1-Blue	pCOG5-RING/U-Box E3-BTB/POZ E3-BLF1_no-GST	ampR
EOS_144	XL1-Blue	pCOG5-RING/U-Box E3-original	AmpR
EOS_146	XL1-Blue	pCOG5-RING/U-Box E3-BLF1_no-GST	AmpR
EOS_148	XL1-Blue	pCOG5-RING/U-Box E3-BTB/POZ E3-BLF1_no-GST	AmpR
EOS_150	XL1-Blue	pCOG5-RING/U-Box E3-RING/U-Box E3_no-BLF1	AmpR
EOS_152	XL1-Blue	pCOG5-RING/U-Box E3-BTB/POZ E3_no-BLF1	AmpR
EOS_154	XL1-Blue	pCOG5-RING/U-Box E3-original	AmpR